UNIVERSITY OF OKLAHOMA

GRADUATE COLLEGE

HOMOGENEOUS VESSELS AS ACTIVE ELEMENTS FOR MEASURING PRESSURE

A DISSERTATION

SUBMITTED TO THE GRADUATE FACULTY

in partial fulfillment of the requirements for the

Degree of

DOCTOR OF PHILOSOPHY

By

MICHAEL DAVID NASH
Norman, Oklahoma
2018

HOMOGENEOUS VESSELS AS ACTIVE ELEMENTS
FOR MEASURING PRESSURE

A DISSERTATION APPROVED FOR THE
SCHOOL OF AEROSPACE AND MECHANICAL ENGINEERING

BY

Dr. David Miller, Chair

Dr. Dean Hougen

Dr. Wilson Merchan-Merchan

Dr. Ramkumar Parthasarathy

Dr. Li Song

Dr. Harold Stalford

Table of Contents

List of Tables

List of Figures

Abstract

This work investigates an approach to pressure sensor design in which a homogeneous vessel is used as the active element to sense pressure. The goal of this project was to synthesize a standard model for the design and development of a pressure sensor predicated on pressure vessel methodologies. Four prototypes were constructed, each implementing the experimental design using a different material and dimensions. A specialized testing apparatus was built to establish a controllable volume to which multiple devices can be connected and tested simultaneously. The data collection and measurement interface is also built into the testing apparatus.

The four prototypes with dissimilar geometries and materials are tested at room temperature for their repeatability in response to pressure and its transduction to voltage. When subjected to controlled pressures of up to 80 psi, strong agreement was observed between the prototypes under test and the actual pressure in the control volume; the physical design was validated for all four devices.

Uncertainty analysis was used to test for failure of the derived theoretical model to predict pressure with the measured voltage from the prototypes. Error limits established by the propagation of uncertainties were not exceeded by the model, and they were not rejected.

Chapter 1

Introduction

1.1 Background

In 1594 Galileo Galilei patented a machine to assist in irrigation by pumping water from a nearby river. The machine had an observed limit of ten meters of water in the suction pump [43]. This limitation was unexplainable at the time, but inspired a wave of research dedicated to discover and understand the phenomena that we would later understand to be the multi-directionally uniform force acting on a unit of area: pressure [36]. Understanding this basic tenet of the physical world would add another physical phenomena to the growing body of knowledge that encompassed our evolving comprehension of the universe.

As engineers, we leverage that collective of discovered phenomena in practical application and the development of technologies to solve the problems of the day. Without fully understanding the nature of this physical phenomenon, Galileo used pressure to engineer a solution to the problem of irrigation. The success of his invention was evidence of the utility of a useful facet of nature, and it ignited imaginations and motivated scientists and engineers the

world over to better understand pressure. Its control would open the door to technologies that would advance civilization to the next level.

In 1644, the first formal quantification of pressure took place when Evangelista Torricelli invented the mercury barometer in the first manometer [24]; the road thus paved for the later advent of steam, combustion engines, hydraulics, aircraft, city water and sewage infrastructures, and reservoir drilling. Today, the control of pressure systems is a cornerstone of the technological civilization in which we live, and it is controllable because it is observable with the use of pressure measurement devices whose designs are as varied as the systems in which they are employed.

Within the decade following Torricelli's manometer, the first pressure measurement devices were widely adopted. Manometers used columns of liquid displaced by the application of pressure. These had the benefits of being accurate, repeatable, and readily observable, but limited in pressure range due to the proportional relationship between the size of the instrument to the upper limit of its measurement range. They were further disadvantaged by their size for a lack in portability. High cost and operating conditions limiting temperature and necessitating stability (e.g. they were difficult to use on ship) was enough to motivate casual research into alternative methods. However, that most people were used to the inconveniences inherent to manometers and acquiesced their shortcomings could explain the 200 years that passed before the debut of a successor.

The advent of the aneroid (Greek "without liquid") barometer in 1843 introduced an instrument that could be designed to fit applications in which manometers would be impractical or inconvenient. Invented by Lucien Vidi,

the seminal design utilized a diaphragm stretched over a cavity. Pressure acting on the diaphragm deflected the surface which was translated into the proportional displacement of an indication needle [49, 50]. The issues of cost, limited operating temperature range, and the necessity of stability with fluid-based manometers furthered the success of aneroid barometers, which were comparatively smaller, less expensive, more robust, and could be made to be more accurate [49].

Present State of Practice

The range of pressures and variety of media in applications today are extreme. The pressures involved range across the gamut from a few pascals in meteorological observations and altimeters to a few terapascals in nuclear fusion research [52]. The flowing substances are not necessarily liquid or gas, but can be exotic and exist somewhere in between; they can be turbid. Media can be corrosive, radioactive, conductive, biologic or saline. They can be accompanied by destructive transport phenomena such as water hammer or cavitation. Extremes of application necessitate the a variety of measurement techniques and sensor designs.

168 years after the inception of the aneroid, diaphragm-based sensors unequivocally dominate the market and the design has become the de facto pressure measurement technique. The vast majority of commercially available pressure sensors utilize a diaphragm as the active element for pressure transduction. To adapt to the computer age, needles which originally translated applied pressure into visible displacement for human measurement have been replaced by transduction elements such as strain gages to translate applied

pressure into a proportionally varied electrical signal suitable for electronic measurement acquisition and logging.

The invention of aneroid gauges was motivated primarily by need for gauge pressure measurement for research laboratories, and atmospheric pressure measurement for weather prediction or altitude estimation [49]. Appreciated for its robustness in the measurement of a short list of media types and narrow pressure range and precision, the scope of applications of the original diaphragm-based aneroids feel uncomfortably limited when considered against the vast range of demanding applications that exist today.

Electronic pressure measurement relies on a transduction mechanism to perform the conversion of an applied pressure into a measurable electrical signal. Flexible diaphragms and Bourdon tubes are the de facto choice in applications and in production. Diaphragm-based pressure transducers have a flexible membrane that is stretched over an opening. In the presence of a pressure imbalance, the membrane deflects toward the side with lower pressure and either the transverse deflection or planar strain in the membrane are captured and considered proportional to the applied pressure. Bourdon tubes are coiled, hollow devices which will uncoil when pressurized. The displacement at the end of the tube will connect to a gauge needle, potentiometer, linear displacement transducer (such as an LVDT), or other mechanism to otherwise convert displacement to electrical signal.

1.2 Pressure Vessel Pressure Transducer

This work introduces the Pressure Vessel Pressure Transducer (PVPT), a new design for an aneroid pressure sensor. Instead of the traditional diaphragm

of most piezoresistive MEMS pressure devices, it uses a homogeneous vessel as the active transduction element. And unlike other attempts at the vessel-based design (Section 2.2), this version has a strict crossed bridge formation (Figure 1.2). The requirements on the shape of the vessel are only that it be cylindrical in shape with constant wall thickness and open at only one end. Such a shape is simple enough that prototypes satisfying the shape requirements could be built using off-the-shelf pipe sections and plumbing components. Further, if the vessel can be constructed using off-the-shelf pipe sections, then a vast landscape of media compatibility opens up by simply selecting copper, aluminum, PVC, or any other pipe that best suits the intended application.

The model consists of constant parameters of design pertaining to vessel geometry (diameter and wall thickness), the material properties of the vessel walls (the modulus of elasticity and Poisson's ratio), and characteristics of the strain gages and bridge circuit (nominal gage resistance, gauge factor, and excitation voltage).

The diameter and thickness of the vessel are all that is needed to satisfy the geometry of the model, and the elastic modulus and Poisson's ratio are the only variables needed to describe the material. The transduction to voltage is done by use of a Wheatstone bridge with piezoresistive strain gages; the additional properties needed by the model are gauge factor, nominal gauge resistance, and excitation voltage. The only other variables of the model are pressure and output voltage, which comprise the stimulus and response transduction couple.

When the interior of the vessel is positively pressurized relative to the exterior, the entire vessel deforms by increasing in both length and circumference.

Four strain gages in a full Wheatstone bridge configuration perform the transduction of wall deformation into voltage response which is measurable by software-aided data acquisition systems and thereby made available for logging and real-time monitoring. A theoretical model has been developed to fully describe the behavior of a vessel based on this design when it is subjected to internal pressure.

The proposed sensor design uses four strain gages attached to the exterior surface of the vessel so that they are deformed when the interior is subjected to sufficiently high process pressure. The four gages are connected together in a Wheatstone bridge. An excitation voltage and ground are applied to opposite sides of the bridge, and the adjacent legs of the bridge produce a ratiometrically-scaled voltage that changes as the resistances in the gages change.

1.3 Problem Statement/Research Problem

Evidence of validity is missing from all works describing similar designs that claim to sense pressure. This research will be the first to contribute a detailed theoretical model, documented physical construction, and the results of testing the system for validity.

1.4 Purpose and Significance of Study

A 1993 assessment [44] of pressure measurement technologies acknowledged the necessity for pressure sensing mechanisms facilitating higher accuracy and reliability for advanced power plant control systems. In particular, the resilience of extant technologies is identified as a desirable area of improvement as the then (and still to this day) common solution of utilizing oil as a buffer between the sensing element and the process fluids invites "insidious" failures that are difficult to identify and rarely obvious, yet they can significantly alter the operability of the sensor. Self-calibration features are of particular interest, as frequent maintenance and testing, which is a significant contributor to operations and maintenance costs, are necessary to ensure normal operation. The assessment emphasized the need in industry for the research and development of a diverse landscape of pressure sensing technologies as the needs of industry are often very specific and varied. This interpretation is evidenced by the broad set of forty conventional and innovational pressure sensors ultimately pooled and compared [44].

Microelectromechanical systems (MEMS) devices are susceptible to adverse effects from environmental conditions due to packaging compatibility, in addition to sensing element compatibility. In conventional sensors, the housing is a separately fabricated component that generally serves the sole purpose of protection of the delicate sensing elements from the environment. MEMS packaging is purposefully designed for the additional burden of compatibility with batch fabrication techniques and must serve to both protect from as well as provide an interface with the outside world [38].

While the main focus of this work is on the research problem and its assessment, this work will also be contributing various articles of knowledge pertaining to the proposed model and design which may serve as an initial basis of interest and encouragement for future research.

1.5 Research Design

The sensor is comprised of two critical parts that work in tandem to facilitate the conversion of physical phenomena to usable information. The physical design is responsible for the appropriate transduction of the stimulus of interest (pressure) to measurable response (voltage) while unresponsive to other stimuli; a rendering of the general physical model is depicted in Figure 1.2. The theoretical model is responsible for incorporating all involved parameters and signals with sufficient completeness and correctly relating them to produce (in this case) the inverse transformation of revealing the hidden stimulus (pressure) based on observable response (voltage) (see Figure 1.1).

The conceptual framework of this project extends from solid mechanics to electrical signal measurement and statistical error analysis. The theoretical framework for the sensing mechanism stems from Lamé's equations which relate internal and external pressure on the vessel surface with the principle deformations that result. For transduction of the mechanical deformation to measurable electrical response signal, a Wheatstone bridge circuit is used with excitation from stable DC power supply.

The validity of the physical device is tested by measuring its repeatability. The experimental procedure follows the guidance of NIST recommendations

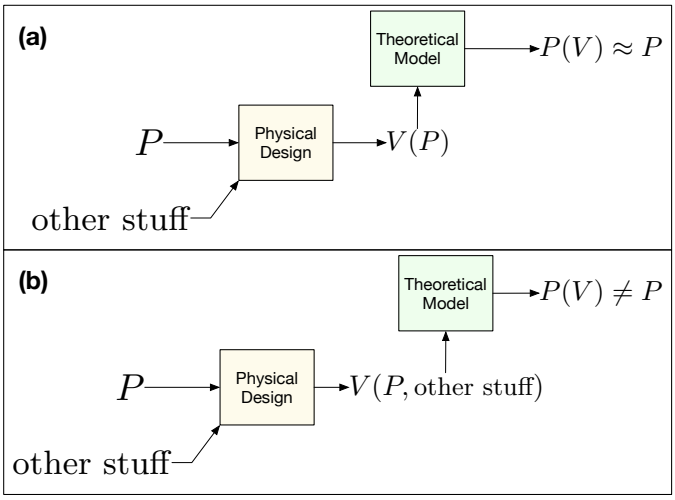

Figure 1.1: (a) The physical design responds with exclusivity to the actual pressure; the value produced by the theoretical model is close to the actual pressure. (b) The physical design responds to the actual pressure but also responds to the other stuff; the value produced by the theoretical model using the dirty signal is unable to match the actual pressure.

for analyzing and establishing repeatability [47]. The following conditions are maintained:

- Experimental tools are consistent and not replaced throughout the study
- Observations are made by the same observer
- The instrument(s) used for measurement are not replaced and they are used under the same conditions for each measurement
- The tests are conducted at the same location
- The repeated measurements are taken over a short duration
- The objectives remain unchanged throughout

The validity of the theoretical model is tested by measuring its ability to produce a predictable result that is within calculable error bounds.

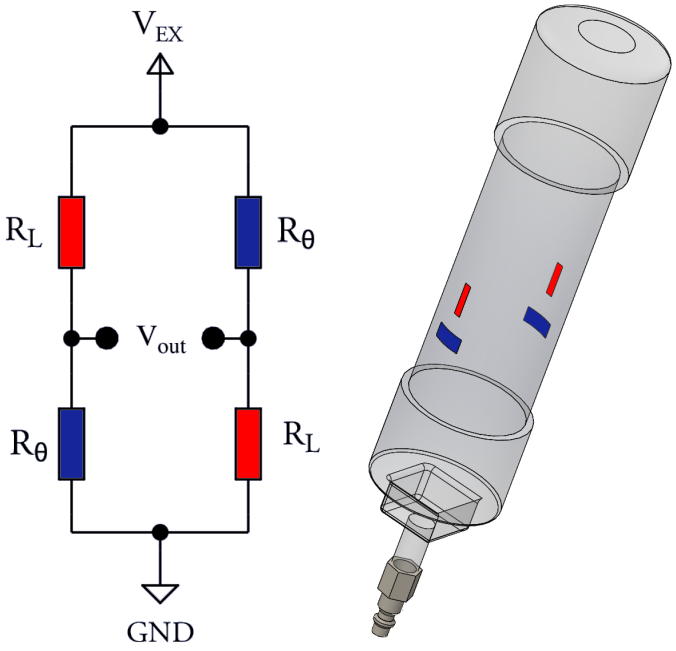

Figure 1.2: 3D Model of the PVPT constructed using PVC.

1.6 Research Questions and Hypotheses

The ability of the model to repeatedly and predictably describe the hidden stimulus based on the transformation of the apparent response has not been established; it is not known to what extent the model is complete or accurate.

The objective of the research in this dissertation is to validate the theoretical model as a thorough representation of the real-world system it describes. The model will ultimately be tested by forming the design basis of a physical prototype and that will test it for its ability to exhibit the intended response to pressure with sufficient exclusivity to be a viable sensing mechanism.

If the model adequately describes the transduction of voltage to pressure, the calculated pressure will track the actual pressure. If the model appropriately combines the variables and parameters, then changes in the actual

pressure will be matched by changes in the calculated pressure. In this case, we would consider the model correct in the combination of the variables forming the calculated equations.

The validity of the proposed PVPT is contingent on its ability to produce a repeatable voltage response to the presence of internal pressure, and the ability of the theoretical model of the PVPT system to quantifiably predict the internal pressure given measurements of the voltage response. Accordingly, two experiments are designed to test the validity of the system: the first experiment tests validity of the physical transduction mechanism by testing its repeatability, and the second experiment tests the validity of the theoretical model by testing its prediction accuracy.

1.6.1 Research Question #1

Does the physical design of the PVPT produce a repeatable voltage response to the presence of internal pressure? What is the consistency in the physical PVPT's responses to successive measurements of the same stimuli?

Null Hypothesis

The null hypothesis is that the physical PVPT devices will respond erratically regardless of the applied pressure with no significant consistency that would enable its use as a reliable transduction mechanism. The physical device will produce a response with no discernible consistent influence by external pressure. A least squares regression of the stimulating pressure and the signal response will have a slope of zero.

Alternative Hypothesis

The researched hypothesis is that the physical PVPT devices respond consistently and predictably to the applied pressure. The physical device will noticeably and consistently respond in relation to the external pressure. A least squares regression of the stimulating pressure and signal response will be non-zero.

1.6.2 Research Question #2

Does the theoretical model reliably predict the internal pressure based on measurements of the observable voltage response? This question will be addressed by applying the transformation to collected measurements and comparing the calculated pressure to the actual pressure measured by the standard. Uncertainty analysis will be performed using the model, which will provide quantifiable limits to error between the calculated and actual pressures based on expected uncertainties in the model parameters.

1.7 Assumptions and Limitations

A number of assumptions are made throughout this project, and there are some limitations that are acknowledged. Both are discussed in the following subsections.

1.7.1 Methodological Assumptions

The conclusions drawn by this work are based on observations made of the prototype sensors' responses to pressure and of the standard pressure sensors,

and the observations are assumed clean and without contamination by latent stimuli.

Thermal effects are reduced in the PVPT circuit with the full-bridge Wheatstone bridge design. With each arm of the bridge consisting of a strain gage attached to the surface of the vessel, the effect of temperature on the output signal is reduced by equivalent temperature effects across the bridge. The persistent thermal effects were identified at early stages of the construction of the test equipment, and the applied remediation was tested and established in Section 4.1.2 to justify the subsequent assumption made throughout the research and analyses that thermal effects are negligible.

1.7.2 Assumptions of Theoretical Framework

The derivation of the theoretical model is, in part, rooted from Lamé's equations, which carries with it fundamental assumptions about the nature of the cylindrical body being deformed by the application of a distributed load [23]:

- Cylinder wall material is homogeneous and isotropic
- Planar sections perpendicular to the longitudinal axis of the cylinder wall remain planar under deformation

These stipulations are integrated into the physical prototypes that are the focus of experimentation that *must* be observed in their design and construction. The first assumption is addressed by the decision to use polycarbonate, PVC, brass, and copper wall materials, which can all be assumed homogeneous and isotropic [35, 54, 46]. The second assumption is addressed in the geometry of the cylinder walls. The walls having rotational symmetry

about the longitudinal axis avoids stress concentrations that would likewise bias strain about the body so long as the material is also isotropic (which is enforced with the first assumption).

Hysteresis, if it exists, will be observable in the collected data. During the first experiment, voltage is logged while pressure is increased from 0 psi in increments of 20 psi to a maximum of 80 psi, followed by decrementing by 20 psi until the pressure returns to 0 psi. The repeated pressure measurements in increasing and decreasing fashion will expose any hysteresis. However, although the possibility of the presence of hysteresis is accepted, hysteresis is not in the theoretical model, and if the effect is significantly high then it can invalidate any readings until the signal settles.

1.7.3 Assumptions of Measures

Physical measurements of electrical properties and geometry are treated as uncertain and the uncertainty is formally addressed. Material properties, the modulus of elasticity and Poisson's ratio are acquired through published tables and the uncertainty is based on conservative estimates, but is assessed with the physical and electrical property uncertainty analysis (see Sec 3.2).

The voltage signal read and converted by the ADS1118 analog to digital converter is assumed to be without error. The chip is configured by software to the highest sample rate at the particular reference voltage that is listed in the data sheet [6] to still have 16 effective number of bits.

The temperature measurement from the resistant temperature detector (RTD) signal amplified by the MAX31865 is assumed to be without error. An overall temperature accuracy of 0.5^o C is listed in [4].

1.7.4 Design Flaw Limitations

There are numerous elements of the prototype that contribute to error. In Chapter 3 these elements are consolidated into a series of δ terms which contain the maximum error for the particular term. The δ_{unk} term represents the error contributed by all unknown δ terms. This term can have an infinite number of contributing sources, and its value is unknowable. However, the magnitude of this term is expected to be so small that it will be concealed in the difference between the sum of the actual values of the quantifiable error terms and the maximum acceptable error boundary. Furthermore, although this term is not necessarily constant, its fluctuation is expected to be too small to effect experimental outcomes.

1.8 Expected Outcomes

This study will reveal the adequacy of the system to form the design basis of future pressure sensing devices.

The repeatability of the response to repeated applications of equal stimuli is shown, thereby establishing the validity of the electromechanical device to serve as a sensing mechanism.

The transformed response measurements produce pressure values with predictability and accuracy, remaining within the error boundaries derived from the same model when compared with the actual pressure. This demonstration implies the model is comprised of a sufficiently complete set of physical parameters and measurements (the model is complete), and that those de-

scriptors relate to interact in a manner consistent with physical reality (the model is correct).

1.9 Dissertation Outline

This dissertation comprises six chapters. Chapter 2 reviews literature from which the methodological approach is derived. The review also explores PVPT presence in industry with a patent search and assessment of the inventions that are closest matches. Chapter 3 presents the theoretical model and steps through its derivation and uncertainty analysis. The prototype PVPT design is discussed and the PVPT test bench is introduced. Chapter 4 introduces the research design and formally addresses the parameters of the investigation, the results of which are presented in Chapter 5. Chapter 6 discusses the research results and explores the possibilities in light of the new evidence acquired during this project.

Chapter 2

Literature Review

The following literature review is organized into six sections.

The *Theoretical Orientation for Study* (Section 2.1) reviews work supporting the establishment of the theoretical framework in developing the PVPT model. Primarily, that surrounding the analysis of industrial pressure vessel mechanics; specifically, this section provides some details of the landscape of the pressure vessel design as a segue into its relevancy to this work.

Review of Research on Topic (Section 2.2) focuses on the extant body of research most similar to the design and model proposed in the PVPT.

Critique of Previous Research (Section 2.3) probes the embodiments presented in the *Review of Research on Topic* for flaws in application of established theory and differences from the PVPT design and model being proposed with the PVPT.

Review of Methodological Literature (Section 2.4) reviews literature on the testing and analysis of sensors and the theoretical models describing their behavior.

Synthesis of Research Findings (Section 2.5) pulls together the theoretical framework, extant topical literature, and methodological literature to form the coherent basis of this work.

2.1 Theoretical Orientation for Study

The approach to sensing pressure developed in this dissertation was preceded with the hypothesis that the deformation in a cylindrical body bounding a pressurized volume could be reliably modeled and predicted. This notion is supported in abundance by established research in pressure vessel design.

By the most general definition, a pressure vessel is a device that maintains a volume at a significantly higher or lower pressure than its surroundings. Pressure vessels are commonplace in the modern world. Compressed gas tanks, aerosol cans, pressure cookers, and even submarines and airplane cabins can be considered pressure vessels as they are all designed to maintain a pressure significantly different from the pressure of the surrounding environment. The contained media is often corrosive, flammable, combustible or at extreme high or low temperature in addition to being highly pressurized. If the vessel is poorly designed, poorly fabricated, or the material is of poor choice or quality, the vessel can quickly go from beneficial tool of industry to extremely hazardous liability that puts the lives of any nearby workers at risk; they are inherently dangerous, and when they fail due to mistakes in design or construction the cost in injury and damage has been enormous. It was because of the repeated fulfillment of worst-case scenarios that prompted the formation of a Boiler Code Committee in 1911, and in 1915 the American Society of Mechanical Engineers (ASME) published the first edition of the

Boiler and Pressure Vessel Code (BPVC), a 114 page book created to address the preventable danger of catastrophic failures due to mistakes in design or mistakes in the construction of pressure vessels by establishing guidelines to standardize the process based on proven methodologies. It has expanded to address nearly every conceivable facet of design, application, and scenario; the 2015 ASME BPVC is divided into 12 sections spanning 17,000 pages contained in 31 books [8, 16].

Due to the exceptional level of danger posed to the public if not strictly held to safe standards, the design of pressure vessels has largely become a guided selection process in contrast to the creative freedom enjoyed by designers of general goods and equipment. The additional guidelines outline parameters critical to the safe operation of the proposed vessel, including operating temperature, safety factor, corrosion allowance, operating pressure, and others. These rules and codes are part of the *ASME BPVC Section VIII* which is intended specifically to guide engineers in pressure vessel design [55].

The *ASME BPVC Section VIII* provides guidelines for acceptable equations, manufacturing processes, materials, attachments (including ASME standardized designs), and others facets having influence in the safe operation of the vessel. Pressure vessel standards establish guidelines for their construction and operation.

The pressure vessel design roadmap that is *ASME Section VIII* is subdivided into sections dedicated to specific situations and needs. For the vast majority of applications, engineers need only choose from *ASME Section VIII, Division 1* or *ASME Section VIII, Division 2* [55].

ASME Section VIII, Division 1 presents a *Design-by-Rule* approach. The engineers utilize the approach to size pressure vessels for common media and constructed of common materials. It is a very streamlined vessel-design-on-rails experience, though often at excess cost, as designs tend to be very conservative in safety factors and other design criterion [9].

ASME Section VIII, Division 2 presents a *Design-by-Analysis* approach which demands a more active role on the part of the engineer in defining and analyzing design criteria in higher detail. The approach permits the design of vessels for specific applications and environments with greater customizability and greater detail in stress and loading analyses [56], [10].

The design process is heavily, if not primarily, focused on the operating temperature and pressure, vessel material, vessel shape, diameter, and wall thickness. A staple of the design process consists of calculating the minimum wall thickness based on material properties and operating pressure demands, calculating maximum operating pressure based on wall thickness and material properties, and repeat as the design is tweaked. The analytical treatment calculates the mechanical behavior of the pressure vessel when subjected to pressurized media. This methodology and these calculations are founded on Lamé's equations, which supports their use as the foundation of a closed-form solution to pressure when all that can be measured is the deformation of vessel walls.

Much of the calculation effort of the engineer is spent on the geometry and material selection of the vessel under expected operating conditions. For example, no vessel is designed without calculating either the minimum wall

thickness or maximum allowable working pressure depending on which is the limiting factor [40].

The cornerstone of pressure vessel design and analysis is the set of equations relating internal and external pressure to stress and strain in the vessel walls. The "sizing" process begins by deciding a conservative design pressure and maximum allowable working pressure. Maximum and minimum design temperatures often naturally follow the pressure limitations. Vessel wall material selection with consideration for corrosion allowance is based on the media and environment, and these design guides directed the vessels constructed for this research.

2.2 Review of Research on the Topic

Literature exploring designs similar to the PVPT is rare. Although instances of academic research are sparse, patent space is home to a handful of concepts spanning from 1943, [39], to as recently as 2008, [28].

The earliest was also one of the more ambitious approaches. In 1943, Ostergren filed for a patent embodying a set of pipe sections with strain gages affixed to their sides (Figure 2.1). On each device is a set of four strain gages, two oriented longitudinally and two oriented circumferentially. The intended use of the devices is to serve as permanent part of the plumbing of a hydraulic line, not unlike a smart pipe section wherein that pipe section can provide a pressure measurement. Each concept has a post-fabrication feature intended to increase the sensitivity of the response to the signal. The strain gages are connected in a quarter Wheatstone bridge configuration, where two arms are fixed resistors, one is trim resistance wire, and the last arm is the

strain gage. The bridge in this application is somewhat unique in that the resistance wire arm and the gage arm both have two resistive elements in series. In his description, Ostergren explains the gage pair connected in series are to protect against bending stress from seeping into the response signal. Using gages on opposite sides of the beam, when the beam bends (assuming it is not bending on the plane that bisects the two gages) one gage increases in resistance while the other decreases, and the effect will cancel when the resistances are added. However, the end-result in this application is actually a neutralization of the signal output as both upper and lower arms of the gage-laden divider would remain equal in resistance when pressurized 2.2.

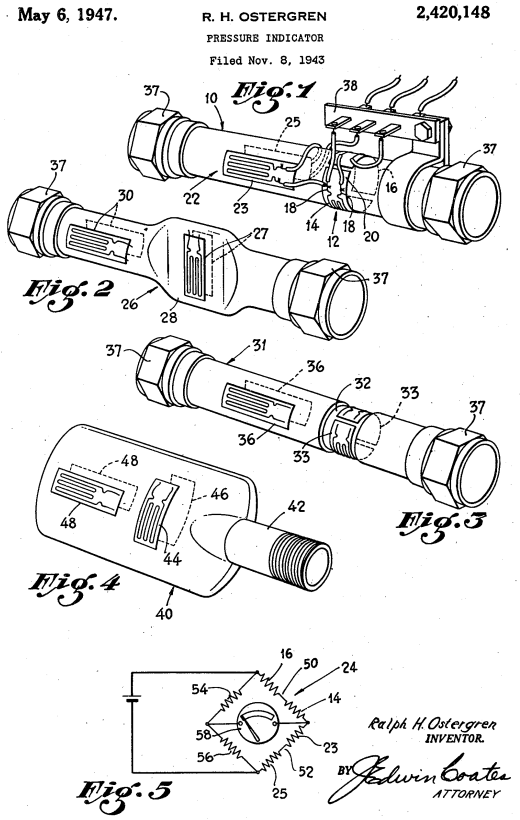

Figure 2.1: US Patent 2,420,148 *Pressure Indicator* [39].

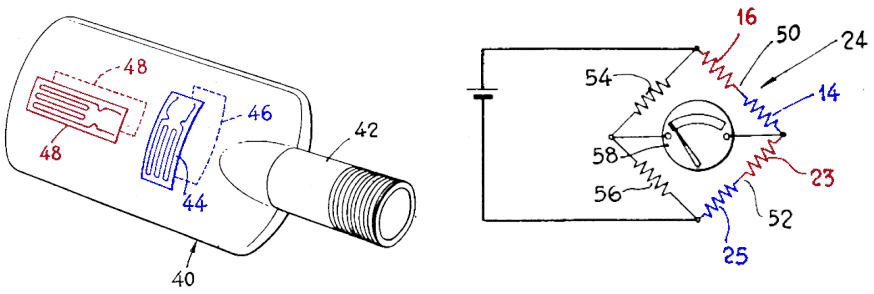

Figure 2.2: US Patent 2,420,148 *Pressure Indicator single-ended manifestation* [39].

Filing in 1946, Guillemin's "Strain Gauge Manometer", [22], was a corrugated tube around which four identical lengths of gage wire is wrapped and then connected in a Wheatstone bridge circuit (Figure 2.3). The device is boasted to be adapted for very rapid pressure changes such as those found in airplanes whose canopy is ruptured by gunfire and in ordinance testing. He attributes this capability to successful reduction of moving parts. The two innermost coils are connected to opposite diagonal arms of the Wheatstone bridge, which effectively doubles its voltage response to deformation. The two outermost coils are not bonded to the cylinder, so they act as fixed resistors in the bridge but they add the benefit of thermal compensation. Assuming the strain gages are all the same temperature, the lengths of gage wire being equal in size likewise have the same thermal drift. And because they all drift equally, the output voltage from the bridge is unaffected.

In 1970, Calhoun filed "Fluid Pressure Measuring Device", [13], described a device which had an empty cavity and measured connected 2 strain gages each in the longitudinal and circumferential directions. The bridge circuit makes sense and appears effective, having circumferential and longitudinal gages on opposite sides of the bridge from their pairs 2.4. But the design

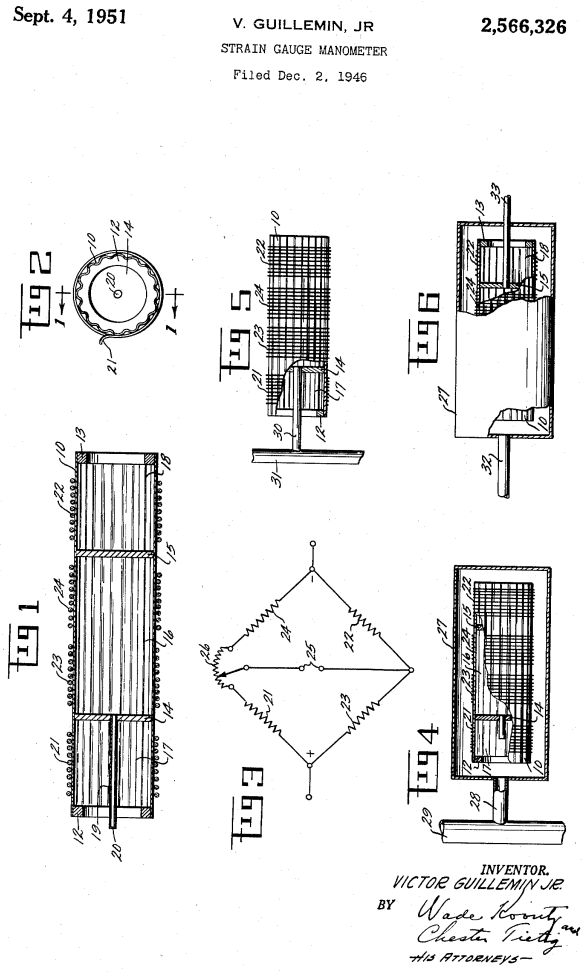

Figure 2.3: US Patent 2,566,326 *Strain Gauge Manometer* [22].

uses an unnecessarily complicated vessel shape and walls which would make it difficult to fabricate with precision, even more difficult to repeatedly fabricate devices at the same dimensions. Those complicated design features including the sharp interior and exterior angles will host stress concentrations which will reduce the reliability of any deformation prediction for a theoretical model.

Jumping ahead almost 40 years, in 1983 Dunemann et al. filed a patent for an "Arrangement for Measuring the Pressure in Cylindrical Cavities" [18]. The device has four gages mounted to the walls, two longitudinally and two

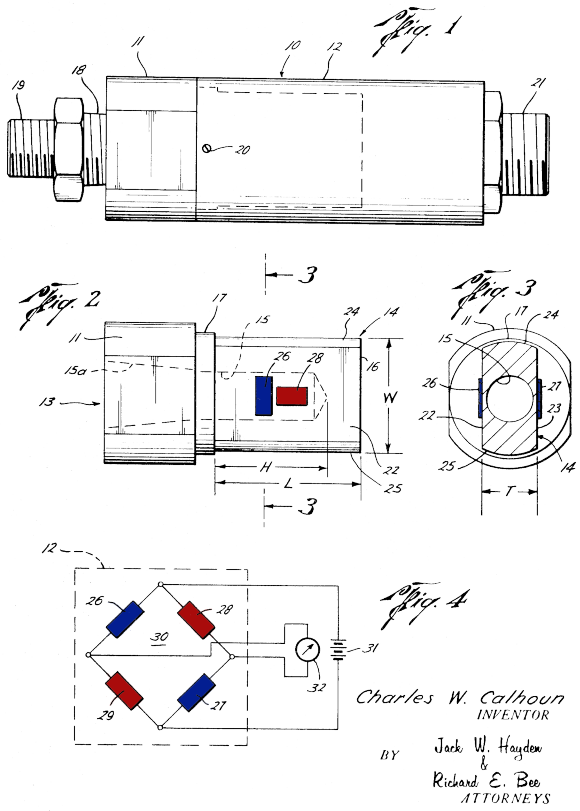

Figure 2.4: US Patent 3,645,136 *Fluid Pressure Measuring Device* [13]

circumferentially (Figure 2.5). The bridge circuit is well designed and should produce a proportional signal output with internal pressure. However, the author makes the assumption that the vessel, under pressure, will elongate along the longitudinal axis while constricting circumferentially with a reduction in diameter and circumference (Figure 2.5 'FIG. 1'). In actuality, the vessel will both elongate longitudinally and dilate circumferentially [42]. The physical design of the sensor was likely successful insofar as it produced a proportional voltage response to the application of pressure, but the usefulness of the design for reproduction and customization would be severely limited without

an accurate theoretical model and dependency on calibrations to adapt it to every application or design variant.

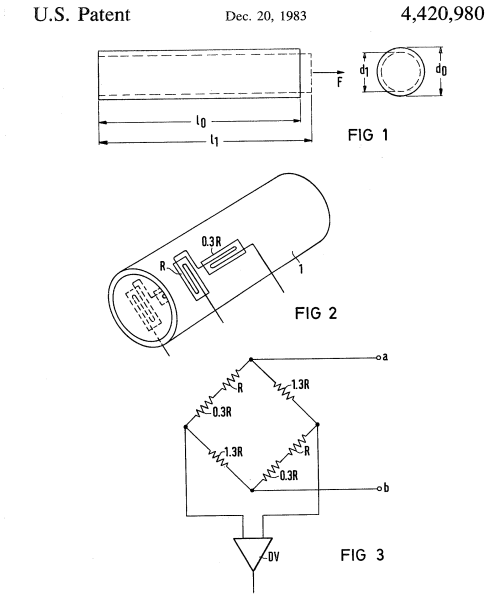

Figure 2.5: US Patent 4,420,980 *Arrangement for Measuring the Pressure in Cylindrical Cavities* [18].

Kempf's patent awarded in 1988, "Apparatus for Performing Pressure, Normal, Force, and Bending Measurements on Pipelines" [25], depicts a cylindrical shell with six strain gages; two circumferentially oriented and four longitudinally (Figure 2.6). The invention is another smart pipe section, this version however incorporates a series of amplifiers instead of a connecting the gages into a bridge circuit, and intends to measure external forces through bending effects as well as pressure effects. This work is unique in that it intends to measure multiple effects, pressure being one of them. The system uses six gages: four longitudinal and two circumferential, all of which measured separately and with independent amplification circuits.

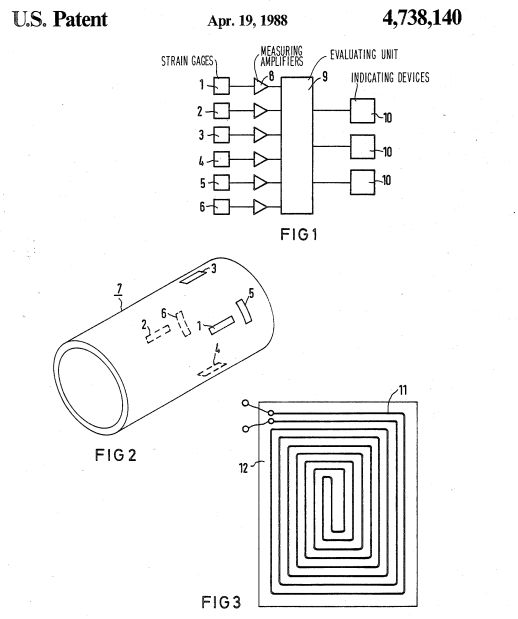

Figure 2.6: US Patent 4,738,140 *Apparatus for Performing Pressure, Normal Force and Bending Measurements on Pipelines* [25].

In 2008, Lohr et al. filed a patent application for a "High Pressure Sensor" [28] which describes a pressure sensor with vessel-like space and intended to elongate and dilate when under pressure 2.7. There is also a correct reference to the hoop-longitudinal strain ratio in terms of Poisson's ratio, which is evidence of proper solid mechanics and crucial for a valid theoretical model. However, the strain ratio is applicable to a cylindrical vessel, which Lohr's sensor is not.

2.3 Critique of Previous Research

Designs in [39, 18, 25, 22] contain two open-ends but measure longitudinal strain as fundamental basis in their measurement technique. Such a design ignores the support added by the plumbing that is attached to the open

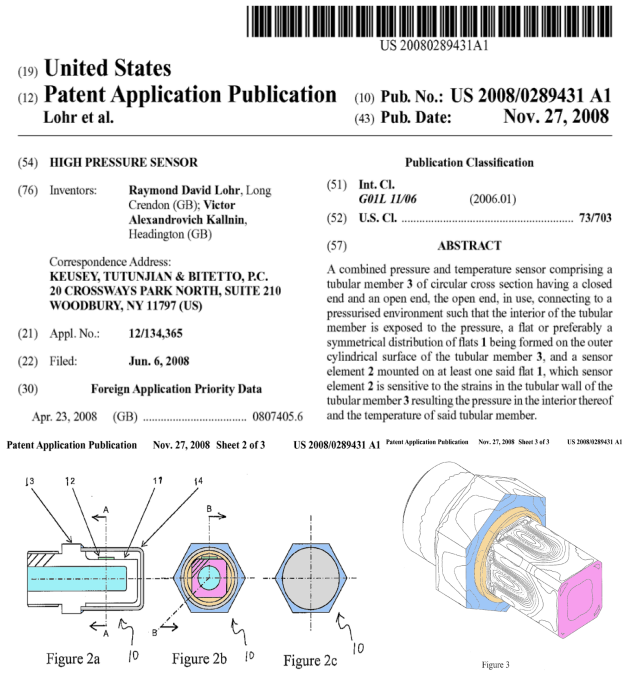

US 20080289431A1

(19) **United States**

(12) **Patent Application Publication**
Lohr et al.

(10) **Pub. No.: US 2008/0289431 A1**
(43) **Pub. Date: Nov. 27, 2008**

(54) **HIGH PRESSURE SENSOR**

(76) Inventors: **Raymond David Lohr**, Long Crendon (GB); **Victor Alexandrovich Kallnin**, Headington (GB)

Correspondence Address:
KEUSEY, TUTUNJIAN & BITETTO, P.C.
20 CROSSWAYS PARK NORTH, SUITE 210
WOODBURY, NY 11797 (US)

(21) Appl. No.: **12/134,365**

(22) Filed: **Jun. 6, 2008**

(30) **Foreign Application Priority Data**

Apr. 23, 2008 (GB) 0807405.6

Publication Classification

(51) **Int. Cl.**
G01L 11/06 (2006.01)

(52) **U.S. Cl.** **73/703**

(57) **ABSTRACT**

A combined pressure and temperature sensor comprising a tubular member **3** of circular cross section having a closed end and an open end, the open end, in use, connecting to a pressurised environment such that the interior of the tubular member is exposed to the pressure, a flat or preferably a symmetrical distribution of flats **1** being formed on the outer cylindrical surface of the tubular member **3**, and a sensor element **2** mounted on at least one said flat **1**, which sensor element **2** is sensitive to the strains in the tubular wall of the tubular member **3** resulting the pressure in the interior thereof and the temperature of said tubular member.

Patent Application Publication Nov. 27, 2008 Sheet 2 of 3 US 2008/0289431 A1

Patent Application Publication Nov. 27, 2008 Sheet 3 of 3 US 2008/0289431 A1

Figure 2a Figure 2b Figure 2c

Figure 3

Figure 2.7: US Patent Application 2008/028932 A1 *High Pressure Sensor* [28].

ends. Consequentially, the longitudinal strain under pressure will vary with each application depending on the particulars of the installation. The PVPT approach maintains a single-ended design so that one end is free to expand longitudinally just as it is free to expand circumferentially due only to the internal pressure.

2.4 Review of Methodological Literature

The validity of the measurement system at the focus of this project is contingent on two critical elements: the ability of the physical device to act as an adequate transduction mechanism, and the ability of the theoretical model to predict the property of interest. Thus, the methodological basis for the design

of the experiments in this project spans two general areas: that of transducer design, and that of system modeling.

2.4.1 Physical Transducer Design

Transducers transform properties of one particular form into another. Generally, the original feature is hidden or obscured from direct observation, but, when stimulated, the transducer translates the original signal into a different signal that is in a accessible form, and insight into a previously hidden aspect of reality is thus provisioned [29]. The transducer derives its worth from the consistency or repeatability of output or response to the input. A transducer that repeatedly produces the same output signal under repeated measurand conditions allows the user to safely infer the nature of the hidden stimulus based solely on the observable response of the sensor.

Repeatability in the physical response of the sensor is the product of functional exclusivity between the response and the stimulus of interest, and the rejection of all others. When a sensor responds to environmental stimuli other than that for which it was designed, it is said to have error. If the measurand has been isolated, then only the measurand signal will be present [34]. Otherwise, the output will have a component of unpredictable uncertainty which translates into error in the measurement. The observable consequence is inconsistency in measurements of a consistent measurand. Although perfect consistency is an unrealistic expectation for a transducer, it is reasonable to expect the range of the unpredictable component of the output signal to be minute compared to that of the measurand.

2.4.2 Theoretical Model Design

With a physical transducer, a complete and correct theoretical model provides the bridge between the hidden measurand of interest and the observable signal with which it responds. It permits the adaptation of a physical sensor to a variety of applications by merely updating parameter values in the model before calculation. Where the physical design fails to control contamination in the response, the preservation of efficacy becomes the responsibility of a complete and correct theoretical model. A model is an abstract mathematical construct that generalizes a part of reality so as to serve a specific purpose [11]. The theoretical model describes the transduction process in the sensor and serves as the basis for the quantification of the hidden stimulus based on observable response. A model that is complete accounts for all the significant effects and phenomena that interact with the sensor and influence its output. A model that is correct properly relates the various phenomena according to known and established physical principles. A felicitous model makes possible the separation of the stimuli of interest from a contaminated response to more than just the stimuli [34, 29].

The complete world can be sorted into one of three categories based on its relationship to the model:

1. The property or effect whose behavior is intended to be described by the model

2. Other effects that significantly influence the output of the model

3. Everything else that is neglected and (presumed) inconsequential by the model

In practice, the other effects are independent variables of the model on which the behavior of the property of interest is dependent. In a physical system, the values of the independent variables are often obtained by measurements with uncertainty due to limitations in instrument accuracy. Every measurement inevitably contains uncertainty, and this uncertainty defines measurement error [48]. Uncertainty in the measurements of independent variables, and the combined effects of everything that is neglected by the model both contribute to the deviation of the modeled world from the actual world, characterizing the overall error of the system.

2.5 Synthesis of Research Findings

It is critical to choose a physical design that responds with sufficient exclusivity to the stimulus of interest so that the response can be predicted by a theoretical model with error limited to incompleteness and noise.

Long established pressure vessel design relies on models combining geometry, pressure, and mechanical properties and stresses. The interactions between these elements is shown to be predictable, reliable, and very applicable to the proposed system where the walls are intended reaction elements instead of containment structures.

Chapter 3

The Theoretical Basis of the PVPT

3.1 Derivation of the Theoretical Model

Lamé's formulae relate pressure in a hollow cylindrical object and the principle stresses in the walls [12], [41]. The equations describe circumferential (also referred to as tangential or hoop), longitudinal, and radial stresses (σ_θ, σ_{L}, and σ_{r}) in thick walled cylinders in terms of internal and external pressures (P_{i} and P_{o}), inner and outer radii (r_{i} and r_{o}), and a distance r from the center (with r limited such that $r_{\mathrm{i}} \leq r \leq r_{\mathrm{o}}$), at which the stresses are evaluated (see Figure 3.1). There does exist a set of stress equations assuming a thin-walled vessel which are less complex, but they are not pursued for the basis of the PVPT theoretical model as they would then limit the validity of the derived model to systems with diameter to thickness ratio greater than 20 (as per the thin-model heuristic [23, 42]), for which the thin-walled assumption is valid. For thick-walled stresses, Lamé's formulae are described in Equations 3.1, 3.2, and 3.3 for hoop, longitudinal, and radial stress, respectively:

$$\sigma_\theta = \frac{r_{\mathrm{i}}^2 P_{\mathrm{i}} - r_{\mathrm{o}}^2 P_{\mathrm{o}}}{r_{\mathrm{o}}^2 - r_{\mathrm{i}}^2} + \frac{r_{\mathrm{i}}^2 r_{\mathrm{o}}^2 (P_{\mathrm{i}} - P_{\mathrm{o}})}{r^2 (r_{\mathrm{o}}^2 - r_{\mathrm{i}}^2)} \tag{3.1}$$

$$\sigma_{\mathrm{L}} = \frac{r_{\mathrm{i}}^2 P_{\mathrm{i}} - r_{\mathrm{o}}^2 P_{\mathrm{o}}}{r_{\mathrm{o}}^2 - r_{\mathrm{i}}^2} \tag{3.2}$$

$$\sigma_{\mathrm{r}} = \frac{P_{\mathrm{i}} r_{\mathrm{i}}^2 (r^2 - r_{\mathrm{o}}^2) - P_{\mathrm{o}} r_{\mathrm{o}}^2 (r^2 - r_{\mathrm{i}}^2)}{r^2 (r_{\mathrm{o}}^2 - r_{\mathrm{i}}^2)} \tag{3.3}$$

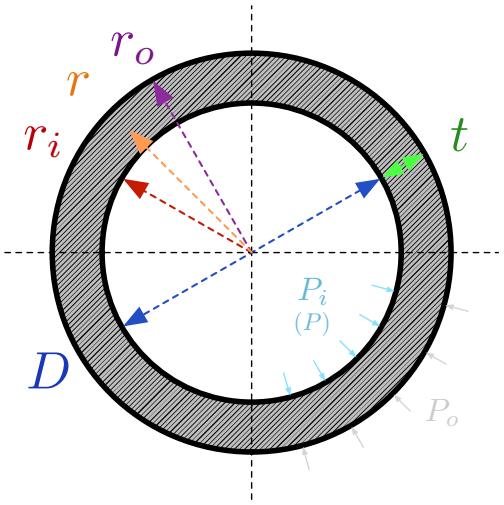

Figure 3.1: Cross-sectional diagram of vessel geometry with respect to nomenclature used in the mathematical model.

For more direct utility in the characterization of PVPT systems, the equations are reformulated here in terms of internal diameter (D) and wall thickness (t) instead of inner and outer radii (see Figure 3.1), and internal pressure simply as P. Stress at the outer surface in the longitudinal (subscript L) in Equation 3.5 and circumferential (subscript θ) in Equation 3.4 directions are then

$$\sigma_\theta = P \frac{D^2}{2t(D+t)} \tag{3.4}$$

$$\sigma_{\mathrm{L}} = P\frac{D^2}{4t(D+t)} \tag{3.5}$$

Further, an Ω term is defined which encapsulates the dimensions in a single term representing the system's geometry

$$\boxed{\Omega = \frac{D^2}{4t(D+t)}} \tag{3.6}$$

The Ω term is used as a geometry term to simplify the stress equations to forms 3.7 and 3.8:

$$\sigma_\theta = 2\Omega P \tag{3.7}$$

$$\sigma_{\mathrm{L}} = \Omega P \tag{3.8}$$

The Ω term of Equation 3.6 can be used as a comparison between designs; generally more sensitive designs will have a higher Ω term (see Section 6.3.1). It can be readily seen in Equations 3.7 and 3.8 that the stresses have a constant relationship:

$$\sigma_\theta = 2\sigma_{\mathrm{L}} \tag{3.9}$$

Strains in the circumferential and longitudinal directions (ε_θ and ε_{L}) extend using the definition for the modulus of elasticity, $E = \frac{\sigma}{\varepsilon}$, and because the two are principle strains acting in the same plane, they effect each other to extents characterized by Poisson's ratio (ν):

$$\varepsilon_\theta = \frac{1}{E}(\sigma_\theta - \nu\sigma_{\mathrm{L}}) \tag{3.10}$$

$$\varepsilon_{\mathrm{L}} = \frac{1}{E}(\sigma_{\mathrm{L}} - \nu\sigma_{\theta}) \tag{3.11}$$

The constant proportionality between the circumferential and longitudinal stresses permit the simplification of Equations 3.10 and 3.11 in combination with 3.7, 3.8 and 3.9 to these final forms

$$\boxed{\varepsilon_{\theta} = \frac{\Omega P}{E}(2 - \nu)} \tag{3.12}$$

$$\boxed{\varepsilon_{\mathrm{L}} = \frac{\Omega P}{E}(1 - 2\nu)} \tag{3.13}$$

which has the notable relationship in 3.14:

$$\frac{\varepsilon_{\theta}}{\varepsilon_{L}} = \frac{2 - \nu}{1 - 2\nu} \tag{3.14}$$

The gauge factor (G_F) of a strain gage relates the relationship between fractional resistance change ($\frac{\Delta R}{R}$) and strain [37] (noting the definition for strain ($\varepsilon = \frac{\Delta L}{L}$)

$$\begin{aligned} G_F &= \frac{\frac{\Delta R}{R_0}}{\frac{\Delta L}{L_0}} \\ &= \frac{\frac{\Delta R}{R_0}}{\varepsilon} \end{aligned} \tag{3.15}$$

$$\frac{\Delta R_n}{R_{n0}} = \varepsilon \cdot G_F \tag{3.16}$$

$$\Delta R_n = R_{n0}(\varepsilon \cdot G_F) \tag{3.17}$$

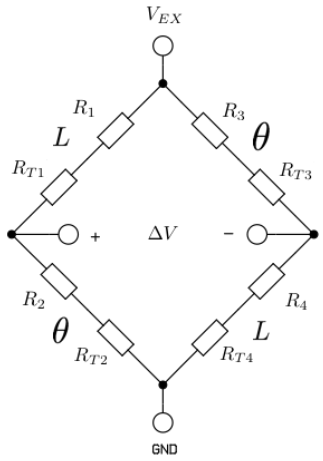

Figure 3.2: Wheatstone bridge circuit. Trim resistors are added to represent both trim resistors and lead wire resistance, both of which are constant.

Where the subscript n specifies position in the Wheatstone bridge (see Figure 3.2), and the subscript 0 refers to the nominal resistance of the strain gage. Rearranging, the final resistance in the presence of strain:

$$\begin{aligned} R_n &= R_{n0}\left(1 + \frac{\Delta R_n}{R_{n0}}\right) \\ &= R_{n0}\left(1 + \varepsilon \cdot G_F\right) \end{aligned} \tag{3.18}$$

$$\begin{aligned} R_n &= R_{n0} + \Delta R_n \\ &= R_{n0} + R_{n0}(\varepsilon \cdot G_F) \end{aligned} \tag{3.19}$$

Given ε definitions (Equations 3.12 and 3.13)

$$R_\theta(P) = R_{n0}\left(1 + G_F \frac{\Omega P}{E}(2 - \nu)\right) \tag{3.20}$$

$$R_L(P) = R_{n0}\left(1 + G_F\frac{\Omega P}{E}(1-2\nu)\right) \tag{3.21}$$

λ terms are introduced to simplify the expressions in the next steps as the model is configured for pressure.

$$\boxed{\lambda_\theta = G_F\frac{\Omega}{E}(2-\nu)} \tag{3.22}$$

$$\boxed{\lambda_{\text{L}} = G_F\frac{\Omega}{E}(1-2\nu)} \tag{3.23}$$

Combining Equations 3.20, 3.21 and 3.22, 3.23, strain gage resistances become

$$R_\theta(P) = R_{n0}\left(1 + P\lambda_\theta\right) \tag{3.24}$$

$$R_L(P) = R_{n0}\left(1 + P\lambda_{\text{L}}\right) \tag{3.25}$$

Strain gages in a Wheatstone bridge wired in a full bridge configuration such as in Figure 3.2 are less susceptible to thermal effects assuming they share the same temperature [17], and the PVPT systems have been designed using this strategy to alleviate major thermal deviations from the predicted solution. Strain gages applied to the outside surface of the vessel are either oriented in parallel with or perpendicular to its axis depending on if it is intended to measure the longitudinal or circumferential strain. The Wheatstone bridge for the proposed devices is designed with the longitudinal and hoop strain gages in a particular arrangement (Figure 3.2) so that the resulting voltage output is proportional to the internal pressure.

The voltage output, by the Wheatstone bridge, $V(P)$ or ΔV, with excitation voltage, V_{Ex}, is related to its resistor configuration, including trim resistors (subscript T) such that:

$$\Delta V = V_{\text{Ex}} \left(\frac{R_2 + R_{2T}}{R_1 + R_{1T} + R_2 + R_{2T}} - \frac{R_4 + R_{4T}}{R_3 + R_{3T} + R_4 + R_{4T}} \right) \tag{3.26}$$

And combining the λ terms, the voltage as a function of pressure may be described (using $Q(P)$ and $W(P)$ for brevity and referring to the voltage at the two ends of the differential voltage output, ΔV):

$$Q(P) = \frac{R_{20}\left(1 + \lambda_\theta P\right) + R_{2T}}{R_{10}\left(1 + \lambda_L P\right) + R_{1T} + R_{20}\left(1 + \lambda_\theta P\right) + R_{2T}} \tag{3.27}$$

$$W(P) = \frac{R_{40}\left(1 + \lambda_L P\right) + R_{4T}}{R_{30}\left(1 + \lambda_\theta P\right) + R_{3T} + R_{40}\left(1 + \lambda_L P\right) + R_{4T}} \tag{3.28}$$

$$V(P) = V_{\text{Ex}}\left(Q(P) - W(P)\right) \tag{3.29}$$

Assuming the system is accurately described by Equation 3.29, the model suggests pressure can be determined by observation of only the voltage output. However, isolating pressure from the bridge equation replete with trim resistor terms is not a trivial exercise.

Considering the bridge equation in a different form is key to the separation of pressure from the Wheatstone equation (Equation 3.27 for isolation and a closed-form solution. Consider the following form:

$$V(P) = \frac{c_1 P + c_2}{c_3 P + c_4} - \frac{c_5 P + c_6}{c_7 P + c_8} \tag{3.30}$$

with coefficients

$$\begin{aligned} c_1 &= R_{20}\lambda_\theta V_{EX} & c_5 &= R_{40}\lambda_L V_{EX} \\ c_2 &= R_{20}V_{EX} + R_{2T}V_{EX} & c_6 &= R_{40}V_{EX} + R_{4T}V_{EX} \\ c_3 &= R_{10}\lambda_L + R_{20}\lambda_\theta & c_7 &= R_{30}\lambda_\theta + R_{40}\lambda_L \\ c_4 &= R_{10} + R_{20} + R_{1T} + R_{2T} & c_8 &= R_{30} + R_{40} + R_{3T} + R_{4T} \end{aligned}$$

This form of the bridge voltage function can be easily differentiated with respect to pressure

$$\frac{\partial V}{\partial P} = \frac{c_1 c_4 - c_2 c_3}{(P c_3 + c_4)^2} - \frac{c_5 c_8 - c_6 c_7}{(P c_7 + c_8)^2} \tag{3.31}$$

which has units of volts per psi and can be considered a statement of the sensitivity of the system as the ratio of voltage response to incremental pressure change.

Equation (3.30) can be further reformulated into a secondary form

$$V(P) = \frac{K_1 P^2 + K_2 P + K_3}{K_4 P^2 + K_5 P + K_6} \tag{3.32}$$

with coefficients defined as

$$K_1 = c_7c_1 - c_5c_3 \qquad K_4 = c_7c_3$$

$$K_2 = c_7c_2 + c_1c_8 - c_5c_4 - c_6c_3 \qquad K_5 = c_7c_4 + c_8c_3$$

$$K_3 = c_8c_2 - c_6c_4 \qquad K_6 = c_8c_4$$

The pressure can be isolated using the form in Equation 3.32, and the rearranged function being one of pressure in terms of the bridge output voltage:

$$\boxed{P(V) = \frac{K_2 - K_5V - \sqrt{M_1V^2 + M_2V + M_3}}{2(K_4V - K_1)}} \tag{3.33}$$

with the last set of coefficients

$$M_1 = K_5^2 - 4K_4K_6$$

$$M_2 = 4K_1K_6 - 2K_2K_5 + 4K_3K_4$$

$$M_3 = K_2^2 - 4K_1K_3$$

The pressure function (Equation 3.33) can be differentiated with respect to voltage to form a formula describing the (non-constant) sensitivity in terms of pressure per volt output.

$$\frac{\partial P}{\partial V} = \frac{K_4\sqrt{M_1V^2 + M_2V + M_3}}{2(K_4V - K_1)^2} - \frac{2M_1V + M_2}{4(K_4V - K_1)\sqrt{M_1V^2 + M_2V + M_3}} + \frac{K_1K_5 - K_2K_4}{2(K_4V - K_1)^2} \tag{3.34}$$

The derivatives derived in Equations 3.31 and 3.34 produce values that can be interpreted as representative of the system's sensitivity between the voltage and pressure. Indeed, the calculation of sensitivity based on a voltage in (3.30) is equivalent to the reciprocal of the sensitivity calculated by (3.33) at the pressure that corresponds with that voltage, as described by established theory regarding derivatives of the inverse functions:

$$\frac{\partial V}{\partial P} = \left(\frac{\partial P}{\partial V}\right)^{-1} \tag{3.35}$$

This fact forms the basis for the initial steps validating the extensive process of isolating the pressure term.

3.2 Model Uncertainty

The theoretical model contains terms that reflect physical parameters that, if not known precisely, must be either measured using tools with imperfect precision and resolution or estimated based on literature. The uncertainty in the PVPT model (δ) is described as a combination of random and systematic uncertainty (δ_{R}, δ_{S}), with an additional term (δ_{unk}) that is the catch-all of uncertainties not mentioned or quantified:

$$\delta = \delta_{\mathrm{R}} + \delta_{\mathrm{S}} + \delta_{\mathrm{unk}} \tag{3.36}$$

The following sub-sections discuss these terms in greater detail and their combination.

3.2.1 δ_{R}: Random Uncertainty

Unlike the other uncertainty terms, the random uncertainty due to measurement noise cannot be quantified *a priori*, and will need to be calculated *a posteriori*. The challenge is separating the random noise from the signal. This term will be derived from data collected during the first experiment.

The separation of the random uncertainty is based on the separation of the high frequency noise from the actual signal which changes at a significantly lower rate. A linear regression model formed from the entirety of the data set which is used to calculate a prediction value for sensor pressure given voltage reading, $\widehat{P}_{M,i}$:

$$\hat{P}_{M,i} = \hat{\beta}_1 V_{M,i} + \hat{\beta}_0 \tag{3.37}$$

[1] $\hat{P}_{M,i}$ is subsequently subtracted from the actual pressure to calculate an error term, ϵ_{P}.

$$\epsilon_{\mathrm{P}_i} = P_\Omega - \hat{P}_{M,i} \tag{3.38}$$

The ϵ_{P} value is fed into a low-pass filter to produce $\epsilon_{\mathrm{P}_{L,i}}$:

$$\epsilon_{\mathrm{P}_{L,i}} = \epsilon_{\mathrm{P}_{L,i-1}} + K(\epsilon_{\mathrm{P}_i} - \epsilon_{\mathrm{P}_{L,i-1}}) \tag{3.39}$$

which is then subtracted from the original ϵ_{P_i}, which effectively acts as a high-pass filter, to produce $\epsilon_{\mathrm{P}_{H,i}}$:

$$\epsilon_{\mathrm{P}_{H,i}} = \epsilon_{\mathrm{P}_i} - \epsilon_{\mathrm{P}_{L,i-1}} \tag{3.40}$$

[1] (see Section 4.4 for thorough explanations of the $\hat{\beta}$ terms).

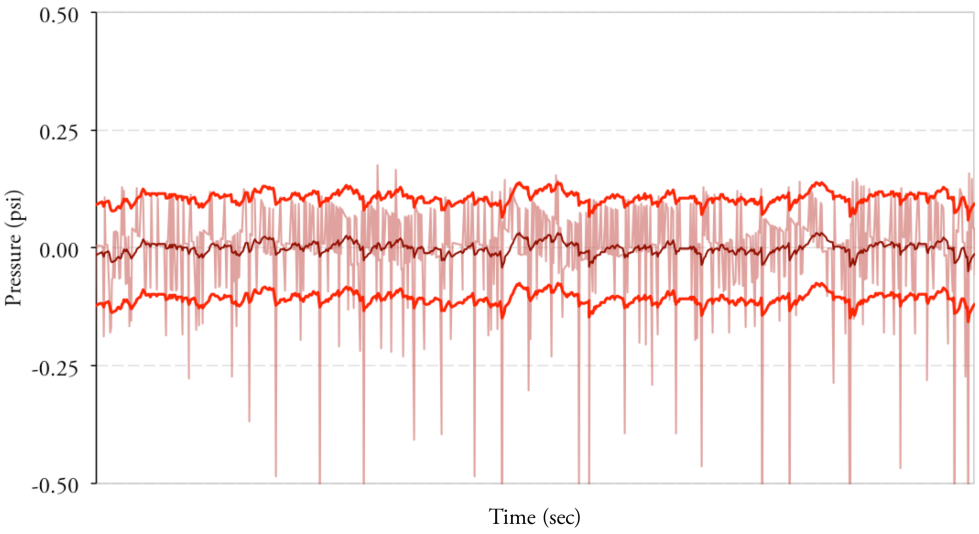

Figure 3.3: A segment of collected data with overlain filtered signal in dark and two red bounding lines marking two standard deviations above and below, illustrating the random measurement noise component of uncertainty, δ_{R}.

The unbiased standard deviation of the high-frequency noise data is calculated, followed by the standard deviation of the mean of the high frequency noise data. The final random uncertainty term (δ_{R}) is the sum of the standard deviation of the mean ($\sigma_{\epsilon_{\mathrm{P}_H}}$) with t-statistic to 95% confidence ($t_{\nu,95\%}$) added with two unbiased standard deviations of the high pass data which ($\alpha_{\epsilon_{\mathrm{P}_H}}$), by the Empirical Rule rule represents about 95% of the data assuming the data is normally distributed [32].

$$\delta_{\mathrm{R}} = \pm(2\sigma_{\epsilon_{\mathrm{P}_H}} + t_{\nu,95\%}\alpha_{\epsilon_{\mathrm{P}_H}}) \tag{3.41}$$

3.2.2 δ_{s}: Instrument and Estimation Uncertainty

The theoretical model consists of unavoidable and unremovable instrument error present when determining the nominal resistances, trim resistances, in-

ner diameter, wall thickness, and excitation voltage, and estimation error in the modulus of elasticity, and Poisson's ratio. If the model was linear, a linear expansion approximation method considering the sum of the squared products of partial derivatives with uncertainty intervals of the uncertain variables is the traditional approach (see Equation 3.42). The model is a multivariate nonlinear model and as such there is no straight-forward method to model overall uncertainty propagation [30]. When the model is relatively simple, multivariable Taylor Series expansions have been employed [26], but when the model is complicated, as is the PVPT model, Monte Carlo simulations are the most reliable approach. However, it has been established that the linear approximation method is reasonably valid on sufficiently small intervals of the uncertainty terms. If the intervals are small enough then this method would be ideal as the model of the approximation of uncertainty propagation for these terms could be extended beyond this work. Any PVPT system constructed will have practical limitations of the properties present as parameters in the theoretical model, quantifiable as measurement and estimation uncertainty terms, and the application of this approximation as an equation (albeit lengthy and complicated) lends itself as a direct calculation method to estimate an expectation range as accuracy in the physical device. Otherwise, a Monte Carlo simulation could serve the same purpose, but would necessitate the calculation be performed on a computer and that the calculation be performed hundreds of thousands of times post hoc to be effective.

For the investigation of a linear approximation model, a model needs to be derived. The basic model for the linear approximation of propagated un-

certainty in a model $V(x_1, x_2, ..., x_n)$ is

$$\Delta_V = \sqrt{\left(\frac{\partial V}{\partial x_1}\Delta_{x_1}\right)^2 + \left(\frac{\partial V}{\partial x_2}\Delta_{x_2}\right)^2 + ... + \left(\frac{\partial V}{\partial x_n}\Delta_{x_n}\right)^2} \tag{3.42}$$

where the Δ terms are the absolute uncertainties. For the theoretical PVPT model (Equation 3.33), the partial derivative terms with respect to the function of pressure were unwieldily. However, the partial derivatives with respect to voltage based on the Wheatstone bridge model were far simpler and more manageable.

$$\begin{Bmatrix} \frac{\partial V}{\partial R_{1N}} & \frac{\partial V}{\partial R_{2N}} & \frac{\partial V}{\partial R_{3N}} & \frac{\partial V}{\partial R_{4N}} \\ \frac{\partial V}{\partial R_{1T}} & \frac{\partial V}{\partial R_{2T}} & \frac{\partial V}{\partial R_{3T}} & \frac{\partial V}{\partial R_{4T}} \\ \frac{\partial V}{\partial D} & \frac{\partial V}{\partial t} & \frac{\partial V}{\partial E} & \frac{\partial V}{\partial \nu} \\ \frac{\partial V}{\partial G_F} & \frac{\partial V}{\partial V_{EX}} & \frac{\partial V}{\partial P} & \end{Bmatrix} \tag{3.43}$$

To convert these partial derivatives into terms of functions of pressure as initially attempted, the key rests in the partial derivative of voltage with respect to pressure. The partial derivative of voltage with respect to pressure is to a function V(P); the inverse function, that is, P(V) which undoes the function V(P) (f^{-1} in common literature) likewise has partial derivative of pressure with respect to voltage, and their product, by the chain rule, is 1,

thereby confirming the validity of the statement

$$\left(\frac{\partial V}{\partial P}\right)^{-1} = \frac{\partial P}{\partial V} \tag{3.44}$$

Further, with the previously stated voltage partial derivative list, the terms can individually be converted from partial derivatives of voltage to the desired partial derivatives of pressure by the partial derivative of pressure with respect to voltage and the chain rule:

$$\frac{\partial P}{\partial V}\begin{Bmatrix} \frac{\partial V}{\partial R_{1N}} & \frac{\partial V}{\partial R_{2N}} & \frac{\partial V}{\partial R_{3N}} & \frac{\partial V}{\partial R_{4N}} \\ \frac{\partial V}{\partial R_{1T}} & \frac{\partial V}{\partial R_{2T}} & \frac{\partial V}{\partial R_{3T}} & \frac{\partial V}{\partial R_{4T}} \\ \frac{\partial V}{\partial D} & \frac{\partial V}{\partial t} & \frac{\partial V}{\partial E} & \frac{\partial V}{\partial \nu} \\ & \frac{\partial V}{\partial G_F} & \frac{\partial V}{\partial V_{EX}} & \end{Bmatrix} = \begin{Bmatrix} \frac{\partial P}{\partial R_{1N}} & \frac{\partial P}{\partial R_{2N}} & \frac{\partial P}{\partial R_{3N}} & \frac{\partial P}{\partial R_{4N}} \\ \frac{\partial P}{\partial R_{1T}} & \frac{\partial P}{\partial R_{2T}} & \frac{\partial P}{\partial R_{3T}} & \frac{\partial P}{\partial R_{4T}} \\ \frac{\partial P}{\partial D} & \frac{\partial P}{\partial t} & \frac{\partial P}{\partial E} & \frac{\partial P}{\partial \nu} \\ & \frac{\partial P}{\partial G_F} & \frac{\partial P}{\partial V_{EX}} & \end{Bmatrix} \tag{3.45}$$

The terms produced by this approach of partial derivatives with respect to voltage and applying the chain rule with the term whose basis is desired are still longer than one would likely want to perform by hand, but they are significantly shorter than the software approach of the calculated partial derivatives of pressure.

The individual absolute uncertainty terms in the measurements and estimations can be listed concisely as Equation 3.46:

$$\left\{ \Delta_R \quad \Delta_L \quad \Delta_V \quad \Delta_{G_F} \quad \Delta_E \quad \Delta_\nu \right\} \tag{3.46}$$

assuming the resistances, voltages and lengths are measured using the same respective instruments. An estimation of the ultimate uncertainty based on Equation 3.42 is valid provided all uncertainties or errors are random and independent [48]. But in any case, it is never greater than the ordinary sum of the individual, unsquared terms; the absolute systemic uncertainty due to measurement and estimation bias used in calculations of uncertainty in Section 5 and which forms Figures 3.5 and 3.6 is expressed in Equation 3.47:

$$\begin{aligned}(\delta_{\mathrm{S}}) = (\Delta_P) \leq \sum_{i=0}^{n} \left[\left(\left| \frac{\partial P}{\partial R_{Ni}} \right| \Delta_R \right) + \left(\left| \frac{\partial P}{\partial R_{Ti}} \right| \Delta_R \right) \right] + \left(\left| \frac{\partial P}{\partial D} \right| \Delta_L \right) \\ + \left(\left| \frac{\partial P}{\partial t} \right| \Delta_L \right) + \left(\left| \frac{\partial P}{\partial E} \right| \Delta_E \right) + \left(\left| \frac{\partial P}{\partial \nu} \right| \Delta_\nu \right) + \left(\left| \frac{\partial P}{\partial G_F} \right| \Delta_{G_F} \right)\end{aligned} \tag{3.47}$$

The question remains, however: are the uncertainty intervals small enough that a linear approximation is a valid model of uncertainty propagation? A Monte Carlo simulation was programmed to test the validity of the linear approximation model. Using the bridge model of voltage as a function of pressure, in increments of 1 psi on the domain from 0 to 250 psi, at each increment 10,000 trials are conducted in which random values for the uncertainty terms in the range of plus or minus the actual measurement and estimation uncertainties are generated. Of the 10,000 trials, the maximum

and minimum calculated voltages are fed into the PVPT model of pressure as a function of voltage, and the higher of the difference between pressure as a function of voltage and the incremental pressure is kept as the maximum uncertainty at the particular pressure value. For the linear approximation method to be considered valid, it will generally agree with the results of the Monte Carlo simulation, ideally being conservative in overestimating but not underestimating the uncertainty. The maximum uncertainty values determined by Monte Carlo simulation are plotted on a chart of uncertainty vs pressure along with the approximated uncertainty generated by the linear approximation (Figure 3.4).

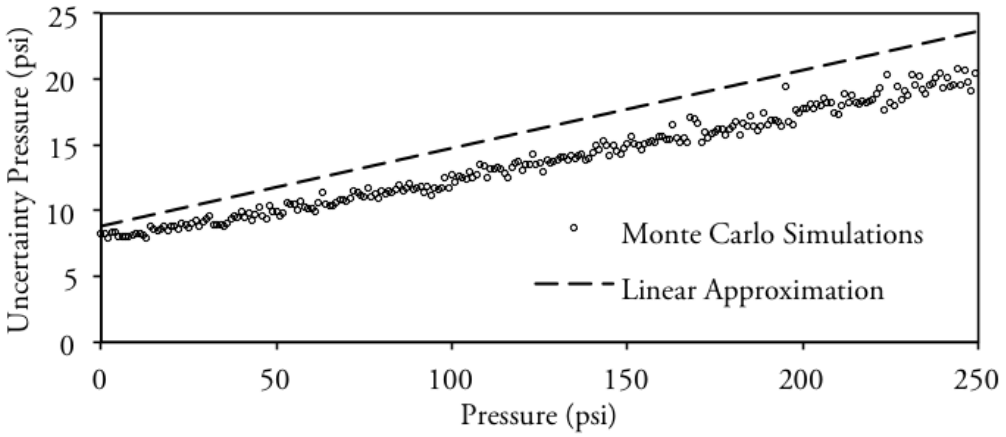

Figure 3.4: The uncertainty predicted by Monte Carlo simulation of 10,000 trials per psi pressure is less than that predicted by linear approximation, indicating that the systemic measurement and estimation biases are on intervals small enough that the linear approximation model is a valid approach to directly calculating the expected uncertainty interval for the theoretical PVPT model.

According to the Monte Carlo simulation comparison, the Linear Approximation model appears a reasonable approximation of uncertainty.

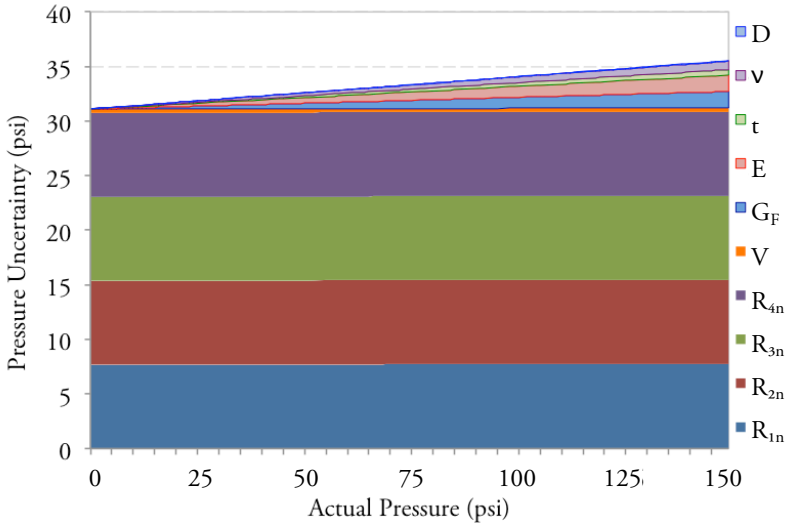

Figure 3.5: Stacked area chart of uncertainty distribution and maximum permissible error with actual pressure. Contributions by nominal gage resistances appear constant and can be removed due to the linear uncertainties intercepting at zero psi.

3.2.3 Differentiation of Constant δ_s and Linearly Dependent δ_s

The derived uncertainty terms, when carried out for hypothetical pressures spanning to 150 psi, provide three important insights. The first is that the vast majority of uncertainty is due to uncertainty in the nominal resistances in the strain gages (Figure 3.5). The second is that the uncertainty due to uncertainty in the nominal resistances is generally constant and uninfluenced by the actual pressure. The third is that the other uncertainty terms are approximately zero in the absence of actual applied pressure. These three points suggest that the largest contributor of error, the error due to the inaccuracy of the nominal gage resistance measurements, can be directly measured when the gage is unpressurized. When the internal (gauge) pressure is zero, the

output from the PVPT can be stored as an error offset term and subtracted from all future readings to remove that error.

Figure 3.6 shows the uncertainty remaining after the large constant sources are removed. Figures 3.6 and 3.5 reflect the nature of the maximum uncertainty behavior when pressure is applied to the PVC PVPT prototype, calculated using the approach described in Section 3.2 for pressure values ranging from 1 psi to 150 psi in 1 psi increments, and using dimensions listed in Table 3.2 and instrument errors listed in Table 4.1.

$$\delta_{\mathrm{S}} = \Phi P_{\mathrm{Act}} + \Psi \tag{3.48}$$

The Φ term is comprised of

$$\Phi = \left(\phi_{\mathrm{D}} + \phi_{\mathrm{t}} + \phi_{\nu} + \phi_{\mathrm{E}} + \phi_{\mathrm{GF}} + \phi_{\mathrm{V}} + \phi_{\mathrm{Vex}}\right) P_{\mathrm{Act}} \tag{3.49}$$

and are presented in isolation in Figure 3.7. The Ψ term is comprised of systematic uncertainty due to the nominal and trim resistor resistances:

$$\Psi = \left(\psi_{R_{1\mathrm{n}}} + \psi_{R_{2\mathrm{n}}} + \psi_{R_{3\mathrm{n}}} + \psi_{R_{4\mathrm{n}}}\right) + \left(\psi_{R_{1\mathrm{t}}} + \psi_{R_{2\mathrm{t}}} + \psi_{R_{3\mathrm{t}}} + \psi_{R_{4\mathrm{t}}}\right) \tag{3.50}$$

These terms also describe the constant (pressure-independent) uncertainties that have a measurable effect at no pressure (see Figure 3.5 at 0 psi) and can thus be logged and removed as a calibration mechanism.

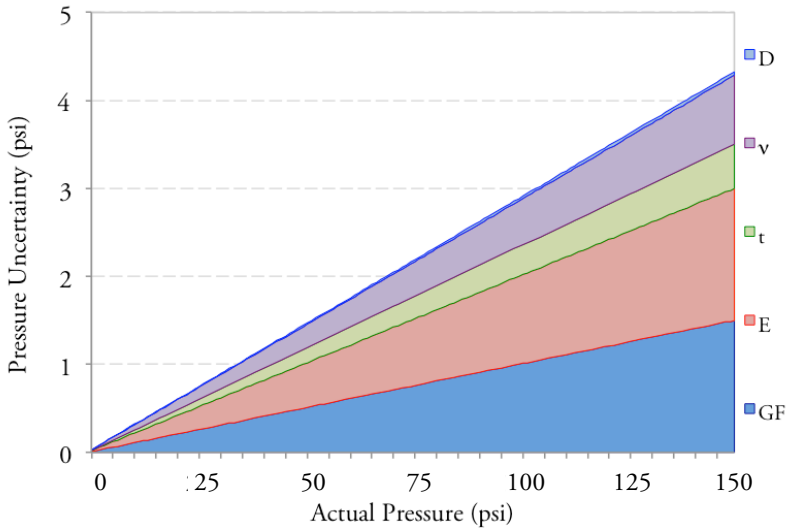

Figure 3.6: Uncertainty variation with actual pressure, excluding those from nominal or trim resistances.

3.2.4 δ_G: Amplification Uncertainty

The partial derivative of voltage with respect to pressure, $\frac{\partial V}{\partial P}$, provides an indication of the sensitivity of the PVPT prototype based on its construction. In particular, based on the nominal resistances in the gages, the trim resistances necessary for balancing, the geometry (diameter and wall thickness), and mechanical properties of the material (modulus of elasticity and Poisson's ratio), the change in voltage per unit pressure can be inferred at a given pressure by the partial derivative of $\frac{\partial V}{\partial P}$. The dependency of the sensitivity on pressure has negligible effect, as shown in Table 4.3 in which the calculated values over the anticipated range of testing are tabulated. The question of adequacy in the analog to digital converter (ADC) to adequately differentiate between levels of pressure in terms of the integer-valued conversion can be answered with the identification of a threshold count as minimum per unit of pressure. In the analysis of the PVPT prototypes, a count of 5 (out of

2^{15}) 'least significant bits' (LSB) per psi for a discretized resolution of ± 0.2 psi per LSB was as a value of general utility to serve as a minimal resolution, $\left(\frac{\Delta_{\text{LSB}}}{\Delta P}\right)_{\text{min}}$. The resolution of the conversion of analog signal to digital value is defined as $\frac{V_{\text{ref}}}{2^{n-1}}$ for differential measurements made on an ADC with n-bits of resolution. The ADS1118s used in this experiment are 16-bit ADCs using an internal reference voltage of 0.256V, resulting in a resolution of 7.8125 $\frac{\mu V}{\text{LSB}}$. Multiplying the sensitivity with a voltage-basis by the resolution converts the resolution to the integer-resolution basis with which the criteria for adequate sensitivity by discretized pressure resolution can be made.

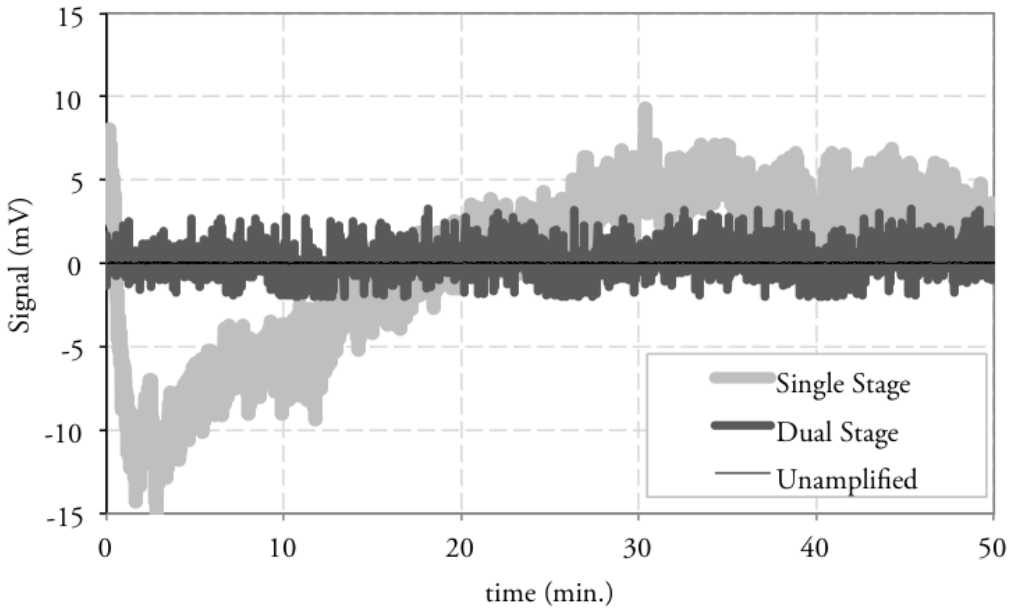

Figure 3.7: Comparison of amplification techniques: unamplified (black), single-stage amplification (dark grey) and two-stage amplification (light grey). The high gain in the single stage amplifier (5000 V/V) is so sensitive that the amplification factor drifts with temperature and static electricity. Each amplifier in the dual-stage configuration has an amplification factor of about 71 V/V.

$$\frac{\Delta_V}{\Delta_P} \times \frac{\Delta_b}{\Delta_V} \geq 5 \frac{\text{LSB}}{\text{PSI}} \tag{3.51}$$

If amplification is deemed necessary, a pair of INA125 instrumentation amplifiers are implemented in a dual-stage topology between the PVPT prototype and the analog to digital converter. While a single amplifier is sufficient to perform amplification up to 10,000 V/V, the amplification factor is governed by the resistance of a resistor bridging pins on the INA125, and the relationship between gain resistance and amplification factor results in large uncertainty at increasing gain factors due to dependence on decreasing resistances but constant resistance uncertainty.

Increasing gain factors require decreasing resistance values, and the uncertainty of the resistance is 0.1Ω, limited by multimeter specifications. Even if equipment were procured that could measure to a higher resolution, various effects (most prominently thermal) will cause the resistance to wander to a maximum of around 1.0Ω. The resulting uncertainty is huge in a single-stage configuration for high gain, but significantly lower in a multi-stage configuration where the output of the first stage is amplified by the second stage. The gain necessary of each stage can be limited to the square root of the overall desired gain (and cube-root if three stages were employed). By reducing the amplification factor needed, a higher gain resistor can be used whose uncertainty will have a much less significant effect after propagating as uncertainty in the gain factor.

From the INA125 datasheet, [1], the equation to determine gain as a function of the gain resistance, R, is

$$G = a + \frac{b}{R} \tag{3.52}$$

where a and b are constant values of 4 and 60000, respectively. Rearranging and solving for resistance based on desired gain, the equation becomes

$$R = \frac{b}{G - a} \tag{3.53}$$

It can then be further deduced that the gain from multiple stages, assuming the output of one stage leads directly to the input of the next, has the form

$$G_{\text{final}} = \prod_{i=1}^{n} G_i \tag{3.54}$$

where G_{final} is the final gain factor for n stages of various individual amplification factors. Further, the linear approximation of uncertainty in the gain value is the traditional form

$$\Delta_G = \sqrt{\sum_{j=1}^{n} \left(\frac{\partial G}{\partial R_j} \Delta_{R_j} \right)^2} \tag{3.55}$$

in units of $\frac{V}{V}$ for n stages with absolute uncertainties Δ_{R_j}, e.g. the smallest measurable resistance increment (0.1 Ω for most multimeters). For a series of stages, the final gain with the absolute uncertainty in the gain can be found

to be

$$G_{\text{final}} \pm \Delta_G = \prod_{i=1}^{n} G_i \pm \sqrt{\sum_{j=1}^{n} \left(\frac{b}{R_j(aR_j + b)} \Delta_R \prod_{i=1}^{n} \left[\frac{(aR_i + b)}{R_i} \right] \right)^2} \tag{3.56}$$

for n stages, each with unique gain resistances. Based on the partial derivative for the single-stage case, it is clear that the uncertainty in the gain is inversely proportional to the resistance used to set the gain. As such, minimization of the gain uncertainty in an n-stage amplification process is realized when the resistances are equal, leading to each individual amplification stage to have a gain factor of the n^{th} root of the overall gain. That is,

$$G_{\text{stage}} = G_{\text{final}}^{\frac{1}{n}} \tag{3.57}$$

then the uncertainty expression reduces to

$$\Delta_G = \frac{n^{\frac{3}{2}}}{b} (a - G^{\frac{1}{n}})^2 G^{1-\frac{1}{n}} \tag{3.58}$$

Uncertainties based on various high-gain amplification schemes are calculated and presented in Table 3.1 to illustrate the relationship between uncertainty and the number of stages.

Table 3.1: Uncertainty in amplification factor at target gains ranging from 1,300 to 10,000 V/V using multiple stages from single to quadruple-stage amplification.

Δ_G	**10,000 V/V**	**5,000 V/V**	**2,500 V/V**	**1,300 V/V**
Single-Stage	832.667	208.000	51.917	13.997
2-Stage	21.722	7.417	2.494	0.873
3-Stage	6.186	2.173	0.731	0.247
4-Stage	2.400	0.771	0.222	0.058

3.2.5 Combining Uncertainty Terms

Although it can be tempting to be overly cautious when estimating uncertainties by estimating high, the effort into estimating the uncertainties to begin with was to have a reasonably accurate estimation of the uncertainty. Needless inflation offsets and scales the estimated uncertainty value thereby degrading the accuracy of the very term desired for precise insight. The gateway to this mistake rests with the universally applicable uncertainty combination statement which will always be greater than or equal to the actual error, $\delta_{\sum}$ of uncertainties δ_{xi} and the model sensitivities $\frac{\partial q}{\partial x_i}$:

$$\delta_{\sum} \leq \sum_{i=1}^{N} \left| \frac{\partial q}{\partial x_i} \right| \delta_{xi} \tag{3.59}$$

For uncertainties of normally distributed (random), independent variables, the actual uncertainty of repeated observations is going to form a normal distribution centered on the mean [48], for which the sum in quadrature has been shown to produce closer estimates:

$$\delta_{\sum} = \sqrt{\sum_{i=1}^{N} \left(\frac{\partial q}{\partial x_i} \delta_{xi} \right)^2} \tag{3.60}$$

Although summing the terms in quadrature has been shown to produce closer estimates than the simple sum, the error cannot be assumed to be random and, although there are analytical tests to determine if the data is in such a state, it will be assumed that the majority of the error (with the exception of random measurement error) is biased and systematic.

Additionally, the intention of the uncertainty analysis will not be to produce an accurate estimate of error in the system, but to produce a maximum error possible in the system. If a measurement crosses the upper or lower error thresholds then it would be strong evidence suggesting a flawed model.

In this research project there are multiple uncertainty terms. The random uncertainties meet the criteria for summing in quadrature, but the systematic uncertainties are only able to be summed. For M systematic uncertainty terms (δ_{Sx}) and N random uncertainty terms (δ_{Rx}), the total uncertainty, which will also define the upper bounds to acceptable measurement error during Experiment 2, is thus:

$$\delta_{\text{Tot}} \leq \sum_{i=1}^{M} \left(\left| \frac{\partial q}{\partial x_i} \right| \delta_{Sxi} \right) + \sqrt{\sum_{j=1}^{N} \left(\frac{\partial q}{\partial x_j} \delta_{Rxj} \right)^2} \tag{3.61}$$

3.2.6 δ_{Ω}: Uncertainty in the Standard

An Omega PX180B-100GV single-ended pressure sensor is connected to one of the peripheral ports for the establishment of a baseline measurement to which the pressure indicated by the PVPT prototypes can be compared. The PX180B-100GV accuracy is rated to ± 0.3 psi [5]. The measured pressure can be considered as the true or actual pressure plus error term:

$$P_{\text{M},\Omega} = P_{\text{Act}} + \delta_{\Omega} \tag{3.62}$$

Although this term is not inherent to the PVPT prototype, it will expand the error region surrounding the difference between the prototype-reported pressure and the pressure measured by the standard [27]. For the purposes of

validity testing, the standard uncertainty term will be treated as defined by the data sheet [5]:

$$\delta_{\Omega} = 0.3\text{psi} \tag{3.63}$$

3.3 Sensor Prototypes

Four prototypes were constructed for this project and experimentation. A PVC prototype (Figure 3.8a), a brass prototype (Figure 3.8b), a polycarbonate (PC) prototype (Figure 3.8c), and a copper prototype (Figure 3.8d).

The prototypes have a standard set of design variables which are chosen, measured, or estimated. Their values are known to within the capabilities of the measurement instruments and within reasonable limits in estimations. The discrepancy between the true value and the idealized value is the basis for systematic error.

The nature of the theoretical model provides choices of variables to use to describe geometry. Inner, outer radii, diameters and wall thickness are all on the table. Inner diameter and wall thickness were chosen strategically for potential future commercialization. Commonly available pipe and plumbing is guided by American Society for Testing and Materials (ASTM) standards; plumbing sizes are in references to the pipe inner diameter, and as such the inner diameter is held to standardized limitations on deviation. The choice simply permits one to fill this variable of the model by inference based on pipe size with the magnitude of the error bounded by ASTM standard [15].

(a) PVC (b) Brass (c) Polycarbonate (PC) (d) Copper (Cu)

Figure 3.8: PVPT prototypes used in experiments.

3.3.1 Design Variables

Table 3.2 lists the absolute uncertainty values describing the limitations of the equipment used in this project and in the calculation of uncertainty boundaries in Section 5.

Table 3.2: PVPT prototype design variable uncertainties (Δ)

	Property	Uncertainty	Source
D	inner diameter	$\pm$0.001 inch	Neiko 01407A Digital Calipers
t	wall thickness	$\pm$0.001 inch	Neiko 01407A Digital Calipers
E	modulus of elasticity	$\pm$10%	[15, 19, 46]
ν	Poisson's ratio	$\pm$10%	[15, 19, 46]
R_{n0}	gage resistance	$\pm$0.1Ω	Radioshack Digital Multimeter
R_{nT}	trim resistance	$\pm$0.1Ω	Radioshack Digital Multimeter
G_F	Gage Factor	$\pm$2%	Omega Datasheet [2, 3]

3.4 Pressure Sensor Test Apparatus

The Pressure Sensor Test Apparatus was constructed to test the PVPT design and theoretical models to determine its validity as a sensor framework. This subsection presents the key variables that are controlled by the platform (Section 3.4.1), the design of the physical apparatus (Section 3.4.2), the electrical system (Section 3.4.3), and the computational platform running logging software and performing the transformation algorithms described by the theoretical model (Section 3.4.4).

3.4.1 Variables

The variables that are controlled by the test apparatus are listed:

V_{EX} Bridge excitation voltage

V_{m} Measured voltage

P_{m} Measured pressure

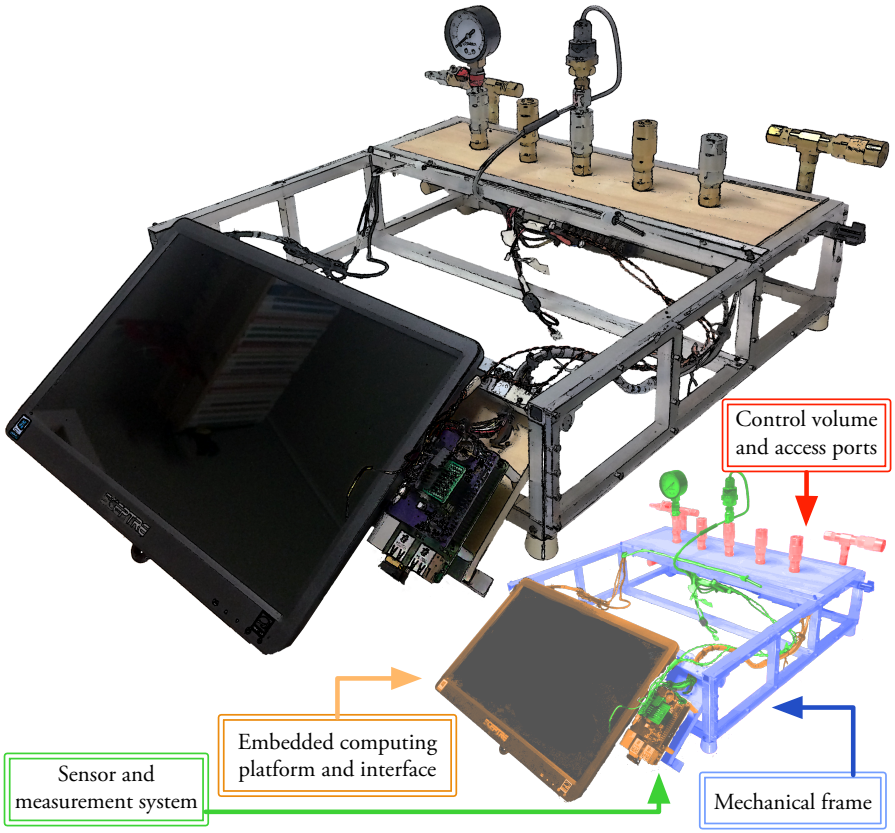

Figure 3.9: PVPT test bench designed for the development and investigation of experimental PVPT prototypes and governing theoretical models.

3.4.2 Mechanical Apparatus

The apparatus has plumbing built in to create a control volume in which air can be pumped to produce a pressurized space that is accessible by standards and devices under test. There are five female quick-connect ports for device connection, and a male quick-connect port with valve for the connection of a compressed air line.

A visual-style (Kobalt^{TM}) pressure gauge with a full scale range of 160 psi is used for visual feedback while pressurizing the control volume.

The structure serves as the cornerstone of the apparatus, providing a sturdy platform to which the electronics, computing, and plumbing systems are mounted so as to minimize alterations to the system's physical state between measurement sessions.

3.4.3 Electrical System

Electronics on the apparatus involve an onboard computing platform which handles the interface with analog to digital converters and other sensors, post-processing of measurements for application of the theoretical model, a display for instantaneous feedback of measured signals, and electronic storage of the measurements, along with a timestamp, to a long-term log archive.

There are two ADS1118 four-channel single/two-channel differential 16-bit ADCs that are contacted over a serial peripheral interface (SPI) bus. The Wheatstone bridge from a PVPT prototype has a pair of analog signals output to be read as a single differential reading. More sensitive prototypes with a characteristic $\frac{\Delta V}{\Delta P}$ that is high enough to be represented by multiple bits of resolution with the analog to digital converter, such as PVC or polycarbonate, can feed their signal directly into the ADC. PVPTs that are not as sensitive are amplified first using INA125 instrumentation amplifiers.

3.4.4 Computing Platform

The computing platform consists of a Raspberry Pi version 2 (Figure 3.12) and contains an operating system based on Linux called Raspbian. The operating

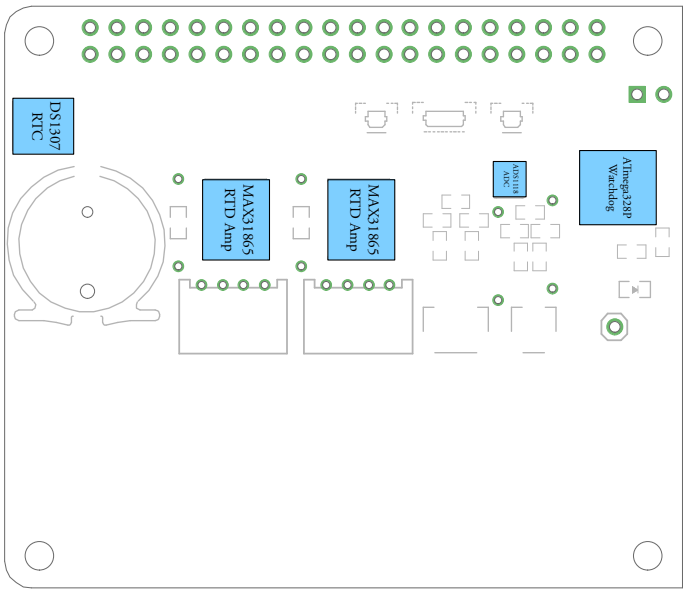

Figure 3.10: A sensor interface shield was designed for the Raspberry Pi to simplify the sensor connection and data retrieval process.

system facilitates the execution of the data collection and logging software, `PVPT-Analysis`. The objective of `PVPT-Analysis` is to retrieve 'readings' by interfacing with peripherals performing analog to digital conversion of sensor signals, and then store the readings to memory.

The Raspberry Pi (Figure 3.12) is running Raspian version "Jesse". Atop the Raspberry Pi is a specially designed shield (Figure 3.11) that has: analog-to-digital converters (ADCs); RTD amplifiers; real-time clock (RTC); and connectors for miscellaneous digital input and output, for convenience.

The software handling the measurement sequence initializes by enabling the analog to digital converters and other peripherals followed by a cycling PVPT measurement for 100 readings. The variance is calculated and com-

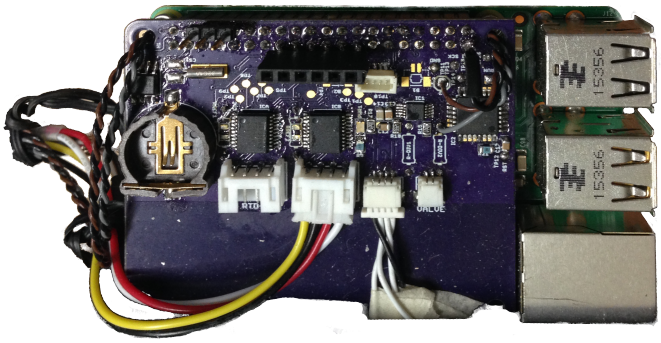

Figure 3.11: The sensor interface board mounted atop the Raspberry Pi.

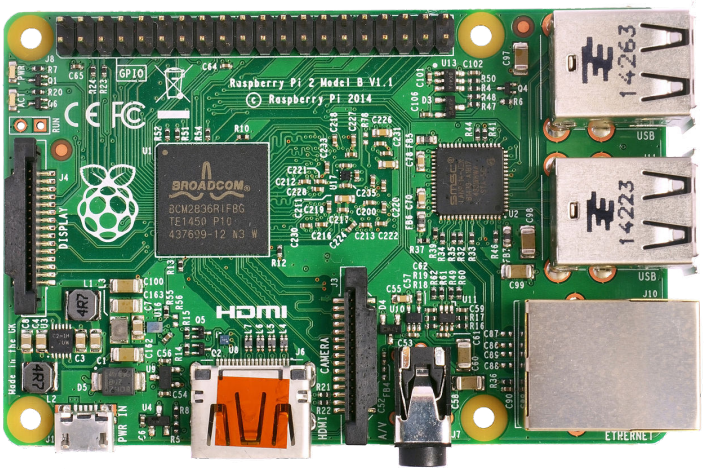

Figure 3.12: A Raspberry Pi hosts the sensor interface and data display and logging software.

pared to a value previously identified to represent the sensor in a steady state of pressure. If steady, the mean is calculated and printed for convenience as an offset to remove the systematic error due to the uncertainty in nominal gage resistances (see Section 3.2.2). The program then moves to the main function.

Upon entry to the main program loop, and repeating with every iteration, the current time and date is read and stored to random access memory. The

date and time are monitored. Each entry includes the date and time, and a single measurement of excitation voltage, ambient temperature, standard pressure, and PVPT voltage measurement, and a calculated pressure measurement from the application of the transformation model using the voltage. Three to five voltage measurements are taken and the median is returned as the official measurement to reduce the likelihood of returning an erroneous reading due to ADC communication errors. The readings are not filtered otherwise, so the raw measurement in its original form .

Chapter 4

Methodology

The previous chapter detailed the theoretical basis for the proposed sensor design and incorporation into physical prototypes. This chapter outlines the experiments that will test the validity of the theoretical model and physical sensor design, beginning with an orientation of the research design.

4.1 Research Design

This research project will test prototype pressure transducers constructed based on the theoretical model outlined in Chapter 3. Validity of the system is contingent on the establishment of validity in its core constituents: the ability of the physical design of the sensors to isolate and respond with exclusivity to pressure, and the completeness of the mathematical model such that it fully incorporates the physical phenomena involved and properly transforms the voltage signal to pressure. There are many opportunities for unintended stimulii to creep in to the system that would be translated into an obfuscating response (see Figure 4.1). The experiment and prototypes are designed to

minimize all but the intended pressure effects from contaminating the output signal.

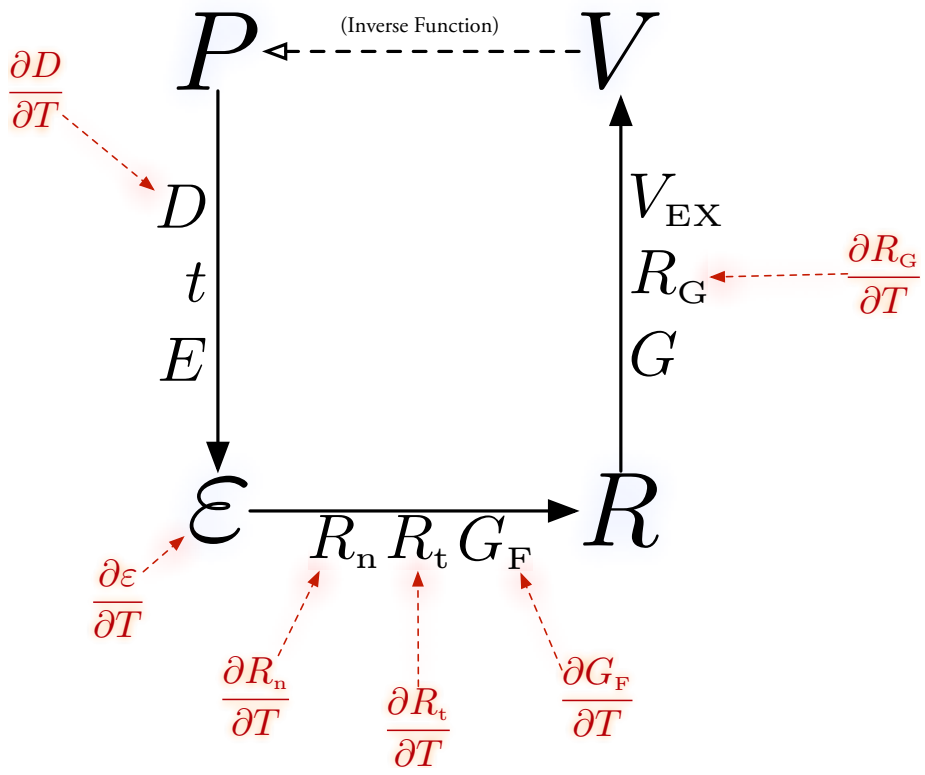

Figure 4.1: High level transduction model including undesirable thermal effects.

Prototype Construction

The model suggests that the only relevant physical properties in the design of the vessel is the diameter, thickness, and the wall material modulus of elasticity and Poisson's ratio. The prototypes are simply constructed using cut sections of piping with end-caps to enclose the vessel. One end is drilled and tapped for 1/4 inch NPT pipe, and a quick-connect coupling is installed. Prior to sealing the ends, the pipe section inner diameter and thickness are measured

with calipers to ±0.001" accuracy. Values for the modulus of elasticity and Poisson's ratio are referenced from literature. Table 4.1 and Table 4.2 contains a summary of the design properties for each prototype.

Table 4.1: PVPT prototype geometry and material properties.

Material	D (in)	t (in)	E (Mpsi)	ν	Source(s)
PC	0.506	0.067	0.25	0.370	[15, 46]
PVC	2.041	0.168	0.45	0.350	[15, 46]
Cu	0.565	0.035	18.8	0.343	[19, 46, 7]
Brass	0.532	0.020	16.0	0.350	[19, 46]

The measurement stage is controlled by a computer program that manages the sample rate and measurement order to reduce unnecessary noise and interference. The control software commits the read measurements to a log archive with timestamp. Data is finally analyzed for validity using error analysis and uncertainty propagation techniques for nonlinear multivariate models, and tested based on statistical analysis of the residuals.

Table 4.2: PVPT prototype nominal gage resistances and trim resistances (both in ohms), gage factors for mounted strain gages, and excitation voltage (in volts).

	R_{10}	R_{20}	R_{30}	R_{40}	R_{1T}	R_{2T}	R_{3T}	R_{4T}	G_F	V_{EX}
PC	349.2	349.9	349.9	349.5	0.0	0.0	0.0	0.0	2.05	5.26
PVC	349.3	349.5	349.5	349.3	0.0	0.0	0.0	0.0	2.14	2.49
Brass	349.7	349.9	348.8	349.6	0.0	0.0	0.8	0.0	2.05	2.49
Cu	349.25	349.55	349.45	349.0	0.0	0.0	0.0	1.2	2.09	2.49

4.1.1 Expected Signal Ranges

The expected signal ranges vary for each prototype based on its geometry and material properties. The mathematical model is a non-linear function of

pressure, and its derivative with respect to pressure is likewise non-linear and the sensitivity varies with respect to the applied pressure (see Table 4.3 and 4.4). The measurability of the sensor is dependent on the signal being large enough to be detectable within the limits of the ADC. In the test setup, the limit of measurability is based on the resolution of the ADC and the reference voltage.

Table 4.3: Voltage response sensitivity to pressure comparison at pressure extrema for PVPT prototypes of different constructions.

Material	$\frac{\Delta V}{\Delta P}\left(\frac{\mu V}{\text{psi}}\right)_{\text{P=1 psi}}$	$\frac{\Delta V}{\Delta P}\left(\frac{\mu V}{\text{psi}}\right)_{\text{P=150 psi}}$
PC	36.273	36.167
PVC	23.177	23.084
Brass	1.378	1.378
Cu	0.575	0.575

Table 4.4: Comparison of unamplified voltage and responses at 150 psi for PVPT prototypes of different constructions and respective integer conversion using a 16-bit differential analog to digital converter with 0.256V reference voltage like that used in this work, and the resulting measurable pressure resolution.

Material	Output Voltage (μV)	LSB	$\frac{\text{psi}}{\text{LSB}}$ Average
PC	5433.1	695	0.216
PVC	3469.5	444	0.338
Brass	206.7	26	5.769
Cu	86.2	11	13.636

4.1.2 Temperature Effects

Thermal effects of various forms are expected to be present with the PVPT prototypes, and their mitigation guides many design aspects of the experimental procedure.

The material constructing the PVPT prototypes will expand and contract based on temperature. Different materials have different rates of thermal expansion, and if the material is known in advance then strain gages can be chosen specifically designed to offset the effects with responsive behavior in the resistance. Alternatively, some gages ship with calibration data in the form of a thermal strain polynomial curve that is a function of temperature which can be used to remove the thermally induced strain. This method of correction can reduce error as low as a half microstrain per degree Fahrenheit [51].

The gages used in the PVPT prototypes are not compensation-matched to the PVPT material, nor are calibration factors being used. Strain gage, lead wire, and ADC properties can also drift with temperature; compensating for the effects of expansion in the material alone is not sufficient. The experiments are designed to keep temperature passively controlled: it is measured and trials are verified to take place in a narrow temperature band and measurements monitored for any ill-effects.

In addition, the PVPT Wheatstone bridge circuit uses a full bridge configuration to reduce temperature effects. With all four gages subjected to the same temperature, the thermally-proportional effects occur on all four arms of the bridge equally thereby maintaining balance. In reality, the gages are not initially equal and so the thermal effects can be expected to vary among the gages leading to imbalance in the bridge [21, 31]. Imperfect as it may be, the effects are nevertheless an improvement compared to a quarter, half, or three-quarter bridge configurations that do not take advantage of the generally balanced thermal effects in the full bridge.

Temperature can further effect the signal when leadwire resistance drifts. This effect can be minimized by using equal length leadwires so that the resistance changes due to temperature variation is equal in all leadwire sets, thereby maintaining general bridge balance [14].

Multiple techniques are designed into the experiment to handle thermal effects but have limitations. The ambient temperature striven to be kept at 72^o F, but drifts by $\pm 3^o$ F. The PVPT utilizes gages configured in a full Wheatstone bridge scheme, with two gages measuring longitudinal strain and two gages measuring circumferential strain (Figure 3.2). The effect of absolute resistance offsets due to thermal variation will be minimized by the bridge design for compensation, but effects on the gauge factor will still be present. Thermal effects on the leadwires is minimized by using leadwires of equal length for each gage.

The ambient temperature is measured using an RTD and logged with the PVPT measurements; in the event that unexplained noise or deviation is observed in the voltage measurements, the temperature measurements can be used to check for correlation that would suggest the noise being thermally induced. Thermal effects were indeed present at early stages of experimentation (Figure 4.2); suspected to be the result of rapid heat transferred unevenly between gages, insulation has been added to the PVPT prototypes leading to the disappearance of the effects (Figure 4.3). Thermal effects are neither incorporated into the theoretical model being tested, nor are they factored into the region of uncertainty bounding acceptable measurements in the investigation of agreement between theoretical model and physical behavior. Thermal effects are handled entirely by avoidance in this study, by insulating

the prototypes and maintaining a fairly consistent lab temperature. Future research should expand to understand how temperature effects the PVPT, but it is outside the scope of this project.

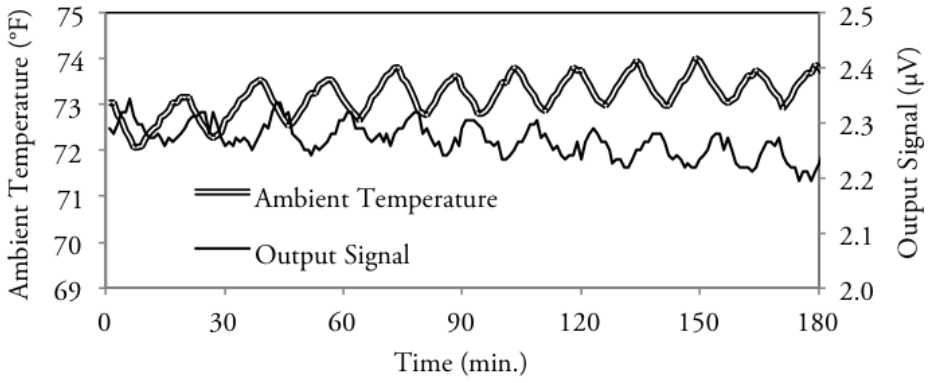

Figure 4.2: Thermal effects were profound at times when the temperature discrepancy between strain gages at opposite sides of the PVPT was more than a couple degrees Fahrenheit, as was typical when operated near a heating vent.

4.1.3 Delayed Response Effects

The response time in the PVPT prototypes is expected to be longer than the diaphragm-based standard. The response time is based on two factors: the volumetric change in the sensing element and the mechanics of the active element material that must deform.

The PVPT prototypes have a much larger volumetric change under pressure than the standard sensor. The increase in volume must be filled with the pressurized medium, and assuming all other characteristics generally equal, it will take less time to supply the volume required by the sensor with the smaller volumetric change. In this case, however, both the PVPT and the standard are subjected to the same larger working volume, and so the sensor

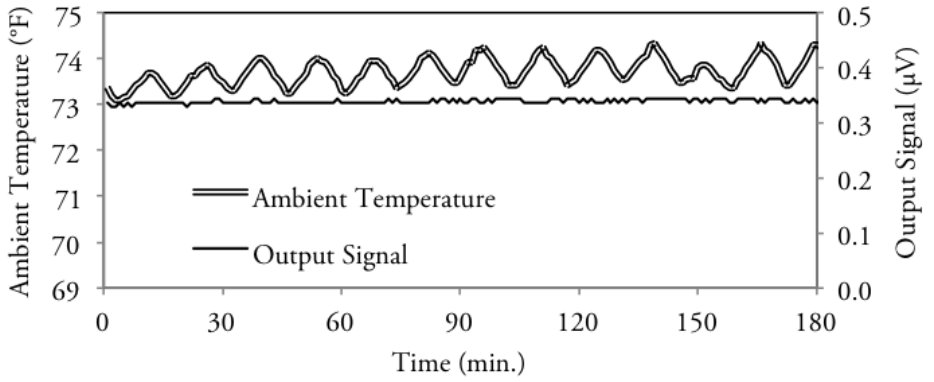

Figure 4.3: The previously observed thermal effects were effectively removed with the addition of a thin layer of insulation. The insulation did not need to maintain a constant temperature, it only needed to promote consistent temperature among the Strain gage in a single PVPT. Note: output voltage signal drop compared to Figure 4.2 due to a reheated solder joint.

with the smaller volume change will simply read the same pressure as the sensor with the larger volume as the larger volume expands. Applications in which the respective sensors are the only sensors to measure the pressure of the media, the PVPT with larger working volume would take longer to reach the steady-state pressure measurement compared to the diaphragm-based sensor with much smaller working volume. The discrepancy would be a function of the volume change, compressibility of the media, and flow rate.

Dynamic analyses and time response characterization for the PVPT system are beyond the scope of this work, but is a vitally important topic of future research assuming this work establishes validity in the fundamental model.

4.2 Experiments

There are two experiments to test the sensor. The first experiment tests the ability of the physical design to respond exclusively to pressure. The second experiment tests the mathematical model to transform the voltage response of the prototypes into pressure.

4.3 Experiment 1 Design

The principle responsibility of a transduction mechanism is to produce a usable output in response to a measurand [20]. The PVPT is intended to be a simple state indicator and its usability is qualified by its consistency of response to the same stimulus (its *repeatability*). The quality of the sensor is a measure of the lack of variability and the extent of indifference to unintended stimulii. To test the physical design, an experiment has been designed to test the repeatability of the output at repeated applications of pressure.

If the resulting variability is so extreme that no correlation can be drawn between pressure and response then the physical model is decisively inconsistent and a poor mechanism for the transduction of pressure to voltage.

4.3.1 Procedure

The prototype sensors are connected to the control volume on the test apparatus and the system is powered on. Once booted, the measurement and logging software is executed.

4.3.2 Hypothesis

Null: The physical device will produce a response with no discernible consistent influence by external pressure. A least squares regression of the stimulating pressure and the signal response will have a slope of zero.

Researched: The physical device will noticeably and consistently respond in relation to the external pressure. A least squares regression of the stimulating pressure and signal response will be non-zero.

4.4 Design Validation

The design validation begins with a least squares regression line fit to the data consisting of pressure and PVPT voltage output:

$$\hat{y} = \hat{\beta}_0 + \hat{\beta}_1 x + \varepsilon \tag{4.1}$$

where $\hat{y}$ is the estimated pressure state, $\hat{\beta}_0$ is the y-intercept term, $\hat{\beta}_1$ is the slope, or the rate of change in the deterministic variable (pressure) with a unit rate of change in the independent variable (PVPT voltage output). The random error component of the regression model, ε, is assumed to have a mean probability of 0, a constant variance of probability distribution for all values of x (the PVPT voltage output), is normally distributed, and errors were neither caused by nor do they have an effect on future errors [32].

Beta terms are defined as

$$\hat{\beta}_0 = \bar{y} - \hat{\beta}_1 \bar{x} = \sum \left(\frac{1}{n} - \frac{\bar{x}(x_i - \bar{x})}{\mathrm{SS}_{xx}} y_i \right) \tag{4.2}$$

$$\hat{\beta}_1 = \frac{\mathrm{SS}_{xy}}{\mathrm{SS}_{xx}} = \frac{\sum(x_i - \bar{x})y_i}{\mathrm{SS}_{xx}} \tag{4.3}$$

where the sum of the squares of the differences between x and $\bar{x}$, SS_{xx}, the sum of the squares of the differences between y and $\bar{y}$, SS_{yy}, the sum of the products of the differences between x and $\bar{x}$ and of the differences between y and $\bar{y}$, SS_{xy}, the sum of the squares of the error, SSE, are defined over a set of measurements as

$$\begin{aligned}
\mathrm{SS}_{xx} &= \sum(x_i - \bar{x})^2 \\
\mathrm{SS}_{xy} &= \sum(x_i - \bar{x})(y_i - \bar{y}) \\
\mathrm{SS}_{yy} &= \sum(y_i - \bar{y})^2 \\
\mathrm{SSE} &= \sum(y - \hat{y})^2 = \mathrm{SS}_{yy} - \hat{\beta}_1 \mathrm{SS}_{xy}
\end{aligned}$$

The Pearson product moment correlation coefficient, R, is a quantitative measure of the strength of the linear relationship between two variables in the sample:

$$R = \frac{\mathrm{SS}_{xy}}{\sqrt{\mathrm{SS}_{xx}\mathrm{SS}_{yy}}} \tag{4.4}$$

Does the linear model adequately relate pressure and voltage? The term $\hat{\beta}_1$ is the slope of the regression line. If the voltage and pressure vary together, then there will be a non-zero slope as pressure is adjusted between 0 and 80 psi. If the two are not coupled, the voltage will not reliably track with pressure and the slope will be zero. Thus forms the basis of the null hypothesis. The T-statistic will be used to test $H_0 : \hat{\beta}_1 = 0$. If they do correlate, the coefficient

of determination, R^2:

$$R^2 = 1 - \frac{\text{SSE}}{\text{SS}_{yy}} \tag{4.5}$$

will suggest the extent of their interactivity with slightly higher prejudice as the coefficient of determination is an indicator of how much of the variance in one variable (voltage) can be explained by variance in the other (pressure) [32].

Rejection Criteria

Rejection of the null hypothesis is on the basis of the β_1 value. The T statistic is of the form

$$T = \frac{\hat{\beta}_1}{s/\sqrt{\text{SS}_{xx}}} \tag{4.6}$$

with rejection region $|T| > t_{\alpha/2}$ where $t_{\alpha/2}$ based on $n-2$ degrees of freedom, is a test of the hypothesis that the slope of the regression line between is zero, indicating no correlation between the two data sets [33, 32]. In this work, $t_{\alpha/2}$ with an α value of 0.05 for 95% confidence is 1.96. The standard deviation, s, or the square root of the variance, s^2:

$$s^2 = \frac{\text{SSE}}{n-2} \tag{4.7}$$

Table 4.5: Experiment variables list.

Variable	Type
$\mathbf{P}$	Independent
$\mathbf{V_M}$	Dependent
Temperature, $\mathbf{V_{EX}}$	Control
D, t, E, ν**,** $\mathbf{R_o}$**,** $\mathbf{R_t}$**,** $\mathbf{G_F}$	Parameter (see Table 3.2)

4.5 Experiment 2 Design

The complete uncertainty model defines the maximum possible deviation for a measurement in a system described by the PVPT theoretical model. The second experiment investigates the deviation of PVPT measurements from the standard pressure. If measurements exceed the uncertainty model threshold and human error can be ruled out, then the model is decisively incomplete and/or incorrect.

4.5.1 Procedure

The procedure for the second experiment up until data analysis is nearly identical to the first experiment. The two differ, however, in the treatment of pressure intervals. The prototype sensors are connected to the control volume on the test apparatus and the system is pressurized. The process is repeated multiple times and with multiple prototypes.

Up to this point, the uncertainty terms in the error model (see Equation 4.11) have all been fully derived with the exception of the random uncertainty component. This remaining term is formed by statistically analyzing the residuals between measurements and standard pressure.

4.5.2 Hypothesis

Null: The applied PVPT transformation *will not* match the direct measurements of a standard to within the function's limits of uncertainty.

Researched: The applied PVPT transformation *will* match the direct measurements of a standard to within the function's limits uncertainty.

4.6 Model Validation

Any measurement of a property, P_{Ω}. in a real system can be represented in terms of the actual property value, P_{A}, plus an error term, $\delta_{\sum}$ which symbolizes the sum of all random, systematic, and unknown error

$$P_{\Omega} = P_{\mathrm{A}} + \delta_{\sum} \tag{4.8}$$

In this experiment, the error term, $\delta_{\sum}$, expanded:

$$P_{\Omega} = \delta_{\mathrm{R}} + \delta_{\mathrm{S}} + \delta_{\mathrm{unk}} \tag{4.9}$$

which is the random, systematic, and unknown uncertainties in the model based on the uncertainty analysis (Section 3.2).

The standard pressure also has an associated uncertainty term (δ_{Ω}) albeit fairly small

$$P_{\Omega} = P_{\mathrm{A}} + \delta_{\mathrm{R}} + \delta_{\mathrm{S}} + \delta_{\mathrm{unk}} + \delta_{\Omega} \tag{4.10}$$

Combining the two pressure expressions forms the acceptance criteria

$$\boxed{\left| P_{\mathrm{M}} - P_{\mathrm{A}} \right| \leq \delta_{\mathrm{R}} + \delta_{\mathrm{S}} + \delta_{\Omega} + \delta_{\mathrm{unk}}} \tag{4.11}$$

Chapter 5

Experiment & Results

The experimental results are presented first in summary (Section 5.1), followed by detail (Section 5.2). Detailed results of the primary tests for repeatability in the physical design and accuracy in the mathematical model are presented in sub-sections 5.2.1 and 5.2.3. Conclusions based on these results follow (Section 5.3).

5.1 Summary of Results

Table 5.1: T statistics ($|T|$) and Coefficients of Determination (R^2) between PVPT output signal and measured pressure in stepped pressure experiments. H_0 rejected if $|T| \geq 1.96$ (Section 4.4).

PVPT	β_1	$\lvert\mathrm{T}\rvert$	R^2
PC	27.99	9955.3	0.9996
PVC	0.19	3101.8	0.9980
Brass	2.22	2962.1	0.9959
Cu	0.35	1683.3	0.9934

Table 5.1 presents a summary of the slopes (β_1) of the least square regression lines, T statistics, and R^2 values.

5.2 Results in Detail

The following section presents the results of experiments 1 and 2 in detail.

5.2.1 Repeatability Results of the Physical Design

Polycarbonate and PVC PVPTs performed exceptionally well with a high degree of repeatability and stability. Copper and brass models were less consistent, but still demonstrated a strong coupling between signal and pressure. Figures 5.1 to 5.4 exhibit trials exemplary of typical behavior across trials, normalized to the scale of pressure for visualization.

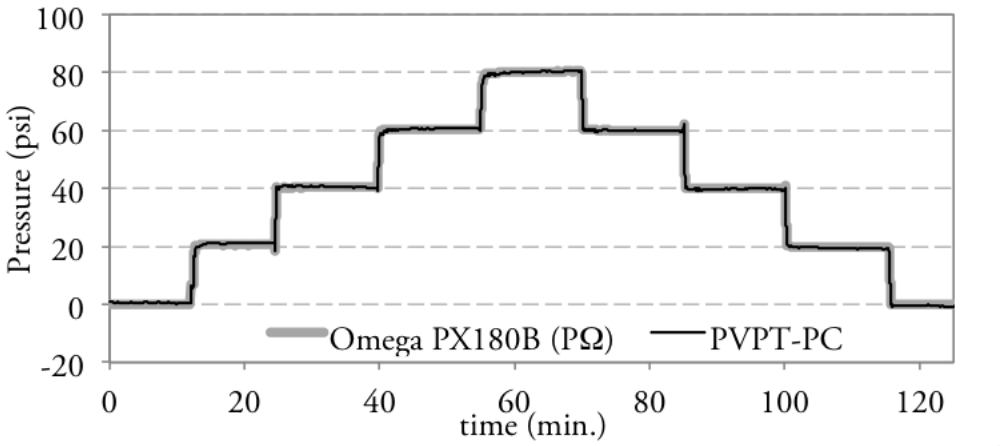

Figure 5.1: Experiment 1 Polycarbonate (PC) PVPT prototype measurements at pressures ($R^2 = 0.9996$).

5.2.2 δ_R Results

The random component of uncertainty due to measurement noise was extracted from the measurements collected in the first experiment. When plotted, the random noise could be clearly seen with the measured signal. Because

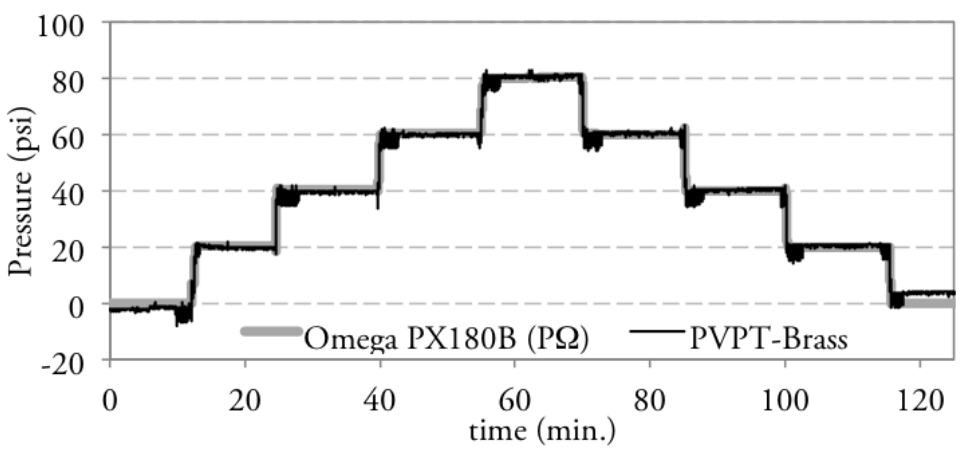

Figure 5.2: Experiment 1 Brass PVPT prototype measurements at pressures ($R^2 = 0.9959$).

the pressure could not be precisely controlled, the measured signal meanders and because this migration is in direct response to the pressure, it must not be discarded. The signal is filtered using a low-pass filter which rejects the high frequency noise (attributed to the random measurement noise). The measurement noise is isolated by subtracting the filtered signal from the original signal [45]. If the noise generally follows a normal distribution, the majority of the spurious signals will be within two standard deviations from the mean, and the mean itself should be nearly zero. Hence, the value for δ_{R} is two standard deviations of the extracted random noise component of the signal added to the standard error to 95% confidence (see Figure 3.3).

Table 5.2: Random uncertainties for each prototype due to measurement noise.

PVPT Prototype	δ_{R} (psi)
PC	8.13×10^{-2}
PVC	1.50×10^{0}
Cu	6.19×10^{-1}
Brass	1.98×10^{0}

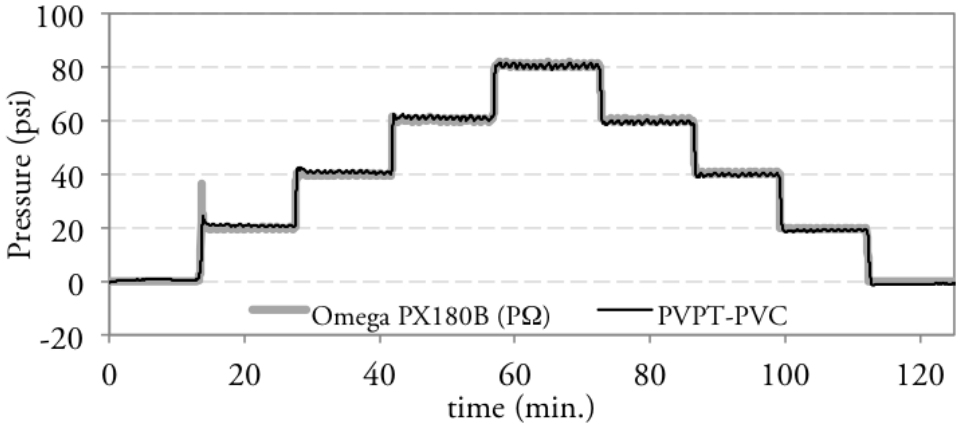

Figure 5.3: Experiment 1 PVC PVPT prototype measurements at pressures ($R^2 = 0.9980$).

5.2.3 Accuracy Results of the Mathematical Model

The model was consistent in transforming voltage into a value for pressure that was within the limits determined by uncertainty analyses (see Figure 5.6 and Figure 5.7). However, there were instances of brief breakouts of the boundaries, likely due to either spurious noise or response lag.

5.3 Conclusion

In all prototypes, the physical design isolated and responded to pressure by generating a voltage signal that scaled proportionally with pressure and did so consistently enough that all had T statistics were high enough to reject the null hypothesis that the pressure and signal responses would be exclusive to the point of being bereft of any correlation.

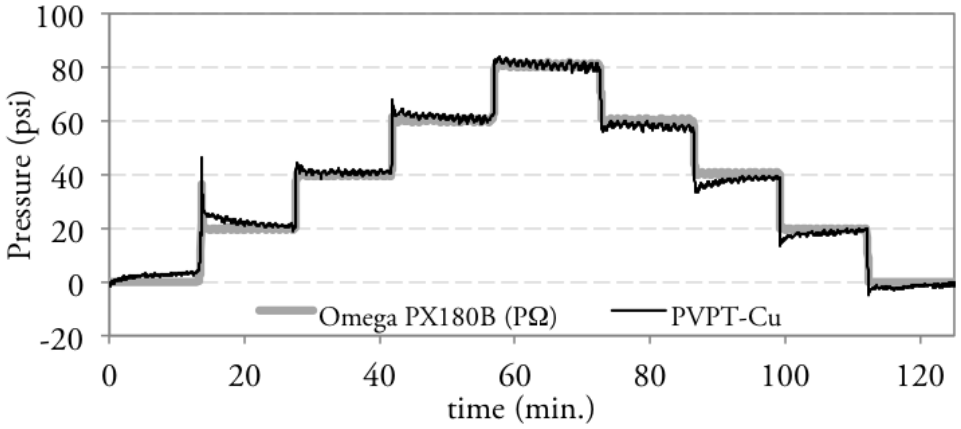

Figure 5.4: Experiment 1 Copper PVPT prototype measurements at pressures ($R^2 = 0.9934$).

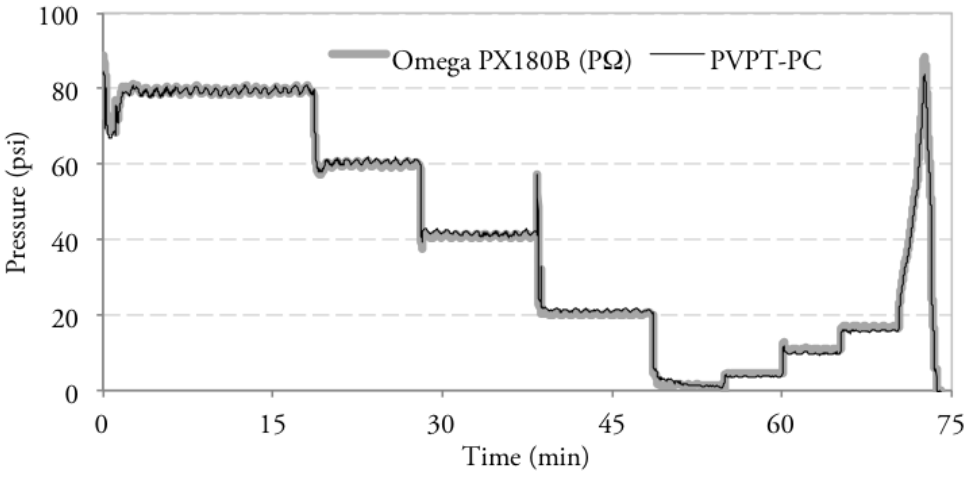

Figure 5.5: Experiment 2 Polycarbonate (PC) PVPT prototype measurements compared to standard.

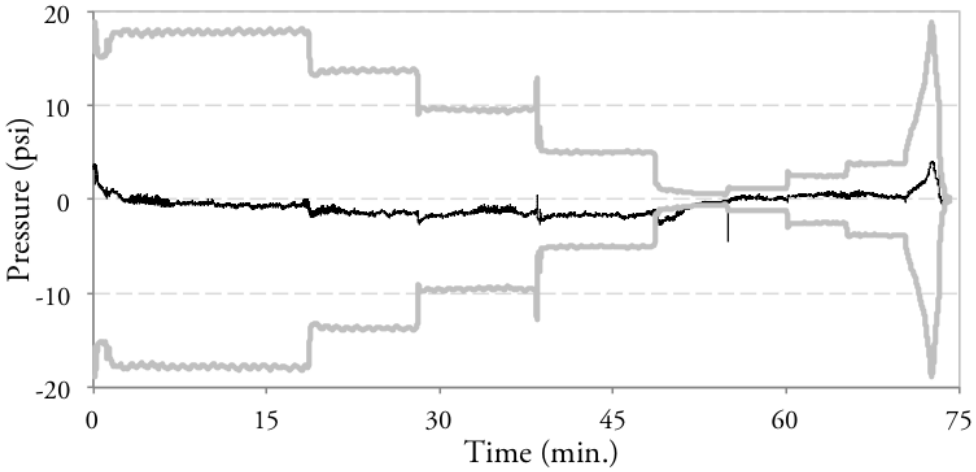

Figure 5.6: Experiment 2 Polycarbonate (PC) PVPT measurement error ($P_{\Omega} - P_{\mathrm{PC}}$) in black. Light grey, thick lines mark error limits based on modeled uncertainty. The prototype breaks the threshold at the pinch-point when the uncertainty tolerances pinched inward during a period of low pressure (see Figure 5.5).

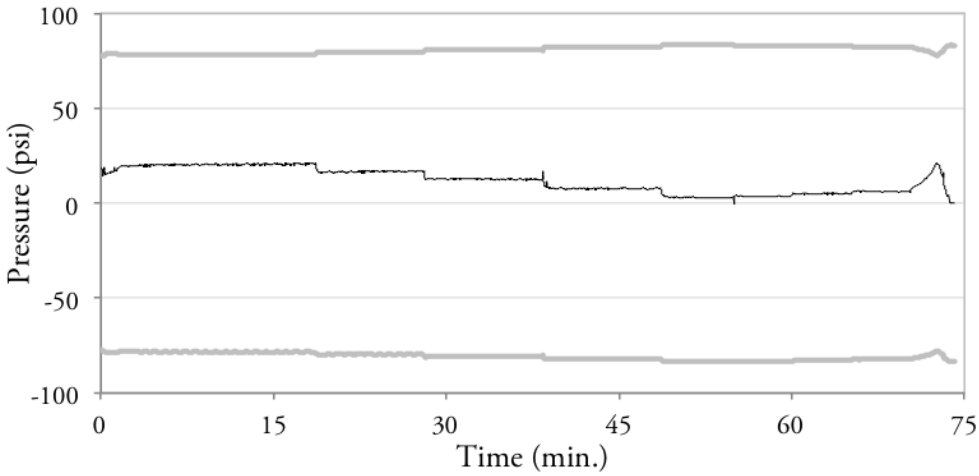

Figure 5.7: Experiment 2 brass PVPT measurement error ($P_{\Omega} - P_{\mathrm{Br}}$) in black. Light grey, thick lines mark error limits based on modeled uncertainty.

Chapter 6

Discussions & Frontiers

6.1 Introduction

This project has introduced a new pressure sensor design strategy and demonstrated its efficacy by direct physical testing at room temperature for pressure ranges from 0 to 100 psi.

The first objective of this project was to test the viability of a pressurized vessel to serve as a mechanism for measuring pressure by direct observation of transduced voltage output from a wheatstone bridge responding to the combined circumferential and longitudinal strains. The results from the design validation advocate the validation of the physical PVPT structure as a sound mechanism for faithfully converting pressure into a usable electric signal response.

The second objective was to test a derived mathematical model intended to provide an analytical solution for pressure using the voltage output and constant parameters of the system. The results from the theoretical model validation support its completeness in consideration of appropriate physical

phenomena and its correctness in how those phenomena are combined and transformed back into the property of interest.

The following subsections offer insights and interesting observations collected over the course of the study, and will serve future research.

6.2 Project Summary

The polycarbonate and PVC PVPTs performed significantly better than the copper and brass. The most obvious explanation is the higher modulus of elasticity in the copper and brass prototypes which results in lower sensitivity in terms of voltage output per unit pressure, stemming from the decreased deformation at similar pressures.

The theoretical model succeeded in predicting the pressure to within the limits of uncertainty, but realistically that capability does not make up for the huge uncalibrated error. What it does, however, is provide evidence to the accuracy of the uncertainty analysis, and if the uncertainty analysis is accurate, then it can guide improvement on the design. The two largest contributors were uncertainty in nominal resistances and the modulus of elasticity. If the material were tightly controlled, and a calibration at null pressure performed, then the accuracy would significantly improve.

6.2.1 Physical Design Validity

The physical design of the prototype sensors was based on the derived theoretical model. The null hypothesis was that the design could not sufficiently isolate pressure so as to respond with sufficient exclusivity, and it was rejected

on the basis of the non-zero $\hat{\beta}_1$ which indicated a correlation between the actual pressure (as measured by the standard) and PVPT voltage response.

6.2.2 Sensor Validity

The pressure vessel approach applied to the design of a mechanism for sensing pressure was shown to be a viable approach to pressure sensor design. The physical design adequately isolated the pressure stimulus, and the theoretical model predicted the pressure to within the uncertainty model.

6.3 Insights

A handful of key insights into the PVPT system have been gleaned from various parts of this research. The following subsections address those that would benefit from further discussion. For more general insights in the way of formulae, etc., see Appendix D.

6.3.1 Designs for Sensitivity

Voltage to pressure sensitivity scales proportionally with the Ω term (see Equation 3.6) for variations of diameter or thickness and inversely with variations to the modulus of elasticity, following the rule

$$\frac{\Omega_1 E_2}{\Omega_2 E_1} \approx \frac{\delta_{V1}}{\delta_{V2}} \tag{6.1}$$

If one has the luxury of choice, some amplification can be substituted with thoughtful design choices. Though the effects are influenced by the setup,

back-of-the-napkin calculations suggest the geometry and modulus of elasticity are the properties with most direct translation to sensitivity. For example, decreasing the wall thickness of a PVPT by 25% increases the output by 35%, while adding 50% to the diameter will increase the voltage output by a little more than 50%. If the modulus of elasticity were decreased by a factor of ten, the voltage output would be increased by a factor of ten.

6.4 Future Research

The following subsections describe possible topics for future research.

6.4.1 Thermal Tolerance

This project restricted the data collection environment to approximately 72^{o}F $\pm$4^{o}F (see Section 4.1.2). By using a full bridge, material-matched strain gages, and short leadwires the PVPT should be able to tolerate a range of temperatures without effecting the output signal.

6.4.2 Heterogeneous, Anisotropic, Composite Vessels

This work has focused solely on homogeneous vessels whose mechanical properties when acted upon are not dependent on orientation with respect to the source of a physical interaction. An alternative material to use would have been something like fiberglass or carbon fiber which would both deform anisotropically due to the structural reinforcement created by the direction of the fiberglass or carbon fiber. Vessels reinforced by carbon fiber or fiberglass would have superior tensile strength in the direction of the fibers. The trade-

off would be a more complicated model. Such vessels are much safer under high pressure and commonly used in compressed gas tanks.

Any plans to investigate the application of the PVPT to high pressures should be preceded by adaptation of the model to work with anisotropic materials so that a safer fiber-wrapped vessel can be employed.

6.4.3 Fatigue and Creep Analyses

The vessel material will fatigue with repeated deformation cycles, but the deformation is very small. How many cycles and at what pressures and material, on average, until the effects become noticeable as measurement error?

It is not uncommon for pressure sensors to be connected to a pressure source that is pressurized around the clock. How long until creep effects the accuracy of the sensor? PVC piping has "50 year creep" pressure ratings to guide their application to limit premature failure due to creep in long-term installations [53], how long would following that guidance extend the effective life of a PVPT before its repeatability has been compromised?

6.4.4 Miniaturization

All of the prototypes constructed for this research project were at least eight inches long and a quarter of an inch in diameter. These dimensions were chosen for ease of construction by hand and to reduce the risk of making mistakes that could potentially compromise the project.

The prototypes in this particular project would have technically been limited to the minimum radius of curvature limits of the strain gages (3.0 mm).

Future research should explore the behavior of the PVPT at similar scale and smaller.

6.5 Frontiers of Research

A number of interesting applications have been imagined over the course of this project that have been neglected in lieu of prioritizing the establishment of validity in the system before investigating uses. The following subsections describe various applications and manifestations of the system, along with a couple of tricks.

6.5.1 Measuring the Modulus of Elasticity

In cases where the pressure is measured with a separate device, Equation 3.33 can be configured to calculate the modulus of elasticity in the PVPT housing material with only minor surgery. The trick lays in the λ terms which were formulated initially to act as shelving to hold a handful of generally constant variables (3.22, 3.23).

$$\gamma_\theta = PG_F\Omega(2-\nu) \tag{6.2}$$

$$\gamma_{\text{L}} = PG_F\Omega(1-2\nu) \tag{6.3}$$

Where the λ terms had $\frac{1}{E}$, the γ terms have swapped with P which migrates the modulus of elasticity all the way out of the equation and moved to the left side. The coefficients defined in Section 3 (Equations 3.30, 3.32 and 3.33)

are reformulated here using γ terms

$$s_1 = R_{20}\gamma_\theta V_{EX} \qquad s_5 = R_{40}\gamma_L V_{EX}$$
$$s_2 = R_{20}V_{EX} + R_{2T}V_{EX} \qquad s_6 = R_{40}V_{EX} + R_{4T}V_{EX}$$
$$s_3 = R_{10}\gamma_L + R_{20}\gamma_\theta \qquad s_7 = R_{30}\gamma_\theta + R_{40}\gamma_L$$
$$s_4 = R_{10} + R_{20} + R_{1T} + R_{2T} \qquad s_8 = R_{30} + R_{40} + R_{3T} + R_{4T}$$

$$L_1 = s_7 s_1 - s_5 s_3 \qquad L_4 = s_7 s_3$$
$$L_2 = s_7 s_2 + s_1 s_8 - s_5 s_4 - s_6 s_3 \qquad L_5 = s_7 s_4 + s_8 s_3$$
$$L_3 = s_8 s_2 - s_6 s_4 \qquad L_6 = s_8 s_4$$

$$W_1 = L_5^2 - 4L_4L_6$$
$$W_2 = 4L_1L_6 - 2L_2L_5 + 4L_3L_4$$
$$W_3 = L_2^2 - 4L_1L_3$$

The modulus of elasticity can then be calculated as a function of measured pressure and measured PVPT voltage

$$E(P,V) = \frac{L_2 - L_5V \pm \sqrt{W_1V^2 + W_2V + W_3}}{2(L_6V - L_3)} \tag{6.4}$$

Like the pressure model, the function contains a quadratic function. Unlike the pressure model, there remains ambiguity in which operator the $\pm$

should be. The simple heuristic I have found through trial and error to work satisfactorily is to calculate assuming addition. If the result is less than 10,000 (psi), then go back and subtract, instead.

Some care must be taken when the pressure is low due to the presence of an asymptote as measured pressure approaches zero. When the measured voltage is at zero, the equation breaks down to

$$E(V=0) = \frac{L_2 \pm \sqrt{W_3}}{-2L_3} \tag{6.5}$$

6.5.2 Measuring Poisson's Ratio

The modulus of elasticity and Poisson's ratio are the two material properties that would typically be retrieved from literature rather than direct measurement. It may be possible to measure these properties by taking two measurements, one in each configuration shown in Figure 6.1.

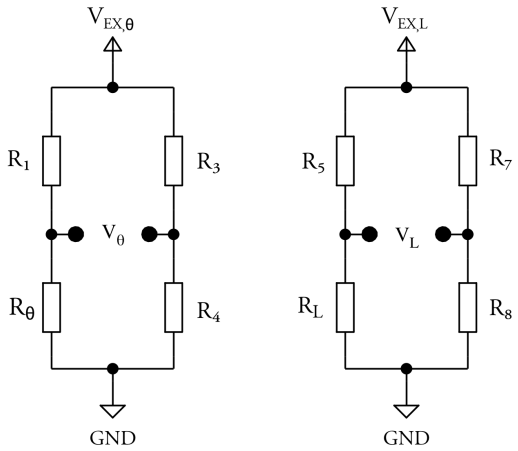

Figure 6.1: Bridge circuits for the solution of Poisson's ratio in PVPT material. Resistors can be shared; output voltages do not need to be read simultaneously.

This technique begins by solving for Poisson's ratio, and then using the result to calculate the modulus of elasticity. The first step is to form an equation with the modulus of elasticity isolated.

Beginning with the longitudinal equation:

$$V_L = V_{\text{EX,L}} \left(\frac{R_L(1 + \frac{P_L \Omega}{4E}(1 - 2\nu)}{R_5 + R_L(1 + \frac{P_L \Omega}{4E}(1 - 2\nu)} - \frac{R_8}{R_7 + R_8} \right) \tag{6.6}$$

and isolating the modulus of elasticity:

$$E = \frac{\Omega R_L P_L (1 - 2\nu)(R_7 V_{\text{EX,L}} - (R_7 + R_8) V_L)}{4((R_5 R_8 - R_L R_7) V_{\text{EX,L}} + (R_5 + R_L)(R_7 + R_H) V_{L,o})} \tag{6.7}$$

With the circumferential equation:

$$V_\theta = V_{\text{EX},\theta} \left(\frac{R_\theta(1 + \frac{P_\theta \Omega}{4E}(2 - \nu)}{R_1 + R_\theta(1 + \frac{P_\theta \Omega}{4E}(2 - \nu)} - \frac{R_4}{R_3 + R_4} \right) \tag{6.8}$$

and substituting modulus of elasticity terms with (6.7) and isolating Poisson's ratio results in the equation:

$$\nu = \frac{(R_3 + R_4) V_\theta \lambda_1 + V_{\text{EX},\theta} \lambda_2}{(R_3 + R_4) V_\theta \lambda_3 + V_{\text{EX},\theta} \lambda_4} \tag{6.9}$$

where λ_1, λ_2, λ_3, and λ_4 refer to:

$$\begin{aligned} \lambda_1 = {} & (R_1 R_L P_L R_7 + R_\theta(2R_5 R_8 P_\theta + R_L R_7(2P_\theta - P_L))) V_{\text{EX,L}} \\ & - (R_1 R_L P_L - R_\theta(2R_5 P_L + R_L(2P_\theta - P_L)))(R_7 + R_8) V_{L,o} \end{aligned} \tag{6.10}$$

$$\lambda_2 = (R_1 R_L P_L R_4 R_7 - R_\theta R_3 (2R_5 R_8 P_\theta - R_L R_7 (2P_\theta - P_L)))V_{\text{EX,L}}$$
$$- (R_1 R_L P_L R_4 + R_\theta R_3 (2R_5 P_L + R_L (2P_\theta - P_L)))(R_7 + R_8)V_{L,o} \quad (6.11)$$

$$\lambda_3 = (2R_1 R_L R_7 P_L + R_\theta (R_5 R_8 P_\theta - R_L R_7 (P_\theta - 2P_L)))V_{\text{EX,L}}$$
$$- (2R_1 R_L P_L - R_\theta (R_5 P_\theta + R_L (P_\theta - 2P_L)))(R_7 + R_8)V_{L,o} \quad (6.12)$$

$$\lambda_4 = (2R_1 R_4 R_L R_7 P_L - R_\theta R_3 (R_5 R_8 P_\theta - R_L R_7 (P_\theta - 2P_L)))V_{\text{EX,L}}$$
$$- (2R_1 R_4 R_L P_L + R_\theta R_3 (R_5 P_\theta + R_L (P_\theta - 2P_L)))(R_7 + R_8)V_{L,o} \quad (6.13)$$

After solving for ν, the modulus of elasticity can be found by back-substitution of ν into Equation 6.6.

6.5.3 Differential Gage Design

It appears possible to use a pair of the PVPTs sharing a single bridge circuit to respond predictably to differential pressure (see Figure 6.2). A mathematical model would certainly be a topic of future research: the bridge equation produces the differential pressure between a pair of voltage dividers.

For a system constructed as in Figure 6.2, the bridge equations can be expressed as

$$\Delta V = V_{\text{EX}} \left(\frac{\frac{1}{\frac{1}{R_{2\text{A}}}+\frac{1}{R_{2\text{B}}}}}{\frac{1}{\frac{1}{R_{1\text{A}}}+\frac{1}{R_{1\text{B}}}} + \frac{1}{\frac{1}{R_{2\text{A}}}+\frac{1}{R_{2\text{B}}}}} - \frac{\frac{1}{\frac{1}{R_{4\text{A}}}+\frac{1}{R_{4\text{B}}}}}{\frac{1}{\frac{1}{R_{3\text{A}}}+\frac{1}{R_{3\text{B}}}} + \frac{1}{\frac{1}{R_{4\text{A}}}+\frac{1}{R_{4\text{B}}}}} \right) \tag{6.14}$$

$$\frac{\Delta V}{V_{\text{EX}}} = \frac{(R_{2\text{A}} + R_{2\text{B}})R_{1\text{A}}R_{1\text{B}}}{R_{2\text{B}}(R_{1\text{A}}(R_{1\text{B}} + R_{2\text{A}}) + R_{1\text{B}}R_{2\text{A}}) + R_{1\text{A}}R_{1\text{B}}R_{2\text{A}}} - \frac{(R_{4\text{A}} + R_{4\text{B}})R_{3\text{A}}R_{3\text{B}}}{R_{4\text{B}}(R_{3\text{A}}(R_{3\text{B}} + R_{4\text{A}}) + R_{3\text{B}}R_{4\text{A}}) + R_{3\text{A}}R_{3\text{B}}R_{4\text{A}}} \tag{6.15}$$

The pressure terms in this work correspond to one pressure value, but in a differential model the two pressure terms would need to be removed and the model expressed as a function of the pressure difference.

In an iterative approach, one would write a program to find the pressure difference that corresponds most nearly the measured voltage measurement.

A lookup table could be constructed, and simulations to this extent have suggested the approach would be successful so far as the stimulus and response behave sufficiently linearly.

6.6 Conclusion

This dissertation has explored the potential of the pressure vessel predicated design as a basis for a sensor that can sense pressure. Results have shown promise in the application and raised potential applications in need of future work to expand the frontier of its use.

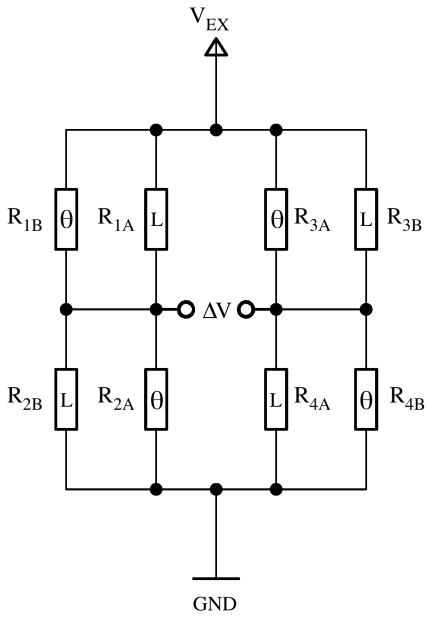

Figure 6.2: The differential PVPT configuration needs a bridge that produces consistent differential voltages with repeated conditions of differential pressure. Initial simulations have produced encouraging results for this nested bridge design.

References

[1] *Instrumenation Amplifier with Precision Voltage Reference.* Texas Instruments. INA125. Sep 2008.

[2] *Omega KFH Series Pre-Wired Strain Gages.* Omega Engineering, Inc. KFH Series. 2003.

[3] *Precision Strain Gages - 1-Axis General Purpose.* Omega Engineering, Inc. SGD Series. 2003.

[4] *RTD-to-Digital Converter.* Maxim Integrated. MAX31865. Rev. 3. Jul 2015.

[5] *Silicon/brass pressure transducers with millivolt output.* Omega Engineering, Inc. PX180B Series. 2004.

[6] *Ultrasmall, Low-Power, SPI-Compatible, 16-bit Analog-to-Digital Converter with Internal Reference and Temperature Sensor.* Texas Instruments. ADS1118. Rev. E. Oct 2015.

[7] *The Copper Tube Handbook.* Copper Development Association Inc., 2016.

[8] American Society of Mechanical Engineers. The history of ASME's boiler and pressure vessel code. *https://www.asme.org/engineering-topics/articles/boilers/the-history-of-asmes-boiler-and-pressure*, Accessed Feb 2018.

[9] ASME Boiler and Pressure Vessel Committee on Pressure Vessels. *Rules for Construction of Pressure Vessels.* ASME Boiler and Pressure Vessel Code, Section VIII, Division 1. ASME International, Jul 2010.

[10] ASME Boiler and Pressure Vessel Committee on Pressure Vessels. *Rules for Construction of Pressure Vessels: Alternative Rules.* ASME Boiler and Pressure Vessel Code, Section VIII, Division 2. Annex 5.F pages 139-146, ASME International, Jul 2010.

[11] Edward Bender. *An introduction to mathematical modeling*. Courier Corporation, 2012.

[12] Richard Budyna. *Advanced strength and applied stress analysis*. McGraw-Hill Education, 1999.

[13] Charles W. Calhoun. Fluid pressure measuring device. U.S. Patent 3,645,136, Apr. 1970.

[14] Steve Carter, Alex Ned, John Chivers, and Andy Bemis. Selecting piezoresistive vs. piezoelectric pressure transducers. Application note: An 102, 2016.

[15] Designation: D 2466. *Standard Specification for Poly(Vinyl Chloride) (PVC) Plastic Pipe Fittings, Schedule 40*, volume 08.04 of *Annual Book of ASTM Standards*. ASTM International, 2002.

[16] Dave Dewees. Essential for safety. *Mechanical Engineering*, pages 32–35, Nov 2014.

[17] Richard Dorf, editor. *The Electrical Engineering Handbook*. CRC Press, LLC, 1st edition, 2000.

[18] Klaus Dunemann and Harald Fritz. Arrangement for measuring the pressure in cylindrical cavities. U.S. Patent 4,420,980, Sep 1981.

[19] Wilson Gabauer. *The Estimation of Uncertainties in Hardness Measurements*. Standards Measurement & Testing, Sep 2000.

[20] Wolfgang Göpel, Joachim Hesse, Jay Zemel, Thomas Grandke, and Wen Ko. *Fundamentals and general aspects*, volume 1 of *Sensors: a comprehensive survey*. VCH Publishers Inc., 1989.

[21] JH Greenwood. The constraints on the design and use of silicon-diaphragm pressure sensors. *Electronics and Power*, 29(2):170–174, 1983.

[22] Victor Guillemin. Strain gauge manometer. U.S. Patent 2,566,326, Dec. 1946.

[23] Ronald Huston and Harold Josephs. *Practical stress analysis in engineering design*. CRC Press, 3rd edition, 2008.

[24] Institute and Museum of History of Science. Evangelista torricelli; 3.4 the barometric experiment. *http://www.imss.fi.it/multi/torricel/etorat34.html*, Accessed Jun 2017.

[25] Burkhard Kempf. Apparatus for performing pressure, normal force and bending measurements on pipelines. U.S. Patent 4,738,141, Apr. 1988.

[26] Sanghoon Lee and Wei Chen. A comparative study of uncertainty propagation methods for black-box-type problems. *Structural and Multidisciplinary Optimization*, 37(3):239–253, 2009.

[27] Béla Lipták. *Process measurement and analysis*, volume 1 of *The Instrument Engineers' Handbook*. CRC Press, 4th edition, 2003.

[28] Raymond Lohr and Victor Kallnin. High pressure sensor. U.S. Patent Application 2008/0289431-A1, Nov. 2008.

[29] Jerry Lyons. *The Designer's Handbook Of Pressure-Sensing Devices*. Van Nostrand Reinhold Company, 1980.

[30] John Mandel. *The statistical analysis of experimental data*. Courier Corporation, 2012.

[31] Kulite Strain Gage Manual. Kulite semiconductor products. *Inc., One Willow Tree Road, Leonia, New Jersey, 2011*, https://www.kulite.com/assets/media/2017/05/ StrainGageManualDigital.pdf Accessed April 2018.

[32] William Mendenhall and Terry Sincich. *Statistics for Engineering and the Sciences*. Prentice-Hall, Inc., 5th edition, 2006.

[33] David Moore and Stephane Kirkland. *The basic practice of statistics*, volume 2. WH Freeman New York, 2007.

[34] Foster Morrison. *The art of modeling dynamic systems: forecasting for chaos, randomness and determinism*. Courier Corporation, 2012.

[35] deV Naylor. Polymer membranes-materials, structures and separation performance. *Rapra Review Reports*, 8(5), 1996.

[36] Harry Norton. *Handbook of transducers*. Prentice Hall Englewood Cliffs, 1989.

[37] Omega. The strain gage. *https://www.omega.com/literature/transactions /volume3/strain.html*, Accessed Apr 2018.

[38] Chad O'Neal, Ajay Malshe, Sushila Singh, William Brown, and William Eaton. Challenges in the packaging of mems. In *Advanced Packaging Materials: Processes, Properties and Interfaces, 1999. Proceedings. International Symposium on*, pages 41–47. IEEE, 1999.

[39] Ralph Ostergren. Pressure indicator. U.S. Patent 2,420,148, Nov 1943.

[40] Apurva Pendbhaje, Mahesh Gaikwad, Nitin Deshmukh, and Rajkumar Patil. Design and analysis of pressure vessel. *International Journal of Innovative Research in Technology and Science*, 2(3):2321–1156, 2012.

[41] Purushothama Raj and Van Ramasamy. *Strength of Materials*. Pearson, 2012.

[42] Raymond Roark and Warren Young. *Formulas for stress and strain*. McGraw-Hill, 1975.

[43] Sensorland. The history of pressure measurement. *http://www.sensorland.com/HowPage059.html*, Accessed Jun 2017.

[44] Rick Shepard and Leroy Thacker. Evaluation of pressure sensing concepts: a technology assessment. Technical report, Oak Ridge National Lab, 1993.

[45] Cecil Smith. *Basic process measurements*. John Wiley & Sons, 2011.

[46] Colin Smithells, William Gale, and Terry Totemeier. *Smithells Metals Reference Book*. Elsevier Butterworth-Heinemann, 7th edition, 2004.

[47] Barry Taylor and Chris Kuyatt. *Guidelines for evaluating and expressing the uncertainty of NIST measurement results*. National Institute of Standards and Technology, 1994.

[48] John Taylor. *Introduction to error analysis, the study of uncertainties in physical measurements*. University Science Books, 2nd edition, 1997.

[49] Barometer Fair. History of the barometer. *http://www.barometerfair.com/history_of_the_barometer.html*, Accessed Jun 2017.

[50] The National Museum of American History. Aneroid barometer. *http://americanhistory.si.edu/collections/search/object/nmah_1183996*, Accessed Jun 2017.

[51] Strain Gage Based Transducers. Their design and construction. Technical report, technical report, Measurements Group Inc., Raleigh, NC, 1988.

[52] Martin Vargic. Scale of pressure (2015). *http://www.halcyonmaps.com/infographics/#/scale-of-pressure/*, Accessed Jun 2017.

[53] Vinidex Pty Limited. PVC Properties. *http://www.vinidex.com.au/technical/material-properties/pvc-properties/*, Accessed Mar 2018.

[54] Jack Vinson. *The behavior of sandwich structures of isotropic and composite materials*. CRC Press, 1999.

[55] Kashyap Vyas. Pressure vessel design by analysis versus design by rule. *Processing Magazine*, 2018.

[56] Larry Zick. Stresses in large horizontal cylindrical pressure vessels on two saddle supports. *Welding Journal Research Supplement*, 30(9):435–445, 1951.

Appendices

Appendix A

Model C Code

A.1 Model Calculation Subroutines

Table A.1: {Parameters}

double Rn1	**double** Rn2	**double** Rn3	**double** Rn4
double Rn1	**double** Rn2	**double** Rn3	**double** Rn4
double Rt1	**double** Rt2	**double** Rt3	**double** Rt4
double P	**double** Di	**double** t	
double v	**double** YoungsMod	**double** GF	**double** Vex

A.1.1 Function List

```
double V_from_P( {Parameters} )
double P_from_V( {Parameters}, double V_measured)
double E_from_PV( {Parameters}, double V_measured, double P_measured )
double dVdR1n( {Parameters} )
double dVdR2n( {Parameters} )
double dVdR3n( {Parameters} )
double dVdR4n( {Parameters} )
double dVdR1t( {Parameters} )
double dVdR2t( {Parameters} )
```

```
double dVdR3t(  {Parameters} )
double dVdR4t(  {Parameters} )
double dVdP(  {Parameters} )
double dVdD(  {Parameters} )
double dVdt(  {Parameters} )
double dVdv(  {Parameters} )
double dVdY(  {Parameters} )
double dVdGF( {Parameters} )
double dVdVex(  {Parameters} )
```

A.1.2 Functions

```
double V_from_P(double Rn1,double Rn2,double Rn3,double Rn4,
    double Rt1,double Rt2,double Rt3,double Rt4,
    double P,double Di,double t,
    double v, double YoungsMod,double GF,double Vex)
{
  return Vex*((Rn2*(1 + GF * (P * (Di*Di/
  (4*YoungsMod*t*(Di + t))) * (2 - v))) /
  (Rn1*(1 + GF * (P * (Di*Di/
  (4*YoungsMod*t*(Di + t))) * (1 - 2*v))) +
  Rn2*(1 + GF * (P * (Di*Di/
  (4*YoungsMod*t*(Di + t))) * (2 - v))) + Rt1 + Rt2)) -
  (Rn4*(1 + GF * (P * (Di*Di/
  (4*YoungsMod*t*(Di + t))) * (1 - 2*v))) /
  (Rn3*(1 + GF * (P * (Di*Di/
  (4*YoungsMod*t*(Di + t))) * (2 - v))) +
  Rn4*(1 + GF * (P * (Di*Di/
  (4*YoungsMod*t*(Di + t))) * (1 - 2*v))) +
  Rt3 + Rt4)));
}
```

```
double P_from_V(double V_measured,
    double Rn1,double Rn2,double Rn3,double Rn4,
    double Rt1,double Rt2,double Rt3,double Rt4,
    double P,double Di,double t,
    double v, double YoungsMod,double GF,double Vex)
{
  double V = V_measured;
  double lambda_H = ((Di*Di)/(4*t*(Di+t))) * (GF/YoungsMod) * (2.0 - v);
  double lambda_L = ((Di*Di)/(4*t*(Di+t))) * (GF/YoungsMod) * (1.0 - v*2.0);

  double aa = Vex * Rn2 * lambda_H;
  double bb = Vex * (Rn2 + Rt2);
  double cc = Rn1 * lambda_L + Rn2 * lambda_H;
  double dd = Rn1 + Rt1 + Rn2 + Rt2;

  double ee = Vex * Rn4 * lambda_L;
  double ff = Vex * (Rn4 + Rt4);
  double gg = Rn3 * lambda_H + Rn4 * lambda_L;
  double hh = Rn3 + Rt3 + Rn4 + Rt4;

  double A = gg*aa - ee*cc;
  double B = gg*bb + aa*hh - ee*dd - ff*cc;
  double C = hh*bb - ff*dd;
  double D = gg*cc;
  double E = gg*dd + hh*cc;
  double F = hh*dd;

  double M = E*E - 4.0*D*F;
  double N = 4.0*A*F - 2.0*B*E + 4.0*C*D;
```

```
  double O = B*B - 4.0*A*C;

  double P_num = ( B - E*V - sqrt( M*V*V + N*V + O) );
  double P_den = 2.0*(D*V - A);
  double r_P = P_num/P_den;
  return r_P;
}


double E_from_PV(double V_measured, double P_measured,
    double Rn1,double Rn2,double Rn3,double Rn4,
    double Rt1,double Rt2,double Rt3,double Rt4,
    double P,double Di,double t,
    double v, double YoungsMod,double GF,double Vex)
{
  double V = V_measured;
  double P = P_measured;

  double lambda_H = ((Di*Di)/(4*t*(Di+t)))*(GF*P)*(2.0 - v);
  double lambda_L = ((Di*Di)/(4*t*(Di+t)))*(GF*P)*(1.0 - v*2.0);

  double aa = Vex * R2n * lambda_H;
  double bb = Vex * (R2n + R2t);
  double cc = R1n * lambda_L + R2n * lambda_H;
  double dd = R1n + R1t + R2n + R2t;

  double ee = Vex * R4n * lambda_L;
  double ff = Vex * (R4n + R4t);
  double gg = R3n * lambda_H * R4n * lambda_L;
  double hh = R3n + R3t + R4n + R4t;
```

```
  double A = gg*aa - ee*cc;
  double B = gg*bb + aa*hh - ee*dd - ff*cc;
  double C = hh*bb - ff*dd;
  double D = gg*cc;
  double E = gg*dd + hh*cc;
  double F = hh*dd;

  double M = E*E - 4.0*D*F;
  double N = 4.0*A*F - 2.0*B*E + 4.0*C*D;
  double O = B*B - 4.0*A*C;

  double E_den = 2.0*(F*V - C);
  double E_num = (B - E*V) + sqrt( M*V*V + N*V + O);
  if( fabs(E_num/E_den) < 1e5 )
    E_num = (B - E*V) - sqrt( M*V*V + N*V + O);

  return E_num/E_den;
}



double dVdR1n(double Rn1,double Rn2,double Rn3,double Rn4,
     double Rt1,double Rt2,double Rt3,double Rt4,
     double P,double Di,double t,
     double v, double YoungsMod,double GF,double Vex)
{
    return -((Rn2*Vex*(1 + (pow(Di,2)*GF*P*(1 - 2*v))/
    (4.*t*(Di + t)*YoungsMod))*(1 + (pow(Di,2)*GF*P*(2 - v))/
    (4.*t*(Di + t)*YoungsMod)))/
```

```
    pow(Rt1 + Rt2 + Rn1*(1 + (pow(Di,2)*GF*P*(1 - 2*v))/
    (4.*t*(Di + t)*YoungsMod)) + Rn2*(1 + (pow(Di,2)*GF*P*(2 - v))/
    (4.*t*(Di + t)*YoungsMod)),2)) ;
}

double dVdR2n(double Rn1,double Rn2,double Rn3,double Rn4,
     double Rt1,double Rt2,double Rt3,double Rt4,
     double P,double Di,double t,
     double v, double YoungsMod,double GF,double Vex)
{
    return Vex*((1 + (pow(Di,2)*GF*P*(2 - v))/(4.*t*(Di + t)*YoungsMod))/
    (Rt1 + Rt2 + Rn1*(1 + (pow(Di,2)*GF*P*(1 - 2*v))/
    (4.*t*(Di + t)*YoungsMod)) + Rn2*(1 + (pow(Di,2)*GF*P*(2 - v))/
    (4.*t*(Di + t)*YoungsMod))) - (Rn2*pow(1 + (pow(Di,2)*GF*P*(2 - v))/
    (4.*t*(Di + t)*YoungsMod),2))/
    pow(Rt1 + Rt2 + Rn1*(1 + (pow(Di,2)*GF*P*(1 - 2*v))/
    (4.*t*(Di + t)*YoungsMod)) + Rn2*(1 + (pow(Di,2)*GF*P*(2 - v))/
    (4.*t*(Di + t)*YoungsMod)),2)) ;
}

double dVdR3n(double Rn1,double Rn2,double Rn3,double Rn4,
     double Rt1,double Rt2,double Rt3,double Rt4,
     double P,double Di,double t,
     double v, double YoungsMod,double GF,double Vex)
{
    return (Rn4*Vex*(1 + (pow(Di,2)*GF*P*(1 - 2*v))/
    (4.*t*(Di + t)*YoungsMod))*(1 + (pow(Di,2)*GF*P*(2 - v))/
    (4.*t*(Di + t)*YoungsMod)))/
    pow(Rt3 + Rt4 + Rn4*(1 + (pow(Di,2)*GF*P*(1 - 2*v))/
    (4.*t*(Di + t)*YoungsMod)) + Rn3*(1 + (pow(Di,2)*GF*P*(2 - v))/
```

```
    (4.*t*(Di + t)*YoungsMod)),2) ;
}

double dVdR4n(double Rn1,double Rn2,double Rn3,double Rn4,
     double Rt1,double Rt2,double Rt3,double Rt4,
     double P,double Di,double t,
     double v, double YoungsMod,double GF,double Vex)
{
    return Vex*(-((1 + (pow(Di,2)*GF*P*(1 - 2*v))/
    (4.*t*(Di + t)*YoungsMod))/
    (Rt3 + Rt4 + Rn4*(1 + (pow(Di,2)*GF*P*(1 - 2*v))/
    (4.*t*(Di + t)*YoungsMod)) + Rn3*(1 + (pow(Di,2)*GF*P*(2 - v))/
    (4.*t*(Di + t)*YoungsMod)))) + (Rn4*pow(1 + (pow(Di,2)*GF*P*(1 - 2*v))/
    (4.*t*(Di + t)*YoungsMod),2))/
    pow(Rt3 + Rt4 + Rn4*(1 + (pow(Di,2)*GF*P*(1 - 2*v))/
    (4.*t*(Di + t)*YoungsMod)) + Rn3*(1 + (pow(Di,2)*GF*P*(2 - v))/
    (4.*t*(Di + t)*YoungsMod)),2)) ;
}


double dVdR1t(double Rn1,double Rn2,double Rn3,double Rn4,
     double Rt1,double Rt2,double Rt3,double Rt4,
     double P,double Di,double t,
     double v, double YoungsMod,double GF,double Vex)
{
    return -((Rn2*Vex*(1 + (pow(Di,2)*GF*P*(2 - v))/
    (4.*t*(Di + t)*YoungsMod)))/
     pow(Rt1 + Rt2 + Rn1*(1 + (pow(Di,2)*GF*P*(1 - 2*v))/
     (4.*t*(Di + t)*YoungsMod)) + Rn2*(1 + (pow(Di,2)*GF*P*(2 - v))/
     (4.*t*(Di + t)*YoungsMod)),2)) ;
```

```
}

double dVdR2t(double Rn1,double Rn2,double Rn3,double Rn4,
     double Rt1,double Rt2,double Rt3,double Rt4,
     double P,double Di,double t,
     double v, double YoungsMod,double GF,double Vex)
{
    return -((Rn2*Vex*(1 + (pow(Di,2)*GF*P*(2 - v))/
    (4.*t*(Di + t)*YoungsMod)))/
    pow(Rt1 + Rt2 + Rn1*(1 + (pow(Di,2)*GF*P*(1 - 2*v))/
    (4.*t*(Di + t)*YoungsMod)) + Rn2*(1 + (pow(Di,2)*GF*P*(2 - v))/
    (4.*t*(Di + t)*YoungsMod)),2)) ;
}

double dVdR3t(double Rn1,double Rn2,double Rn3,double Rn4,
     double Rt1,double Rt2,double Rt3,double Rt4,
     double P,double Di,double t,
     double v, double YoungsMod,double GF,double Vex)
{
    return (Rn4*Vex*(1 + (pow(Di,2)*GF*P*(1 - 2*v))/
   (4.*t*(Di + t)*YoungsMod)))/
    pow(Rt3 + Rt4 + Rn4*(1 + (pow(Di,2)*GF*P*(1 - 2*v))/
   (4.*t*(Di + t)*YoungsMod)) + Rn3*(1 + (pow(Di,2)*GF*P*(2 - v))/
   (4.*t*(Di + t)*YoungsMod)),2) ;
}

double dVdR4t(double Rn1,double Rn2,double Rn3,double Rn4,
     double Rt1,double Rt2,double Rt3,double Rt4,
     double P,double Di,double t,
     double v, double YoungsMod,double GF,double Vex)
```

```
{
    return (Rn4*Vex*(1 + (pow(Di,2)*GF*P*(1 - 2*v))/
   (4.*t*(Di + t)*YoungsMod)))/
    pow(Rt3 + Rt4 + Rn4*(1 + (pow(Di,2)*GF*P*(1 - 2*v))/
   (4.*t*(Di + t)*YoungsMod)) + Rn3*(1 + (pow(Di,2)*GF*P*(2 - v))/
   (4.*t*(Di + t)*YoungsMod)),2) ;
}


double dVdP(double Rn1,double Rn2,double Rn3,double Rn4,
     double Rt1,double Rt2,double Rt3,double Rt4,
     double P,double Di,double t,
     double v, double YoungsMod,double GF,double Vex)
{
    return Vex*((Rn4*(1 + (pow(Di,2)*GF*P*(1 - 2*v))/
   (4.*t*(Di + t)*YoungsMod))*((pow(Di,2)*GF*Rn4*(1 - 2*v))/
   (4.*t*(Di + t)*YoungsMod) + (Rn3*pow(Di,2)*GF*(2 - v))/
   (4.*t*(Di + t)*YoungsMod)))/
    pow(Rt3 + Rt4 + Rn4*(1 + (pow(Di,2)*GF*P*(1 - 2*v))/
   (4.*t*(Di + t)*YoungsMod)) + Rn3*(1 + (pow(Di,2)*GF*P*(2 - v))/
   (4.*t*(Di + t)*YoungsMod)),2) - (Rn2*((Rn1*pow(Di,2)*GF*(1 - 2*v))/
   (4.*t*(Di + t)*YoungsMod) + (Rn2*pow(Di,2)*GF*(2 - v))/
   (4.*t*(Di + t)*YoungsMod))* (1 + (pow(Di,2)*GF*P*(2 - v))/
   (4.*t*(Di + t)*YoungsMod)))/
    pow(Rt1 + Rt2 + Rn1*(1 + (pow(Di,2)*GF*P*(1 - 2*v))/
   (4.*t*(Di + t)*YoungsMod)) + Rn2*(1 + (pow(Di,2)*GF*P*(2 - v))/
   (4.*t*(Di + t)*YoungsMod)),2) + (Rn2*pow(Di,2)*GF*(2 - v))/
    (4.*t*(Di + t)*(Rt1 + Rt2 + Rn1*(1 + (pow(Di,2)*GF*P*(1 - 2*v))/
   (4.*t*(Di + t)*YoungsMod)) + Rn2*(1 + (pow(Di,2)*GF*P*(2 - v))/
   (4.*t*(Di + t)*YoungsMod)))*YoungsMod) - (pow(Di,2)*GF*Rn4*(1 - 2*v))/
```

```
    (4.*t*(Di + t)*(Rt3 + Rt4 + Rn4*(1 + (pow(Di,2)*GF*P*(1 - 2*v))/
   (4.*t*(Di + t)*YoungsMod)) + Rn3*(1 + (pow(Di,2)*GF*P*(2 - v))/
   (4.*t*(Di + t)*YoungsMod)))*YoungsMod)) ;
}


double dVdD(double Rn1,double Rn2,double Rn3,double Rn4,
     double Rt1,double Rt2,double Rt3,double Rt4,
     double P,double Di,double t,
     double v, double YoungsMod,double GF,double Vex)
{
    return Vex*(-((Rn4*(-(pow(Di,2)*GF*P*(1 - 2*v))/
   (4.*t*pow(Di + t,2)*YoungsMod) + (Di*GF*P*(1 - 2*v))/
   (2.*t*(Di + t)*YoungsMod)))/
    (Rt3 + Rt4 + Rn4*(1 + (pow(Di,2)*GF*P*(1 - 2*v))/
   (4.*t*(Di + t)*YoungsMod)) + Rn3*(1 + (pow(Di,2)*GF*P*(2 - v))/
   (4.*t*(Di + t)*YoungsMod)))) + (Rn4*(Rn4*(-(pow(Di,2)*GF*P*(1 - 2*v))/
   (4.*t*pow(Di + t,2)*YoungsMod) + (Di*GF*P*(1 - 2*v))/
   (2.*t*(Di + t)*YoungsMod)) + Rn3*(-(pow(Di,2)*GF*P*(2 - v))/
   (4.*t*pow(Di + t,2)*YoungsMod) + (Di*GF*P*(2 - v))/
   (2.*t*(Di + t)*YoungsMod)))* (1 + (pow(Di,2)*GF*P*(1 - 2*v))/
   (4.*t*(Di + t)*YoungsMod)))/
    pow(Rt3 + Rt4 + Rn4*(1 + (pow(Di,2)*GF*P*(1 - 2*v))/
   (4.*t*(Di + t)*YoungsMod)) + Rn3*(1 + (pow(Di,2)*GF*P*(2 - v))/
   (4.*t*(Di + t)*YoungsMod)),2) + (Rn2*(-(pow(Di,2)*GF*P*(2 - v))/
   (4.*t*pow(Di + t,2)*YoungsMod) + (Di*GF*P*(2 - v))/
   (2.*t*(Di + t)*YoungsMod)))/
    (Rt1 + Rt2 + Rn1*(1 + (pow(Di,2)*GF*P*(1 - 2*v))/
   (4.*t*(Di + t)*YoungsMod)) + Rn2*(1 + (pow(Di,2)*GF*P*(2 - v))/
   (4.*t*(Di + t)*YoungsMod))) - (Rn2*(Rn1*(-(pow(Di,2)*GF*P*(1 - 2*v))/
```

```
  (4.*t*pow(Di + t,2)*YoungsMod) + (Di*GF*P*(1 - 2*v))/
  (2.*t*(Di + t)*YoungsMod)) + Rn2*(-(pow(Di,2)*GF*P*(2 - v))/
  (4.*t*pow(Di + t,2)*YoungsMod) + (Di*GF*P*(2 - v))/
  (2.*t*(Di + t)*YoungsMod)))* (1 + (pow(Di,2)*GF*P*(2 - v))/
  (4.*t*(Di + t)*YoungsMod)))/
   pow(Rt1 + Rt2 + Rn1*(1 + (pow(Di,2)*GF*P*(1 - 2*v))/
  (4.*t*(Di + t)*YoungsMod)) + Rn2*(1 + (pow(Di,2)*GF*P*(2 - v))/
  (4.*t*(Di + t)*YoungsMod)),2)) ;
}

double dVdt(double Rn1,double Rn2,double Rn3,double Rn4,
     double Rt1,double Rt2,double Rt3,double Rt4,
     double P,double Di,double t,
     double v, double YoungsMod,double GF,double Vex)
{
    return Vex*(-((Rn4*(-(pow(Di,2)*GF*P*(1 - 2*v))/
  (4.*t*pow(Di + t,2)*YoungsMod) - (pow(Di,2)*GF*P*(1 - 2*v))/
  (4.*pow(t,2)*(Di + t)*YoungsMod)))/
   (Rt3 + Rt4 + Rn4*(1 + (pow(Di,2)*GF*P*(1 - 2*v))/
  (4.*t*(Di + t)*YoungsMod)) + Rn3*(1 + (pow(Di,2)*GF*P*(2 - v))/
  (4.*t*(Di + t)*YoungsMod)))) + (Rn4*(Rn4*(-(pow(Di,2)*GF*P*(1 - 2*v))/
  (4.*t*pow(Di + t,2)*YoungsMod) - (pow(Di,2)*GF*P*(1 - 2*v))/
  (4.*pow(t,2)*(Di + t)*YoungsMod)) + Rn3*(-(pow(Di,2)*GF*P*(2 - v))/
  (4.*t*pow(Di + t,2)*YoungsMod) - (pow(Di,2)*GF*P*(2 - v))/
  (4.*pow(t,2)*(Di + t)*YoungsMod)))* (1 + (pow(Di,2)*GF*P*(1 - 2*v))/
  (4.*t*(Di + t)*YoungsMod)))/
   pow(Rt3 + Rt4 + Rn4*(1 + (pow(Di,2)*GF*P*(1 - 2*v))/
  (4.*t*(Di + t)*YoungsMod)) + Rn3*(1 + (pow(Di,2)*GF*P*(2 - v))/
  (4.*t*(Di + t)*YoungsMod)),2) + (Rn2*(-(pow(Di,2)*GF*P*(2 - v))/
  (4.*t*pow(Di + t,2)*YoungsMod) - (pow(Di,2)*GF*P*(2 - v))/
```

```
   (4.*pow(t,2)*(Di + t)*YoungsMod)))/
    (Rt1 + Rt2 + Rn1*(1 + (pow(Di,2)*GF*P*(1 - 2*v))/
   (4.*t*(Di + t)*YoungsMod)) + Rn2*(1 + (pow(Di,2)*GF*P*(2 - v))/
   (4.*t*(Di + t)*YoungsMod))) - (Rn2*(Rn1*(-(pow(Di,2)*GF*P*(1 - 2*v))/
   (4.*t*pow(Di + t,2)*YoungsMod) - (pow(Di,2)*GF*P*(1 - 2*v))/
   (4.*pow(t,2)*(Di + t)*YoungsMod)) + Rn2*(-(pow(Di,2)*GF*P*(2 - v))/
   (4.*t*pow(Di + t,2)*YoungsMod) - (pow(Di,2)*GF*P*(2 - v))/
   (4.*pow(t,2)*(Di + t)*YoungsMod)))* (1 + (pow(Di,2)*GF*P*(2 - v))/
   (4.*t*(Di + t)*YoungsMod)))/
    pow(Rt1 + Rt2 + Rn1*(1 + (pow(Di,2)*GF*P*(1 - 2*v))/
   (4.*t*(Di + t)*YoungsMod)) + Rn2*(1 + (pow(Di,2)*GF*P*(2 - v))/
   (4.*t*(Di + t)*YoungsMod)),2)) ;
}

double dVdv(double Rn1,double Rn2,double Rn3,double Rn4,
     double Rt1,double Rt2,double Rt3,double Rt4,
     double P,double Di,double t,
     double v, double YoungsMod,double GF,double Vex)
{
    return Vex*((Rn4*(-(Rn3*pow(Di,2)*GF*P)/
   (4.*t*(Di + t)*YoungsMod) - (pow(Di,2)*GF*Rn4*P)/
   (2.*t*(Di + t)*YoungsMod))*(1 + (pow(Di,2)*GF*P*(1 - 2*v))/
   (4.*t*(Di + t)*YoungsMod)))/
    pow(Rt3 + Rt4 + Rn4*(1 + (pow(Di,2)*GF*P*(1 - 2*v))/
   (4.*t*(Di + t)*YoungsMod)) + Rn3*(1 + (pow(Di,2)*GF*P*(2 - v))/
   (4.*t*(Di + t)*YoungsMod)),2) - (Rn2*(-(Rn1*pow(Di,2)*GF*P)/
   (2.*t*(Di + t)*YoungsMod) - (Rn2*pow(Di,2)*GF*P)/
   (4.*t*(Di + t)*YoungsMod))*(1 + (pow(Di,2)*GF*P*(2 - v))/
   (4.*t*(Di + t)*YoungsMod)))/
    pow(Rt1 + Rt2 + Rn1*(1 + (pow(Di,2)*GF*P*(1 - 2*v))/
```

```
  (4.*t*(Di + t)*YoungsMod)) + Rn2*(1 + (pow(Di,2)*GF*P*(2 - v))/
  (4.*t*(Di + t)*YoungsMod)),2) - (Rn2*pow(Di,2)*GF*P)/
  (4.*t*(Di + t)*(Rt1 + Rt2 + Rn1*(1 + (pow(Di,2)*GF*P*(1 - 2*v))/
  (4.*t*(Di + t)*YoungsMod)) + Rn2*(1 + (pow(Di,2)*GF*P*(2 - v))/
  (4.*t*(Di + t)*YoungsMod)))*YoungsMod) + (pow(Di,2)*GF*Rn4*P)/
  (2.*t*(Di + t)*(Rt3 + Rt4 + Rn4*(1 + (pow(Di,2)*GF*P*(1 - 2*v))/
  (4.*t*(Di + t)*YoungsMod)) + Rn3*(1 + (pow(Di,2)*GF*P*(2 - v))/
  (4.*t*(Di + t)*YoungsMod)))*YoungsMod)) ;
}

double dVdY(double Rn1,double Rn2,double Rn3,double Rn4,
     double Rt1,double Rt2,double Rt3,double Rt4,
     double P,double Di,double t,
     double v, double YoungsMod,double GF,double Vex)
{
    return Vex*((Rn4*(-(pow(Di,2)*GF*Rn4*P*(1 - 2*v))/
  (4.*t*(Di + t)*pow(YoungsMod,2)) - (Rn3*pow(Di,2)*GF*P*(2 - v))/
  (4.*t*(Di + t)*pow(YoungsMod,2)))* (1 + (pow(Di,2)*GF*P*(1 - 2*v))/
  (4.*t*(Di + t)*YoungsMod)))/
   pow(Rt3 + Rt4 + Rn4*(1 + (pow(Di,2)*GF*P*(1 - 2*v))/
  (4.*t*(Di + t)*YoungsMod)) + Rn3*(1 + (pow(Di,2)*GF*P*(2 - v))/
  (4.*t*(Di + t)*YoungsMod)),2) - (Rn2*(-(Rn1*pow(Di,2)*GF*P*(1 - 2*v))/
  (4.*t*(Di + t)*pow(YoungsMod,2)) - (Rn2*pow(Di,2)*GF*P*(2 - v))/
  (4.*t*(Di + t)*pow(YoungsMod,2)))* (1 + (pow(Di,2)*GF*P*(2 - v))/
  (4.*t*(Di + t)*YoungsMod)))/
   pow(Rt1 + Rt2 + Rn1*(1 + (pow(Di,2)*GF*P*(1 - 2*v))/
  (4.*t*(Di + t)*YoungsMod)) + Rn2*(1 + (pow(Di,2)*GF*P*(2 - v))/
  (4.*t*(Di + t)*YoungsMod)),2) - (Rn2*pow(Di,2)*GF*P*(2 - v))/
   (4.*t*(Di + t)*(Rt1 + Rt2 + Rn1*(1 + (pow(Di,2)*GF*P*(1 - 2*v))/
  (4.*t*(Di + t)*YoungsMod)) + Rn2*(1 + (pow(Di,2)*GF*P*(2 - v))/
```

```
   (4.*t*(Di + t)*YoungsMod)))*pow(YoungsMod,2)) +
   (pow(Di,2)*GF*Rn4*P*(1 - 2*v))/
    (4.*t*(Di + t)*(Rt3 + Rt4 + Rn4*(1 + (pow(Di,2)*GF*P*(1 - 2*v))/
   (4.*t*(Di + t)*YoungsMod)) + Rn3*(1 + (pow(Di,2)*GF*P*(2 - v))/
   (4.*t*(Di + t)*YoungsMod)))*pow(YoungsMod,2)));
}

double dVdGF(double Rn1,double Rn2,double Rn3,double Rn4,
      double Rt1,double Rt2,double Rt3,double Rt4,
      double P,double Di,double t,
      double v, double YoungsMod,double GF,double Vex)
{
    return Vex*((Rn4*(1 + (pow(Di,2)*GF*P*(1 - 2*v))/
   (4.*t*(Di + t)*YoungsMod))*((pow(Di,2)*Rn4*P*(1 - 2*v))/
   (4.*t*(Di + t)*YoungsMod) + (Rn3*pow(Di,2)*P*(2 - v))/
   (4.*t*(Di + t)*YoungsMod)))/
    pow(Rt3 + Rt4 + Rn4*(1 + (pow(Di,2)*GF*P*(1 - 2*v))/
   (4.*t*(Di + t)*YoungsMod)) + Rn3*(1 + (pow(Di,2)*GF*P*(2 - v))/
   (4.*t*(Di + t)*YoungsMod)),2) - (Rn2*((Rn1*pow(Di,2)*P*(1 - 2*v))/
   (4.*t*(Di + t)*YoungsMod) + (Rn2*pow(Di,2)*P*(2 - v))/
   (4.*t*(Di + t)*YoungsMod))* (1 + (pow(Di,2)*GF*P*(2 - v))/
   (4.*t*(Di + t)*YoungsMod)))/
    pow(Rt1 + Rt2 + Rn1*(1 + (pow(Di,2)*GF*P*(1 - 2*v))/
   (4.*t*(Di + t)*YoungsMod)) + Rn2*(1 + (pow(Di,2)*GF*P*(2 - v))/
   (4.*t*(Di + t)*YoungsMod)),2) + (Rn2*pow(Di,2)*P*(2 - v))/
    (4.*t*(Di + t)*(Rt1 + Rt2 + Rn1*(1 + (pow(Di,2)*GF*P*(1 - 2*v))/
   (4.*t*(Di + t)*YoungsMod)) + Rn2*(1 + (pow(Di,2)*GF*P*(2 - v))/
   (4.*t*(Di + t)*YoungsMod)))*YoungsMod) - (pow(Di,2)*Rn4*P*(1 - 2*v))/
    (4.*t*(Di + t)*(Rt3 + Rt4 + Rn4*(1 + (pow(Di,2)*GF*P*(1 - 2*v))/
   (4.*t*(Di + t)*YoungsMod)) + Rn3*(1 + (pow(Di,2)*GF*P*(2 - v))/
```

```
   (4.*t*(Di + t)*YoungsMod)))*YoungsMod)) ;
}

double dVdVex(double Rn1,double Rn2,double Rn3,double Rn4,
      double Rt1,double Rt2,double Rt3,double Rt4,
      double P,double Di,double t,
      double v, double YoungsMod,double GF,double Vex)
{
    return -((Rn4*(1 + (pow(Di,2)*GF*P*(1 - 2*v))/
   (4.*t*(Di + t)*YoungsMod)))/
    (Rt3 + Rt4 + Rn4*(1 + (pow(Di,2)*GF*P*(1 - 2*v))/
   (4.*t*(Di + t)*YoungsMod)) + Rn3*(1 + (pow(Di,2)*GF*P*(2 - v))/
   (4.*t*(Di + t)*YoungsMod)))) + (Rn2*(1 + (pow(Di,2)*GF*P*(2 - v))/
   (4.*t*(Di + t)*YoungsMod)))/
    (Rt1 + Rt2 + Rn1*(1 + (pow(Di,2)*GF*P*(1 - 2*v))/
   (4.*t*(Di + t)*YoungsMod)) + Rn2*(1 + (pow(Di,2)*GF*P*(2 - v))/
   (4.*t*(Di + t)*YoungsMod))) ;
}
```

Appendix B

Partial Derivatives

Table B.1: Variable interpretations for the partial derivatives in this section.

a, b, c, h	R_{n1}, R_{n2}, R_{n3}, R_{n4}
l, m, n, o	R_{t1}, R_{t2}, R_{t3}, R_{t4}
y, g, p, d, t	E, P, G_F, D, t
ν_θ, ν_L	$(2-\nu)$, $(1-2\nu)$

$$\begin{bmatrix} \frac{\partial V}{\partial R_{n1}} \\ \frac{\partial V}{\partial R_{n2}} \\ \frac{\partial V}{\partial R_{n3}} \\ \frac{\partial V}{\partial R_{n4}} \end{bmatrix} = \begin{bmatrix} -\frac{bV_{\mathrm{EX}}\left(\frac{gp\Omega\nu_L}{y}+1\right)\left(\frac{gp\Omega\nu_\theta}{y}+1\right)}{\left(l+m+a\left(\frac{gp\Omega\nu_L}{y}+1\right)+b\left(\frac{gp\Omega\nu_\theta}{y}+1\right)\right)^2} \\ V_{\mathrm{EX}}\left(\frac{\frac{gp\Omega\nu_\theta}{y}+1}{l+m+a\left(\frac{gp\Omega\nu_L}{y}+1\right)+b\left(\frac{gp\Omega\nu_\theta}{y}+1\right)}-\frac{b\left(\frac{gp\Omega\nu_\theta}{y}+1\right)^2}{\left(l+m+a\left(\frac{gp\Omega\nu_L}{y}+1\right)+b\left(\frac{gp\Omega\nu_\theta}{y}+1\right)\right)^2}\right) \\ \frac{hV_{\mathrm{EX}}\left(\frac{gp\Omega\nu_L}{y}+1\right)\left(\frac{gp\Omega\nu_\theta}{y}+1\right)}{\left(n+o+h\left(\frac{gp\Omega\nu_L}{y}+1\right)+c\left(\frac{gp\Omega\nu_\theta}{y}+1\right)\right)^2} \\ V_{\mathrm{EX}}\left(\frac{h\left(\frac{gp\Omega\nu_L}{y}+1\right)^2}{\left(n+o+h\left(\frac{gp\Omega\nu_L}{y}+1\right)+c\left(\frac{gp\Omega\nu_\theta}{y}+1\right)\right)^2}-\frac{\frac{gp\Omega\nu_L}{y}+1}{n+o+h\left(\frac{gp\Omega\nu_L}{y}+1\right)+c\left(\frac{gp\Omega\nu_\theta}{y}+1\right)}\right) \end{bmatrix} \tag{B.1}$$

$$\begin{bmatrix} \frac{\partial V}{\partial R_{T1}} \\ \frac{\partial V}{\partial R_{T2}} \\ \frac{\partial V}{\partial R_{T3}} \\ \frac{\partial V}{\partial R_{T4}} \end{bmatrix} = \begin{bmatrix} -\frac{bV_{\mathrm{EX}}\left(\frac{gp\Omega\nu_\theta}{y}+1\right)}{\left(l+m+a\left(\frac{gp\Omega\nu_L}{y}+1\right)+b\left(\frac{gp\Omega\nu_\theta}{y}+1\right)\right)^2} \\ -\frac{bV_{\mathrm{EX}}\left(\frac{gp\Omega\nu_\theta}{y}+1\right)}{\left(l+m+a\left(\frac{gp\Omega\nu_L}{y}+1\right)+b\left(\frac{gp\Omega\nu_\theta}{y}+1\right)\right)^2} \\ \frac{hV_{\mathrm{EX}}\left(\frac{gp\Omega\nu_L}{y}+1\right)}{\left(n+o+h\left(\frac{gp\Omega\nu_L}{y}+1\right)+c\left(\frac{gp\Omega\nu_\theta}{y}+1\right)\right)^2} \\ \frac{hV_{\mathrm{EX}}\left(\frac{gp\Omega\nu_L}{y}+1\right)}{\left(n+o+h\left(\frac{gp\Omega\nu_L}{y}+1\right)+c\left(\frac{gp\Omega\nu_\theta}{y}+1\right)\right)^2} \end{bmatrix} \tag{B.2}$$

$$\frac{\partial V}{\partial P} = V_{\mathrm{EX}} \left(\begin{bmatrix} \frac{bg\nu_\theta d^2}{4t(d+t)\left(l+m+a\left(\frac{gp\Omega\nu_L}{y}+1\right)+b\left(\frac{gp\Omega\nu_\theta}{y}+1\right)\right)y} - \\ \frac{gh\nu_L d^2}{4t(d+t)\left(n+o+h\left(\frac{gp\Omega\nu_L}{y}+1\right)+c\left(\frac{gp\Omega\nu_\theta}{y}+1\right)\right)y} + \\ \frac{h\left(\frac{gp\Omega\nu_L}{y}+1\right)\left(\frac{gh\nu_L d^2}{4t(d+t)y}+\frac{cg\nu_\theta d^2}{4t(d+t)y}\right)}{\left(n+o+h\left(\frac{gp\Omega\nu_L}{y}+1\right)+c\left(\frac{gp\Omega\nu_\theta}{y}+1\right)\right)^2} - \\ \frac{b\left(\frac{ag\nu_L d^2}{4t(d+t)y}+\frac{bg\nu_\theta d^2}{4t(d+t)y}\right)\left(\frac{gp\Omega\nu_\theta}{y}+1\right)}{\left(l+m+a\left(\frac{gp\Omega\nu_L}{y}+1\right)+b\left(\frac{gp\Omega\nu_\theta}{y}+1\right)\right)^2} \end{bmatrix} \right) \tag{B.3}$$

$$\frac{\partial V}{\partial D} = V_{\mathrm{EX}} \left(\left[\begin{array}{c} -\frac{h\left(\frac{dgp\nu_L}{2t(d+t)y} - \frac{d^2 gp\nu_L}{4t(d+t)^2 y}\right)}{n+o+h\left(\frac{gp\Omega\nu_L}{y}+1\right)+c\left(\frac{gp\Omega\nu_\theta}{y}+1\right)} + \\ \\ \frac{h\left(h\left(\frac{dgp\nu_L}{2t(d+t)y} - \frac{d^2 gp\nu_L}{4t(d+t)^2 y}\right)+c\left(\frac{dgp\nu_\theta}{2t(d+t)y} - \frac{d^2 gp\nu_\theta}{4t(d+t)^2 y}\right)\right)\left(\frac{gp\Omega\nu_L}{y}+1\right)}{\left(n+o+h\left(\frac{gp\Omega\nu_L}{y}+1\right)+c\left(\frac{gp\Omega\nu_\theta}{y}+1\right)\right)^2} + \\ \\ \frac{b\left(\frac{dgp\nu_\theta}{2t(d+t)y} - \frac{d^2 gp\nu_\theta}{4t(d+t)^2 y}\right)}{l+m+a\left(\frac{gp\Omega\nu_L}{y}+1\right)+b\left(\frac{gp\Omega\nu_\theta}{y}+1\right)} - \\ \\ \frac{b\left(a\left(\frac{dgp\nu_L}{2t(d+t)y} - \frac{d^2 gp\nu_L}{4t(d+t)^2 y}\right)+b\left(\frac{dgp\nu_\theta}{2t(d+t)y} - \frac{d^2 gp\nu_\theta}{4t(d+t)^2 y}\right)\right)\left(\frac{gp\Omega\nu_\theta}{y}+1\right)}{\left(l+m+a\left(\frac{gp\Omega\nu_L}{y}+1\right)+b\left(\frac{gp\Omega\nu_\theta}{y}+1\right)\right)^2} \end{array} \right] \right) \tag{B.4}$$

$$\frac{\partial V}{\partial t} = V_{\mathrm{EX}} \left(\left[\begin{array}{c} -\frac{h\left(-\frac{gp\nu_L d^2}{4t^2(d+t)y} - \frac{gp\nu_L d^2}{4t(d+t)^2 y}\right)}{n+o+h\left(\frac{gp\Omega\nu_L}{y}+1\right)+c\left(\frac{gp\Omega\nu_\theta}{y}+1\right)} + \\ \\ \frac{h\left(h\left(-\frac{gp\nu_L d^2}{4t^2(d+t)y} - \frac{gp\nu_L d^2}{4t(d+t)^2 y}\right)+c\left(-\frac{gp\nu_\theta d^2}{4t^2(d+t)y} - \frac{gp\nu_\theta d^2}{4t(d+t)^2 y}\right)\right)\left(\frac{gp\Omega\nu_L}{y}+1\right)}{\left(n+o+h\left(\frac{gp\Omega\nu_L}{y}+1\right)+c\left(\frac{gp\Omega\nu_\theta}{y}+1\right)\right)^2} + \\ \\ \frac{b\left(-\frac{gp\nu_\theta d^2}{4t^2(d+t)y} - \frac{gp\nu_\theta d^2}{4t(d+t)^2 y}\right)}{l+m+a\left(\frac{gp\Omega\nu_L}{y}+1\right)+b\left(\frac{gp\Omega\nu_\theta}{y}+1\right)} - \\ \\ \frac{b\left(a\left(-\frac{gp\nu_L d^2}{4t^2(d+t)y} - \frac{gp\nu_L d^2}{4t(d+t)^2 y}\right)+b\left(-\frac{gp\nu_\theta d^2}{4t^2(d+t)y} - \frac{gp\nu_\theta d^2}{4t(d+t)^2 y}\right)\right)\left(\frac{gp\Omega\nu_\theta}{y}+1\right)}{\left(l+m+a\left(\frac{gp\Omega\nu_L}{y}+1\right)+b\left(\frac{gp\Omega\nu_\theta}{y}+1\right)\right)^2} \end{array} \right] \right) \tag{B.5}$$

$$\frac{\partial V}{\partial v} = V_{\text{EX}} \left(\begin{bmatrix} -\frac{bgpd^2}{4t(d+t)\left(l+m+a\left(\frac{gp\Omega\nu_L}{y}+1\right)+b\left(\frac{gp\Omega\nu_\theta}{y}+1\right)\right)y}+ \\ \frac{ghpd^2}{2t(d+t)\left(n+o+h\left(\frac{gp\Omega\nu_L}{y}+1\right)+c\left(\frac{gp\Omega\nu_\theta}{y}+1\right)\right)y}+ \\ \frac{h\left(-\frac{cgpd^2}{4t(d+t)y}-\frac{ghpd^2}{2t(d+t)y}\right)\left(\frac{gp\Omega\nu_L}{y}+1\right)}{\left(n+o+h\left(\frac{gp\Omega\nu_L}{y}+1\right)+c\left(\frac{gp\Omega\nu_\theta}{y}+1\right)\right)^2}- \\ \frac{b\left(-\frac{agpd^2}{2t(d+t)y}-\frac{bgpd^2}{4t(d+t)y}\right)\left(\frac{gp\Omega\nu_\theta}{y}+1\right)}{\left(l+m+a\left(\frac{gp\Omega\nu_L}{y}+1\right)+b\left(\frac{gp\Omega\nu_\theta}{y}+1\right)\right)^2} \end{bmatrix} \right) \tag{B.6}$$

$$\frac{\partial V}{\partial E} = V_{\text{EX}} \left(\begin{bmatrix} -\frac{bgp\nu_\theta d^2}{4t(d+t)\left(l+m+a\left(\frac{gp\Omega\nu_L}{y}+1\right)+b\left(\frac{gp\Omega\nu_\theta}{y}+1\right)\right)y^2}+ \\ \frac{ghp\nu_L d^2}{4t(d+t)\left(n+o+h\left(\frac{gp\Omega\nu_L}{y}+1\right)+c\left(\frac{gp\Omega\nu_\theta}{y}+1\right)\right)y^2}+ \\ \frac{h\left(-\frac{ghp\nu_L d^2}{4t(d+t)y^2}-\frac{cgp\nu_\theta d^2}{4t(d+t)y^2}\right)\left(\frac{gp\Omega\nu_L}{y}+1\right)}{\left(n+o+h\left(\frac{gp\Omega\nu_L}{y}+1\right)+c\left(\frac{gp\Omega\nu_\theta}{y}+1\right)\right)^2}- \\ \frac{b\left(-\frac{agp\nu_L d^2}{4t(d+t)y^2}-\frac{bgp\nu_\theta d^2}{4t(d+t)y^2}\right)\left(\frac{gp\Omega\nu_\theta}{y}+1\right)}{\left(l+m+a\left(\frac{gp\Omega\nu_L}{y}+1\right)+b\left(\frac{gp\Omega\nu_\theta}{y}+1\right)\right)^2} \end{bmatrix} \right) \tag{B.7}$$

$$\frac{\partial V}{\partial G} = V_{\mathrm{EX}} \left(\begin{bmatrix} \frac{bp\nu_\theta d^2}{4t(d+t)\left(l+m+a\left(\frac{gp\Omega\nu_L}{y}+1\right)+b\left(\frac{gp\Omega\nu_\theta}{y}+1\right)\right)y} - \\ \\ \frac{hp\nu_L d^2}{4t(d+t)\left(n+o+h\left(\frac{gp\Omega\nu_L}{y}+1\right)+c\left(\frac{gp\Omega\nu_\theta}{y}+1\right)\right)y} + \\ \\ \frac{h\left(\frac{gp\Omega\nu_L}{y}+1\right)\left(\frac{hp\nu_L d^2}{4t(d+t)y}+\frac{cp\nu_\theta d^2}{4t(d+t)y}\right)}{\left(n+o+h\left(\frac{gp\Omega\nu_L}{y}+1\right)+c\left(\frac{gp\Omega\nu_\theta}{y}+1\right)\right)^2} - \\ \\ \frac{b\left(\frac{ap\nu_L d^2}{4t(d+t)y}+\frac{bp\nu_\theta d^2}{4t(d+t)y}\right)\left(\frac{gp\Omega\nu_\theta}{y}+1\right)}{\left(l+m+a\left(\frac{gp\Omega\nu_L}{y}+1\right)+b\left(\frac{gp\Omega\nu_\theta}{y}+1\right)\right)^2} \end{bmatrix} \right) \tag{B.8}$$

$$\frac{\partial V}{\partial V_{\mathrm{EX}}} = \frac{b\left(\frac{gp\Omega\nu_\theta}{y}+1\right)}{l+m+a\left(\frac{gp\Omega\nu_L}{y}+1\right)+b\left(\frac{gp\Omega\nu_\theta}{y}+1\right)} - \frac{h\left(\frac{gp\Omega\nu_L}{y}+1\right)}{n+o+h\left(\frac{gp\Omega\nu_L}{y}+1\right)+c\left(\frac{gp\Omega\nu_\theta}{y}+1\right)} \tag{B.9}$$

Appendix C

Circuits

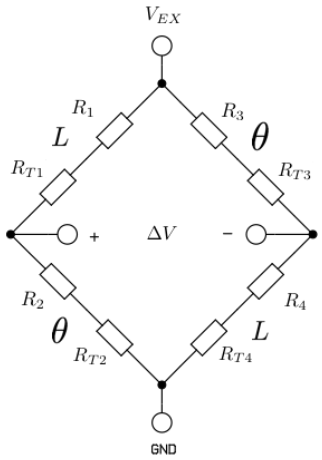

Figure C.1: Wheatstone bridge circuit. Trim resistors are added to represent both trim resistors and lead wire resistance, both of which are constant.

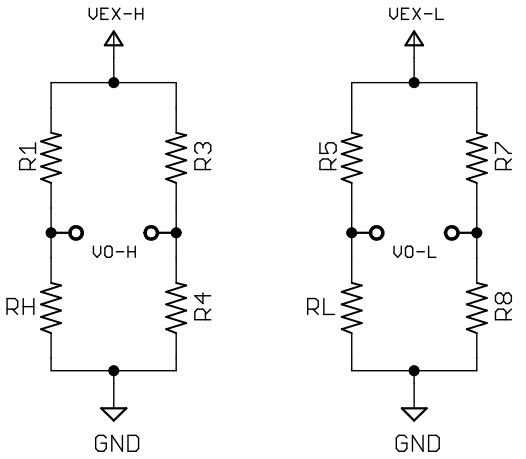

Figure C.2: Bridge circuits for the solution of Poisson's ratio in PVPT material. Resistors can be shared; output voltages do not need to be read simultaneously.

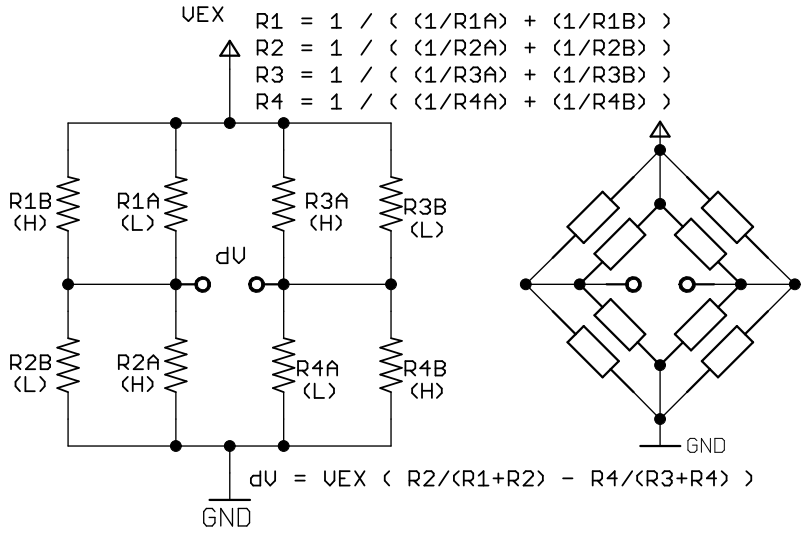

Figure C.3: The differential PVPT configuration needs a bridge that produces consistent differential voltages with repeated conditions of differential pressure. Initial simulations have produced encouraging results for this nested bridge design.

Appendix D

Summary of Key Insights

D.1 Equations

Geometry term, Equation (3.6)

$$\Omega = \frac{D^2}{4t(D+t)}$$

Stress equations (3.7, 3.8); strain equations (3.12, 3.13):

$$\sigma_\theta = 2\Omega P_{\text{i}} \qquad \sigma_{\text{L}} = \Omega P_{\text{i}}$$
$$\varepsilon_\theta = \frac{\Omega P_{\text{i}}}{E}(2-\nu) \qquad \varepsilon_{\text{L}} = \frac{\Omega P_{\text{i}}}{E}(1-2\nu)$$

$$R_n = R_{n0}\,(1 + \varepsilon_n \cdot G_F)$$

Lambda Equations 3.22, 3.23

$$\lambda_\theta = \frac{\Omega}{E}(2-\nu) \qquad \lambda_{\text{L}} = \frac{\Omega}{E}(1-2\nu)$$
$$R_\theta(P) = R_{n0}\,(1 + P\lambda_\theta) \qquad R_L(P) = R_{n0}\,(1 + P\lambda_{\text{L}})$$

Wheatstone bridge equation which transforms pressure to voltage output

$$V(P) = \Delta V = V_{\text{Ex}} \left(\frac{R_2 + R_{2T}}{R_1 + R_{1T} + R_2 + R_{2T}} - \frac{R_4 + R_{4T}}{R_3 + R_{3T} + R_4 + R_{4T}} \right)$$

Voltage to pressure transformation model, Equation 3.33

$$P(V) = \frac{K_2 - K_5 V - \sqrt{M_1 V^2 + M_2 V + M_3}}{2(K_4 V - K_1)}$$

$$c_1 = R_{20}\lambda_\theta V_{EX} \qquad c_5 = R_{40}\lambda_L V_{EX}$$

$$c_2 = R_{20}V_{EX} + R_{2T}V_{EX} \qquad c_6 = R_{40}V_{EX} + R_{4T}V_{EX}$$

$$c_3 = R_{10}\lambda_L + R_{20}\lambda_\theta \qquad c_7 = R_{30}\lambda_\theta + R_{40}\lambda_L$$

$$c_4 = R_{10} + R_{20} + R_{1T} + R_{2T} \qquad c_8 = R_{30} + R_{40} + R_{3T} + R_{4T}$$

$$K_1 = c_7 c_1 - c_5 c_3 \qquad K_4 = c_7 c_3$$

$$K_2 = c_7 c_2 + c_1 c_8 - c_5 c_4 - c_6 c_3 \qquad K_5 = c_7 c_4 + c_8 c_3$$

$$K_3 = c_8 c_2 - c_6 c_4 \qquad K_6 = c_8 c_4$$

$$M_1 = K_5^2 - 4K_4K_6$$

$$M_2 = 4K_1K_6 - 2K_2K_5 + 4K_3K_4$$

$$M_3 = K_2^2 - 4K_1K_3$$

Amplifier gain and uncertainty, Equation 3.56:

$$G_{\text{final}} \pm \Delta_G = \prod_{i=1}^{n} G_i \pm \sqrt{\sum_{j=1}^{n} \left(\prod_{i=1}^{n} \left[\frac{(aR_i + b)}{R_i} \right] \frac{b}{(aR_j + b)} \Delta_R \right)^2}$$

D.2 Relationships

Equation 3.9 relates hoop stress to longitudinal stress:

$$\sigma_\theta = 2\sigma_{\mathrm{L}}$$

which is a constant property of pressure vessels both thin and thick-walled.

Equation 3.14 relates hoop strain to longitudinal strain:

$$\frac{\varepsilon_\theta}{\varepsilon_L} = \frac{2-\nu}{1-2\nu}$$

When in a Wheatstone bridge configuration as in Figure C.1, a larger ratio results in increased sensitivity.

$$\frac{\Omega_1 E_2}{\Omega_2 E_1} \approx \frac{\delta_{V1}}{\delta_{V2}}$$

D.3 Prototype Parameter Tables

Table D.1: PVPT prototype geometry and material properties.

Material	D (in)	t (in)	E (Mpsi)	ν	Source(s)
PC	0.506	0.067	0.25	0.370	[15, 46]
PVC	2.041	0.168	0.45	0.350	[15, 46]
Cu	0.565	0.035	18.8	0.343	[19, 46, 7]
Brass	0.532	0.020	16.0	0.350	[19, 46]

Table D.2: PVPT prototype gage resistances and trim resistances.

	R_{10}	R_{20}	R_{30}	R_{40}	R_{1T}	R_{2T}	R_{3T}	R_{4T}
PC	349.2	349.9	349.9	349.5	0.0	0.0	0.0	0.0
PVC	349.3	349.5	349.5	349.3	0.0	0.0	0.0	0.0
Brass	349.7	349.9	348.8	349.6	0.0	0.0	0.8	0.0
Cu	349.25	349.55	349.45	349.0	0.0	0.0	0.0	1.2

Table D.3: PVPT prototype design variable uncertainties (Δ)

	Property	Uncertainty	Source
D	inner diameter	$\pm$0.001 inch	Neiko 01407A Digital Calipers
t	wall thickness	$\pm$0.001 inch	Neiko 01407A Digital Calipers
E	modulus of elasticity	$\pm$10%	[15, 19, 46]
ν	Poisson's ratio	$\pm$10%	[15, 19, 46]
R_{n0}	gage resistance	$\pm$0.1Ω	Radioshack Digital Multimeter
R_{nT}	trim resistance	$\pm$0.1Ω	Radioshack Digital Multimeter
G_F	Gage Factor	$\pm$2%	Omega Datasheet [2, 3]